Ocean Biogeochemical Dynamics

Chapter 10: Oceanic carbon cycle, atmospheric CO$_2$, and climate

by

Jorge L. Sarmiento and Nicolas Gruber

Princeton University Press

September 10, 2004

Contents

iv

Throughout most of this book, our discussions have focused on the steady-state characteristics of the cycles of biogeochemically important elements in the ocean. However, as more about the past behavior of these cycles was learned, we have to come to realize that these cycles have seldom been in a "true" steady-state. It appears that variability is as much a fundamental property of these biogeochemical cycles as it is a property of the climate system in general (see discussion in section 2.5). In this last chapter, we explore the variability of these cycles on a range of time-scales, ranging from a few years to several hundred thousand years. In trying to understand the mechanisms that give rise to these variations, we will apply many of the tools and concepts that we have learned in the previous 9 chapters. We will focus on the carbon cycle, given its central role in biogeochemical cycling and its interaction with climate as a result of the greenhouse gas properties of CO_2 in the atmosphere. This cycle is also of particular interest given the fact that mankind has began to perturb the global carbon cycle dramatically and likely will continue to do so.

10.1 Introduction

A very good indicator for the state of the global carbon cycle is atmospheric CO_2, since it represents the concentration of a relatively small reservoir that acts as a conveyor for the exchange of carbon between the two other important reservoirs of the global carbon cycle : the terrestrial biosphere including the soils, and the ocean including its sediments (Figure 10.1.1). The amount of CO_2 in the atmosphere is also small compared with the gross exchange fluxes between it and the ocean and terrestrial biosphere, as reflected in the short residence time of about 6 to 8 years for CO_2 in the atmosphere with respect to these exchange fluxes. Atmospheric CO_2 is therefore expected to react sensitively to changes in the global carbon cycle.

Thanks to the preservation of tiny air-bubbles in ice-cores, researchers have been able to reconstruct concentrations of atmospheric CO_2 over the last 400,000 years with great precision [*Indermühle et al.*, 1999, *Petit et al.*, 1999]. A summary of such reconstructions in Figure 10.1.2 shows that atmospheric CO_2 has varied by nearly 100 ppm over the last 400,000 years, indicating that substantial changes must have occured in the distribution of carbon between the different reservoirs. Several observations stand out in Figure 10.1.2. First, atmospheric CO_2 has varied quasi-periodically over the last 400,000 years between approximately 180 ppm and 280 ppm. These variations occured in close concert with the quasi-periodic glacial/inter-glacial cycles, with fully glacial conditions coinciding with the lower bound CO_2 concentration of about 180 ppm, and inter-glacial conditions experiencing the upper bound concentrations of about 280 ppm. This upper-bound appears to be rather stable, and also characterizes the largest part of the current inter-glacial, the

Holocene.

The cause for these glacial-interglacial changes must be connected with the oceanic carbon cycle, since this reservoir controls atmospheric CO_2 on any time-scale longer than a few hundred years. We will discuss many hypotheses and mechanisms that have been proposed over the last two decades to explain these observed changes, but as it turns out, no mechanism proposed so far has been able to explain all existing constraints. In the near future, as scientists learn more about ocean circulation, biogeochemistry and their interaction with the climate system during ice ages from detailed analyses of climate records, we likely will be able to correctly identify the mechanisms. However, at the moment the causes of the glacial-interglacial variations in atmospheric CO_2 remain one of the greatest puzzles of the global carbon cycle.

A second outstanding feature revealed in Figure 10.1.2 is the dramatic increase of atmospheric CO_2 since the beginning of the industrial revolution in the late 18th century, a period we will refer to as the *Anthropocene* [*Crutzen and Stoermer*, 2000]. This increase is a consequence of anthropogenic activities, mainly the burning of fossil fuels, but also the conversion of forests and other pristine areas into lands for agricultural and other human use. About half of the emissions from these anthropogenic activities have remained in the atmosphere leading to an increase that is now approaching the change that occurred from glacial to interglacial periods. However, this human induced increase happened within less than 200 years, whereas it took atmospheric CO_2 several thousand years to change from glacial to interglacial levels.

CO_2 is the most important anthropogenic greenhouse gas in the atmosphere (see next subsection) and its increase is cause for concern as it may lead to signifcant changes in climate with major consequences for human beings. Efforts have started now at an international level to curb emissions of CO_2 and other greenhouse gases. However, since fossil fuels are the primary source of energy and heat in the industrial world, and therefore are tightly linked to our current economy, CO_2 emission reductions are coupled to major economic investments. It is therefore of great importance to be able to quantify the redistribution of the emitted CO_2 in the global carbon system, since only the fraction remaining in the atmosphere adds to the greenhouse warming.

The observation that a substantial fraction of the emitted CO_2 has remained in the atmosphere is actually surprising at first, since one would intuitively assume that the emitted CO_2 would be redistributed between the atmosphere and ocean with the same 1:65 ratio as the present distribution. Estimates of the actual oceanic uptake suggest that only about a third of the total anthropogenic CO_2 emissions has been taken up by the oceans. Why is the oceanic uptake so small? This is mainly a consequence of kinetic constraints imposed by the limited rate of ocean circulation. However, even if the ocean was mixing extremely rapidly, the fraction taken up by the ocean without further

reaction with the CaCO$_3$ in the sediments would only be around 80 to 85%, substantially smaller than the 98% that would be predicted from the present distribution. This rather surprising result is caused by one of the many peculiarities of the oceanic CO$_2$ system. In the following subsection, we will first discuss briefly the greenhouse effect and explain why it is so important for climate.

GREENHOUSE EFFECT

Climate and the biogeochemical cycling of major elements on earth are tightly interwoven. One of the most important coupling points exists in the biogeochemical controls on the composition of Earth's atmosphere, in particular of those gases that interact with solar and terrestrial radiation and change how the energy is redistributed within the climate system. Those gases that absorb energy at infrared wavelengths typical of terrestrial radiation are called *Greenhouse gases*, with CO$_2$ being one of the most important ones.

Biogeochemical cycles can influence the physical climate system also through changes in other climate-relevant properties at earth's surface, e.g. by changing the albedo, i.e. the fraction of shortwave radiation from the sun that is directly reflected back, or by interacting with the hydrological cycle, altering the latent heat fluxes associated with condensation and evaporation (see Figure 10.1.3 and e.g. *Betts* [2000]). We will limit our discussion here to the *Greenhouse Effect*.

The Earth receives short-wavelength radiation emitted from the sun, and re-radiates this energy back to space at longer wavelengths. Figure 10.1.3 shows the flow of energy through the atmosphere, starting from the short-wave solar radiation received at the top-of-the-atmosphere proceeding down to the surface of earth. Along the way, more than half of the radiation either gets absorbed by the atmosphere and clouds, or gets reflected back into space.

The short wavelength energy absorbed by earth's surface warms the planet, and earth itself acts as a blackbody radiatior, but because its temperature is much lower than that of the sun, most of its emitted radiation occurs at much longer wavelengths (Wien's law), i.e. in the infrared band. In the absence of an atmosphere, the surface temperature of the Earth would warm until the surface of the planet radiated heat to space at the same rate as it intercepts radiation from the sun. This equilibrium temperature is given by the Stefan-Boltzmann Law of blackbody radiation, $Q = \sigma T^4$, where Q is the heat flux, $\sigma = 5.670 \times 10^{-8}$ W m^{-2} K^{-4} is the Stefan-Boltzmann constant, and T is the temperature in degrees Kelvin. The earth receives an average solar radiation of about 235 W m^{-2} after subtracting off the 30% of the incoming solar radiation reflected back to space (Figure 10.1.3). In this case with no atmosphere, the equilibrium temperature for the earth is thus a frigid 255 K (-19 °C).

The presence of an atmosphere with gases that absorb at infrared wavelengths, i.e.

greenhouse gases, turns Earth into a much more habitable planet. The impact of such gases is illustrated by Figure 10.1.4, which shows the flux of energy emitted by the surface of the earth as a function of wavelength. The dashed lines are the ideal blackbody radiation with no atmospheric interference. The solid line is the calculated clear-sky radiation flux for a surface temperature of 294 K with the effect of greenhouse gas absorption by the atmosphere included. This is what a satellite outside the atmosphere would see if there were no clouds. The deviation of the solid line from the dashed line for 294 K is due to absorption of outgoing radiation by greenhouse gases in the atmosphere. The minimum in outgoing radiation centered at 15 μm is due to absorption by CO_2, and that near 9 to 10 μm is due to absorption by ozone. The largest absorber of all is water vapor (Table 10.1.1), which absorbs across a broad range of wavelengths. The energy absorbed by the radiatively active gases in the atmosphere is re-emitted from within the atmosphere (see Figure 10.1.3. This re-emission occurs in all directions, therefore to a substantial degree also in a downward direction, reducing the efficiency with which the surface of earth is able to cool itself. One way to think about the resulting trapping of radiation is that if you were in outer space looking at the earth at a wavelength of 15 μm, most of what you would see would be radiation emitted from the sky.

Because radiation is trapped in the atmosphere and is re-emitted at some height above the surface, the average equilibrium radiative blackbody temperature of 255 K occurs at some elevation that is well above the surface of the earth. Because air is compressible, the atmosphere warms as one descends from this elevation to the surface. Temperature at the surface of the earth is thus warmer than the radiative equilibrium temperature, giving the observed average surface temperature of 288 K. The warming of the surface of the earth due to the presence of the greenhouse effect is thus a remarkable 33 K.

GLOBAL WARMING

Human activities have increased the atmospheric burdens of many radiatively active gases, including CO_2, methane (CH_4), nitrous oxide (N_2O), and chlorofluorocarbons (CFCs). Methane, nitrous oxide, and CFCs tend to absorb terrestrial radiation in a wave-length window where the atmosphere is currently relatively transparent, i.e. where little absorption by other atmospheric constituents takes place. As a result, the release to the atmosphere of these trace gases has an important effect on the radiative balance even at very low levels of concentration. Atmospheric CO_2, on the other hand, is already absorbing most of the radiation in its absorption band, and any additional CO_2 acts by increasing the absorption towards the edges of the band. As a consequence, a proportionally larger increase in the atmospheric CO_2 burden is necessary to affect significantly the radiative balance of the atmosphere. Table 10.1.2 gives the relative efficiencies of the major greenhouse gases, expressed as forcing per molecule normalized to CO_2.

Table 10.1.1 summarizes the contributions of each of the greenhouse gases to the radiative balance of the atmosphere due to their concentration increases between 1765 and 1990. Despite its high background concentration, the addition of CO_2 to the atmosphere has been so large that it accounts for about 61% of the enhanced capacity of the atmosphere to absorb long-wavelength radiation emitted from the surface. CH_4 and N_2O account for about 27% of the total anthropogenic radiative forcing, and chlorofluorocarbons for the remaining 12%.

An estimate of the surface warming that will result from the increased greenhouse trapping can be obtained by use of a simple zero-dimensional heat balance model:

$$H\frac{\mathrm{d}\Delta T}{\mathrm{d}t} = \Delta Q - \lambda\,\Delta T \tag{10.1.1}$$

where H (W m^{-2} K^{-1} s) is the heat capacity of the combined ocean and atmosphere system, ΔT is the change in surface temperature, ΔQ (W m^{-2}) is the radiative forcing given in Table 10.1.1, and λ (W m^{-2} K^{-1}), is referred to as the climate sensitivity parameter. In equilibrium (10.1.1) gives

$$\Delta T = \frac{\Delta Q}{\lambda}. \tag{10.1.2}$$

The value of λ is usually determined from the response of a variety of climate models to perturbations in radiative forcing [*Cubasch et al.*, 2001]. A value of 3.3 W m^{-2} K^{-1} is obtained by assuming that absorption of infrared radiation by greenhouse gases occurs without any feedbacks. However, global warming increases the water vapor content, which further increases the absorption. It also modifies the vertical gradient of temperature (lapse rate) in the atmosphere. Further feedbacks include changes in snow and ice cover, which affect albedo; cloud cover, and its interaction with short- and long wave radiation; and several more. Consideration of these feedbacks significantly reduces λ to about 1.8±0.7 W m^{-2} K^{-1}, with the uncertainty estimate reflecting the range of results from a variety of models. An analysis of the effect of individual feedbacks shows that cloud feedback is by far the largest contributor to the overall uncertainty. Using this climate sensitivity, we obtain an equilibrium warming of 1.5 to 3.4 K for a CO_2 doubling ($\Delta Q = 3.7$ W m^{-2} [*Ramaswamy et al.*, 2001]). The equilibrium climate warming for a CO_2 doubling reported by *Houghton et al.* [2001] is 1.5 to 4.5 K, which requires $\lambda = 1.7±0.8$ W m^{-2} K^{-1}.

The total increase of 2.43 W m^{-2} in infrared trapping over the last 200 years shown in Table 10.1.1 should thus give an equilibrium warming of 1.0 to 3.0 K. Additional changes in radiative forcing shown in Table 10.1.3 include the effect of increased stratospheric water vapor due to production from methane, changes in tropospheric and stratospheric ozone, direct solar forcing, and the cooling effect of aerosols. Aerosol cooling explains some unusual observations about the pattern of warming. One of these is that the Southern Hemisphere has warmed more than the Northern. This is due to the larger production of

aerosols in the Northern Hemisphere and their limited atmospheric lifetime that prevents them from being spread into the Southern hemisphere. The other is that Northern Hemisphere warming has been greatest at night. Aerosols increase reflection of solar radiation from the earth, so their cooling effect should be felt more during the day. The combined impact of the additional radiative forcing terms reduces the total current radiative forcing to 1.5 W m^{-2}. This gives equilibrium warming of 0.6 to 1.8 K. The observed warming over the last century is still smaller, 0.3 to 0.6 K (Figure 10.1.5). However, our estimate assumes that the temperature of the whole climate system has equilibrated with the increase in radiative forcing, whereas, in reality, the large heat capacity of the ocean and the slow rate of mixing has led to substantial slowdown of the warming rate. Including this effect in fully coupled ocean-atmosphere-land surface climate model simulations (e.g. [*Mitchell et al.*, 2001]) gives a present warming estimate that is very close to the observed one (Figure 10.1.5). The flipside of this effect is that if the growth in radiative forcing were stopped at current levels, the earth would continue to warm up until the equilibrium warming is reached.

While the remainder of this chapter is devoted to CO_2, it is important to recall that of the anthropogenic greenhouse gases shown in Table 10.1.1, N_2O also has important oceanic sources and sinks (see also chapters 3 and 5). Its oceanic source is estimated to be 3.7 to 4.3 Tg N yr^{-1} [*Nevison et al.*, 2004], compared with total sources of 4 to 12 in pre-industrial times, and 13 to 20 today [*Prather et al.*, 2001]. The chlorofluorocarbons have found important use in oceanography as tracers of water motion (see chapter 2), but their net uptake by the oceans is negligible because of their very low solubility and chemical inertness (see chapter 3).

<div align="center">OUTLINE</div>

This chapter is organized as follows. We first address the anthropogenic CO_2 perturbation over the last two hundred years, and discuss in particular the reasons for the slow oceanic uptake of anthropogenic CO_2 and learn about a number of techniques that have been used to identify and quantify anthropogenic CO_2 in the ocean. We will also investigate the role of ocean biology in this process and will see that its influence becomes very important once the climate system moves significantly away from steady-state as a consequence of global climate change. The response of the ocean carbon cycle to such changes are poorly understood and thus very difficult to predict. Observations of interannual to decadal time-scale variability in the climate and global carbon systems provide one of the few means to study these interactions directly. Direct observations of atmospheric CO_2 since 1958 show that the growth rate of atmospheric CO_2 experienced large changes from year to year, while the growth rate of fossil fuel emissions changed only minimally. This indicates that substantial amounts of carbon are transferred between the ocean, atmosphere and

terrestrial biosphere reservoirs on interannual to decadal time scales. However, there is presently little consensus about the relative role of the oceans and of the land biosphere in controlling these changes. Section 10.3 will discuss these issues in more detail. A second important avenue for improving our ability to make prediction for the future is to be able to understand the causes for the changes seen in the past. The last section of this chapter will investigate the glacial-interglacial CO$_2$ problem, one of the most puzzling questions of global carbon cycle research.

TABLES

Table 10.1.1: Major greenhouse gases. Partial pressures, present rate of increase, and increase in radiative forcing are from *Ramaswamy et al.* [2001]. Pre-industrial radiative forcing is from *Dickinson and Cicerone* [1986].

Gas	Gas Partial Pressure in dry air (ppm)		Current rate of increase (%)	Radiative forcing (W m^{-2})	
	1765	1992		pre-industrial < 1765	anthropogenic (1765-1990)
H_2O	-	-	-	94	
CO_2	278	356	0.4	50	1.46
CH_4	0.7	1.71	0.6	1.1	0.48
CFC-11	0.0	0.000268	0.0	0.0	0.07
CFC-12	0.0	0.000503	1.4	0.0	0.17
Other CFC's	-	-	-	-	0.10
N_2O	0.275	0.310	0.25	1.25	0.15
Total				146	2.43

Table 10.1.2: Radiative Forcing per additional molecule relative to the radiative forcing due to one additional molecule of CO_2. Radiative forcing for changes in CO_2 from an initial mixing ratio C_o can be estimated from $\Delta Q = 6.3 \ln (C/C_o)$ W m^{-2} for $CO_2 <$ 1000 ppm. From Houghton et al., [1990].

Gas	Relative forcing
CO_2	1
CH_4	21
N_2O	206
CFC-11	12,400
CFC-12	15,800

Table 10.1.3: Radiative forcing changes between 1765 and early 1990's based on *Ramaswamy et al.* [2001].

		Midpoint (W m^{-1})	Range (W m^{-1})
From Table 10.1.1		2.43	±15%
H$_2$O^a		0.02	
Ozone	troposphere	0.35	(0.2 to 0.5)
	stratosphere	-0.15	(-0.05 to -0.25)
Aerosols	biomass burning	-0.2	(-0.1 to -0.6)
	sulfate	-0.4	(-0.2 to -0.8)
	soot (black carbon)	0.2	(0.1 to 0.4)
	organic carbon	-0.1	(0.03 to 0.3)
	mineral dust	-	(-0.6 to 0.4)
	indirect effect on cloud albedo	-1.0	(0 to -2.0)
Change in solar forcing since 1850		0.3	(0.1 to 0.5)
total		1.5	

^{a}: The increase in radiative forcing for water vapor is only that portion due to the effect of increased methane on water vapor in the stratosphere ([Shine et al., 1995]).

FIGURES

Figure 10.1.1: Schematic diagram of the global carbon cycle. Shown are the reservoir sizes in Pg C and the fluxes in Pg C yr^{-1} (1 Pg = 10^{15} g). The black numbers denote the pre-industrial fluxes and reservoir sizes, whereas the red numbers denote the anthropogenic fluxes and changes in reservoir sizes. Taken from *Sarmiento and Gruber* [2002].

Figure 10.1.2: Variations in the atmospheric CO_2 concentration over time based on ice core reconstructions and direct observations since 1958. (a) CO_2 variations during the last 50 years as directly measured in the atmosphere at Mauna Loa, Hawaii, and the South Pole. (b) CO_2 variations during the last 1000 years as reconstructed from Antarctic ice-cores. (c) CO_2 variations during the holocene based on [*Indermühle et al.*, 1999]. (d) CO_2 variations over the last 400 kyr (1 kyr = 1000 years). This comparison illustrates that the onset of the industrial revolution led to a dramatic increase of the atmospheric CO_2 concentration after a period of relatively stable atmospheric CO_2 concentrations during the last 10,000 years. The present atmospheric CO_2 concentrations are unparalleled in the last 400,000 years. More than 10,000 years ago, atmospheric CO_2 shows relatively regular variations associated with glacial inter-glacial cycles. During the last four glacial maxima, atmospheric CO_2 concentrations are at their lowest concentration around 180 ppm, whereas during the interglacial periods, atmospheric CO_2 concentrations are near 280 ppm. The Mauna Loa and South Pole data are from *Keeling and Whorf* [1998], the Law Dome, Antarctica data from *Etheridge et al.* [1996], the Taylor Dome, Antarctica, data from [*Indermühle et al.*, 1999], and the Vostok, Antarctica, data from [*Petit et al.*, 1999].

Figure 10.1.3: Flow of energy through the atmosphere. Numbers are in watts per square meter of Earth's surface, and some may be uncertain by as much as 20%. The greenhouse effect is associated with the absorption and reradiation of energy by atmospheric greenhouse gases and particles, resulting in a downward flux of infrared radiation from the atmosphere to the surface (back radiation) and therefore in a higher surface temperature. Also shown are the coupling points between biogeochemical cycles and the physical climate system. Adapted from [*Kiehl and Trenberth*, 1997].

Figure 10.1.4: Outgoing clear-sky radiation calculated by K.P. Shine for a region where the surface temperature is 294 K [*Houghton et al.*, 1990]. The dashed lines show the hypothetical energy flux, which would be observed if none of the outgoing radiation were intercepted in the atmosphere.

Figure 10.1.5: Observed warming from 1850 to 1990. Shown are the anomalies relative to the period 1961-1990. The global mean remained essentially constant from 1856 to the 1910s. A first warming of 0.3°C occured through the 1940s, followed by a slight cooling. From the early 1970s to present, the warming exceeded 0.5°C. Data from *Jones and Moberg* [2003].

10.2   The anthropogenic perturbation

Over the Anthropocene, i.e. from about 1800 to 1994, mankind has released about 340 to 420 Pg carbon to the atmosphere in the form of CO_2 (1 Pg C = 10^{15} g C) (see Table 10.2.1) [*Sabine et al.*, 2004]. Most of this carbon stems from the combustion of fossil fuels (about 240 Pg C), but a significant, albeit very uncertain fraction is associated with emissions arising from changes in land use, such as deforestation. About 165 Pg C of these emissions have stayed in the atmosphere leading to an increase in atmospheric CO_2 from a pre-industrial level of about 280 ppm to about 360 ppm in 1994 (Figure 10.1.2). The remainder has been redistributed within the global carbon cycle (Figure 10.1.1). Anthropogenic CO_2 emissions are expected to continue to rise well into the 21st century, despite the initiation of efforts on the international level to curb the emissions. Given the importance of CO_2 as a greenhouse gas, the scientific community needs to be able to predict how much CO_2 the ocean and land biosphere will be taking up from the atmosphere and therefore help to mitigate the anthropogenic CO_2 burden in the atmosphere and the associated increase in radiative forcing.

Before any prediction can be attempted, it is necessary to correctly quantify the redistribution of the anthropogenic carbon that has been emitted since the beginning of the industrial revolution. The budgets for both the entire Anthropocene as well as that for the last two decades have been assessed in detail [*Prentice et al.*, 2001, *LeQuéré et al.*, 2003, *Sabine et al.*, 2004]. According to the budgets recently established by *Sabine et al.* [2004] and shown in Table 10.2.1, the ocean represents the largest sink of anthropogenic CO_2 over the anthropocene, having taken up about 118 $\pm$ 19 Pg C. It is only rivaled by the storage in the atmospheric reservoir. Over the same period, the terrestrial biosphere acted as a net source of 39 $\pm$ 28 Pg C, the sum of an ill constrained source coming from land-use change (about 100 to 180 Pg C), indiciating a sink of somewhere between 61 to 141 Pg C. Over the last two decades, i.e. from 1980 to 1999, the ocean also has acted as a strong sink for anthropogenic CO_2, taking up, on average, about 1.9 Pg C yr^{-1}, i.e. about 27% of the total anthropogenic emissions of about 7.1 Pg C yr^{-1} (Table 10.2.1).

How were these oceanic uptake estimates obtained and what controls the rate of uptake? How might the oceanic sink for anthropogenic CO_2 change in the future when climate is predicted to be significantly altered? These questions are of fundamental importance as the current radiative forcing associated with increased atmospheric CO_2 would be about 30% higher in the absence of the oceanic sink. Furthermore, positive feedbacks could develop if the ocean became less efficient in taking up anthropogenic CO_2 in a warming world, leading to an acceleration of the growth of CO_2 in the atmosphere and therefore an acceleration of global warming.

We address these questions in the next sections. We start with an assessment of the

oceanic uptake capacity after equilibrium has been reached, but will soon realize that there are strong kinetic constraints that prevent the equilibrium from being reached within the next millennium. We then evaluate briefly different methods that have been employed to estimate the present uptake of anthropogenic CO$_2$ by the oceans. We conclude by discussing models that have been used to calculate the past uptake as well as to make predictions for the future.

CAPACITY CONSTRAINTS

If CO$_2$ dissolved in seawater without undergoing chemical reactions like most other gases, about 70% of the CO$_2$ emitted by anthropogenic activities would remain in the atmosphere. However, the uptake capacity of the oceans is greatly enhanced by the reaction of CO$_2$ with the carbonate ion to form bicarbonate, making the carbonate ion concentration the primary determinant for the oceanic uptake capacity for anthropogenic CO$_2$. As seen above (see 8.3.8), the buffering reaction can be written as:

$$CO_2^* + H_2O + CO_3^{2-} \Longleftrightarrow 2HCO_3^- \tag{10.2.1}$$

The carbonate ion content of the ocean is not a conservative property, however. It is tied to the inorganic carbon system in seawater, ($[CO_3^{2-}] \approx$ Alk- DIC) as well as to the large reservoir of CaCO$_3$ in the sediments. The latter can absorb CO$_2$ directly by

$$CO_2^* + CaCO_3 + H_2O \Longleftrightarrow Ca^{2+} + 2\,HCO_3^-. \tag{10.2.2}$$
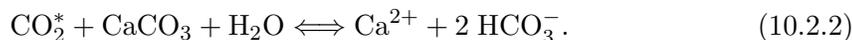
As we will discuss in more detail below, these two buffering reactions operate on two very different time scales, however. The characteristic time for reaching equilibrium between the atmosphere and the ocean alone is of the order of several hundred years. The characteristic time required for reaching equilibrium between the atmosphere, the ocean and the sea floor sediments is of the order of several thousand years [*Broecker and Takahashi*, 1977, *Archer et al.*, 1997]. We therefore separately consider the cases where the anthropogenic CO$_2$ entering the ocean is neutralized by the carbonate concentration in seawater alone, and where it is neutralized by the carbonate ion in seawater plus the calcium carbonate in the sediments. We will also briefly discuss the very long-term sinks of anthropogenic CO$_2$ stemming from the weathering reaction with CaCO$_3$ and silicious rocks on land.

Buffering by dissolved carbonate

Let us first consider the situation for an ocean with uniform chemistry and no sediments. On the basis of what we have learned about the CO$_2$ chemistry so far, we can predict how much of an incremental addition of CO$_2$ to the atmosphere would dissolve in the ocean under the assumption that equilibrium is maintained, i.e. that air-sea gas exchange and ocean mixing are fast enough to keep the oceanic perturbation in equilibrium with that in the atmosphere.

Let the atmospheric increment be:

$$\delta N^{\mathrm{atm}} = \delta x CO_2^{\mathrm{atm}} \, N_{\mathrm{tot}}^{\mathrm{atm}} \tag{10.2.3}$$

where $x CO_2^{\mathrm{atm}}$ is the atmospheric mixing ratio, and where $N_{\mathrm{tot}}^{\mathrm{atm}}$ is the number of moles of air in the atmosphere ($N_{\mathrm{tot}}^{\mathrm{atm}} = 1.8 \times 10^{20}$ moles). The increment in the ocean is given by:

$$\delta N^{\mathrm{oc}} = \delta DIC \, m^{\mathrm{oc}} \tag{10.2.4}$$

where m^{oc} is the mass of the ocean volume under consideration.

Since we assumed that the perturbation in the ocean tracks the perturbation in the atmosphere, the incremental change in oceanic pCO_2 has to be equal to the incremental change in atmospheric pCO_2, which itself is equal to the change in the mixing ratio times the total atmospheric pressure, P^{atm} (see panel 3.2.1, and where we neglect the contribution of water vapor pressure).

$$\delta pCO_2^{\mathrm{oc}} = \delta pCO_2^{\mathrm{atm}} = \delta x CO_2^{\mathrm{atm}} \, P^{\mathrm{atm}} \tag{10.2.5}$$

The change in the atmospheric inventory relative to the change in the oceanic inventory is given by

$$\frac{\delta N^{\mathrm{atm}}}{\delta N^{\mathrm{oc}}} = \frac{\delta x CO_2^{\mathrm{atm}} \, N_{\mathrm{tot}}^{\mathrm{atm}}}{\delta DIC \, m^{\mathrm{oc}}} = \frac{\delta pCO_2^{\mathrm{oc}} \, N_{\mathrm{tot}}^{\mathrm{atm}}}{P^{\mathrm{atm}} \delta DIC \, m^{\mathrm{oc}}} \tag{10.2.6}$$

$$= \gamma_{DIC} \frac{1}{\alpha} \frac{N_{\mathrm{tot}}^{\mathrm{atm}}}{P^{\mathrm{atm}} m^{\mathrm{oc}}} \tag{10.2.7}$$

where γ_{DIC} is the buffer factor defined by (8.3.14), and α is the ratio of mean DIC and mean surface ocean pCO_2. We thereby made the assumption that the increments δ are small enough so that they can be approximated by ∂. However, we are more interested in calculating the fraction f of the emissions taken up by the oceans, thus

$$f = \frac{\delta N^{\mathrm{oc}}}{\delta N^{\mathrm{oc}} + \delta N^{\mathrm{atm}}} = \left(\frac{\delta N^{\mathrm{atm}}}{\delta N^{\mathrm{oc}}} + 1 \right)^{-1} = \left(\frac{\gamma_{DIC}}{\alpha} \frac{N_{\mathrm{tot}}^{\mathrm{atm}}}{m^{\mathrm{oc}}} + 1 \right)^{-1} \tag{10.2.8}$$

If we assume that only the top 75 m of the ocean ($m^{\mathrm{oc}} = 2.7 \times 10^{19}$ kg) is in equilibrium with the atmosphere, and insert global surface average values for DIC, pCO_2 and the buffer factor, we find a fraction f of about 0.08. If the whole ocean were available ($m^{\mathrm{oc}} = 1.35 \times 10^{21}$ kg) then f would be 0.81, thus about 81% of an increment added to the atmosphere would be absorbed by the ocean. Table 10.2.1 informs us that the present fraction f is of the order of 30%, hence the equivalent of only about 8% of the total volume, i.e. about the top 350 m of the ocean, are currently equilibrated with the atmospheric CO_2 perturbation.

This estimate of f is for a small addition only. In order to estimate the equilibrium air-sea distribution after a pulse has been added to the atmosphere, the above equation needs to be integrated over time. In doing so, it is important to note that the buffer factor γ_{DIC} increases, i.e. the buffer capacity decreases, when DIC increases due to the addition of CO_2 from the atmosphere (see equation 8.3.16). This effect can be understood by considering that the uptake of CO_2 from the atmosphere depletes the CO_3^{2-} ion content of the ocean, therefore decreasing its capacity for further uptake.

As a consequence of the reduction in the uptake capacity, the fraction f decreases as the perturbation grows. Table 10.2.2 illustrates this behavior for a simplified ocean atmosphere carbon system. In the pre-industrial steady-state, only about 1.5% of the total carbon is found in the atmosphere, and 98.5% is in the ocean. If we add a perturbation of 1800 Pg C to this system and let it equilibrate, the fraction of the perturbation that goes into the ocean is about 79.2% whereas the fraction now residing in the atmosphere is more than 10 times larger (20.8%) than the pre-industrial steady-state. *Sarmiento et al.* [1995] demonstrated that the effect of a decreasing buffer capacity on the future oceanic uptake of anthropogenic CO_2 is large and neglect of this effect would lead to a substantial over-estimation of the oceanic uptake of anthropogenic CO_2 by the ocean (see Figure 10.2.1). Figure 10.2.1a actually shows the ratio $\partial DIC/\partial[CO_2^*]$, which is related to the buffer factor, γ_{DIC}, by:

$$\frac{\partial DIC}{\partial[CO_2^*]} = \frac{\partial DIC}{\partial(K_0 \, p\text{CO}_2^{oc})} = \frac{DIC}{K_0 \, p\text{CO}_2^{oc}} \frac{1}{\gamma} = \frac{\alpha}{K_0} \frac{1}{\gamma}, \qquad (10.2.9)$$

where K_o is the solubility of CO_2, and where we use α as a shorthand for the ratio of ocean mean DIC and pCO$_2$ (see equation (10.2.7) above). The partial derivative, $\partial DIC/\partial[CO_2^*]$, is therefore proportional to the inverse of γ_{DIC}, and the simulated decrease in $\partial DIC/\partial[CO_2^*]$ corresponds to an increase in the buffer factor γ_{DIC}.

Buffering by sediment $CaCO_3$

In all of the above calculations we have neglected so far the potential reaction of anthropogenic CO_2 with the $CaCO_3$ in the sediments at the sea floor (reaction 10.2.2). If all CO_2 is absorbed by this reaction, the net result of the invasion of anthropogenic CO_2 into the ocean would be to increase the total DIC and Alk content of the ocean by two moles for each mol of CO_2 taken up from the atmosphere. In this case, the CO_3^{2-} ion content, which we can approximate by Alk- DIC, would remain constant. Therefore, this buffering reaction compensates nearly entirely for the decrease in the buffer capacity stemming from the carb ion consumption (see panel 8.3.1), leading to almost no change in γ_{DIC} as anthropogenic CO_2 builds up in the ocean. This can be understood by considering the approximation for the buffer factor given in (8.3.16) and rearranging it to express it in

terms of the Alk/DIC ratio, i.e.

$$\gamma_{DIC} \quad \approx \quad \frac{3[Alk][DIC] - 2[DIC]^2}{(2[DIC] - [Alk])\,([Alk] - [DIC])} \qquad (10.2.10)$$

$$= \quad \frac{2[DIC] - 3[Alk]}{\left(\frac{[Alk]}{[DIC]} - 2\right)\left(\frac{[Alk]}{[DIC]} - 1\right)} \qquad (10.2.11)$$

As DIC and Alk change equally as a result of the buffering reaction of anthropogenic CO_2 with $CaCO_3$ (10.2.2), neither the numerator nor the denominator of (10.2.11) change much, thus explaining why γ_{DIC} changes little in this case. As a consequence of this buffering with $CaCO_3$, the fraction of CO_2 ultimately ending up in the ocean is significantly larger if the dissolution of calcium carbonate at the sea floor is considered as well (see (10.3.6)). *Archer et al.* [1997] find that the buffering by the calcium carbonates in the oceanic sediments increases this fraction by about 10 to 15% depending on the size of the anthropogenic perturbation (see Figure 10.2.2).

Buffering by weathering

In addition to the neutralization of the anthropogenic CO_2 by $CaCO_3$ on the sea floor, an additional fraction will be neutralized by weathering reactions of atmospheric CO_2 with mineral carbonates on land. After complete neutralization with the ocean and $CaCO_3$ rocks, about 8% of a CO_2 release will remain in the atmosphere [*Archer et al.*, 1997, *Archer et al.*, 1998] (see also Figure 10.2.2). The remaining CO_2 will react very slowly with igneous rocks on land by the reaction

$$2CO_2 + CaSiO_3 + 3H_2O \Longleftrightarrow 2HCO_3^- + Ca^{2+} + Si(OH)_4 \qquad (10.2.12)$$
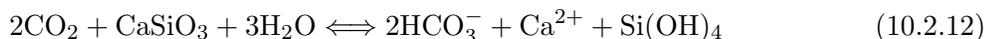
Since the reservoir of these silicious rocks is much larger than the amount of fossil fuel CO_2, all emitted CO_2 will eventually disappear from the atmosphere. This latter reaction is of fundamental importance in controlling atmospheric CO_2 on geological time-scales [*Walker et al.*, 1981] since it balances the CO_2 that is degassed from volcanoes.

KINETIC CONSTRAINTS

The above considerations provide us with a simple tool to estimate the amount of anthropogenic CO_2 that the ocean will have taken up for a given CO_2 emission after equilibrium has been reached between the atmosphere and ocean. Our finding that only a small fraction of the ocean has equilibrated with the anthropogenic CO_2 emissions that ocurred over the last 200 years indicates, however, that the time-scale required for equilibration must be longer than this period. Therefore, one or several of the processes that control the oceanic uptake of anthropogenic CO_2 must be strongly rate limiting, providing strong kinetic constraints on the oceanic uptake of anthropogenic CO_2.

Atmospheric Pulse Response

The time scales associated with the removal of anthropogenic CO$_2$ from the atmosphere can be assessed by investigating how quickly a pulse of CO$_2$ emitted into the atmosphere is disappearing from it [*Maier-Reimer and Hasselmann*, 1987, *Sarmiento et al.*, 1992]. Figure 10.2.3 shows the result of a simulation that followed this approach using a three-dimensional ocean general circulation model, to which a full ocean carbon cycle model was coupled. This model also includes a representation of ocean sediments, as well as a simple parameterization of CO$_2$ consuming weathering processes on land [*Archer et al.*, 1997].

This simulation reveal that it takes about 400 years for the first half of the initial pulse to disappear, and that it takes another 1000 years for an additional 25% of the initial pulse to be removed from the atmosphere. This simulation also shows that after the first 1000 years, the oceanic uptake that is driven by the solution of atmospheric CO$_2$ into seawater and reaction with CO$_3^{2-}$ becomes negligible, and that neutralization of the CO$_2$ by reaction with CaCO$_3$ on the seafloor becomes dominant. At the same time, reaction of atmospheric CO$_2$ with CaCO$_3$ on land begins to be a relevant removal process. After 30,000 years, the contribution of these two processes becomes small, and most of the removal of the initial pulse is governed by the consumption of atmospheric CO$_2$ by weathering of silicate rocks on land.

In summary, chemical buffering by the inorganic carbon chemistry of the sea water sequesters about 70 to 85% of an atmospheric pulse on time scales of several hundred years (see Figure 10.2.3b) [*Archer et al.*, 1997]. Neutralization of CO$_2$ with the calcium carbonate on the sea floor accounts for an additional 9-15% decrease in the atmospheric CO$_2$ pulse on a time scale of about 6000 years. Reaction with CaCO$_3$ on land contributes 3-8%, with a time scale of about 8000 years. After several tens of thousands of years, about 8% of the initial pulse remains in the atmosphere, with the exact numbers depending on the size of the pulse as shown in Figure 10.2.2. On time-scales of several hundred thousands of years, this remaining CO$_2$ will react with igneous rocks on land, so that the entire initial pulse will disappear from the atmosphere on time-scales approaching a million years. What determines the dynamics of these removal processes, particularly those associated with the buffering by the ocean?

Ocean Uptake and buffering with dissolved carbonate

Let us first consider ocean uptake only, i.e. the removal of an atmospheric CO$_2$ perturbation solely driven by the dissolution of CO$_2$ into seawater and subsequent reactions with the CO$_3^{2-}$ ions. There are two possible rate limiting steps that determine the kinetics of the ocean uptake: air-sea gas exchange and transport of CO$_2$ from the surface layers into the interior of the ocean. We have seen in chapter 8 that the characteristic time for a 40 m deep surface layer to reach equilibrium with the atmosphere by air-sea gas exchange is

about 6 months. This is much smaller than the time-scale of the anthropogenic perturbation, which has an e-folding time of several decades, the exact value depending on the time period considered. One can therefore expect that air-sea exchange is generally not the rate limiting step for the oceanic uptake of anthropogenic CO_2 from the atmosphere. This is confirmed by model simulations of oceanic uptake, which demonstrate a modest response of only approximately 10% to a doubling or halving of the gas exchange coefficient.

It therefore must be the downward transport of the anthropogenic CO_2 burden from the surface into the interior of the ocean that is the rate limiting step for the CO_2 uptake by the oceans. In chapter 2, we were able to establish with the help of several tracers that the time-scale for the ventilation of the thermocline is between a couple of years and decades, while the ventilation time-scale for the deep ocean is several hundred years. Given this long time scale for deep water ventilation, it becomes obvious that the time required for an atmospheric CO_2 pulse to reach equilibrium in an ocean-atmosphere system must be of order of a thousand years or more.

We can investigate the transport of anthropogenic CO_2 out of the surface layer into the interior of the ocean by inspecting how quickly a pulse of anthropogenic CO_2 (or any other passive and conservative tracer) that is injected into the mixed layer decays *Joos et al.* [1996]. The mixed layer pulse, in comparison to the atmospheric pulse not only permits us to focus at the oceanic transport out of the surface mixed layer, but it provides a very accurate description of the oceanic uptake of anthropogenic CO_2 by CO_3^{2-} buffering, since it deals explicitly with the problem of a changing buffer factor. In contrast, the atmospheric CO_2 pulse depends on the magnitude of the perturbation, and is therefore more difficult to generalize (see *Joos et al.* [1996] for a detailed discussion). Figure 10.2.4 shows such mixed layer pulse response functions for different ocean carbon models for the first 100 years. All models show a relatively rapid removal of the pulse in the first few years, followed by a strongly deccelerated decrease with time.

em Joos et al. [1996] demonstrated that these pulse-response functions can be very closely approximated by fitting to them a series of exponential functions. In the case of the 3-D circulation model, their fits show that about 64% of the intial pulse disappears with an e-folding time of less than a year. An additional 23% decays with an e-folding time-scale of 2 years, 6% with an e-folding time scale of 15 years, 3% with an e-folding time-scale of 65 years, and 2% with an e-folding time-scale of 348 years. The response function assymptotes to a value of about 2% of the initial pulse, since this constitutes the ocean mean concentration after the whole ocean has equilibrated with the initial pulse. The various time-scales can be interpreted as reflecting how quickly waters are transported into different depth realms of the ocean. Because upper ocean ventilation is relatively vigorous, the anthropogenic CO_2 is, at first, quickly removed from the upper ocean mixed layer. However, ocean ventilation tends to decrease with increasing depth, so it takes

longer for anthropogenic CO$_2$ to be transported into these deeper realms.

These pulse response functions provide not only a measure of time-scales, but also quantitatively describe the entire dynamics of the transport of anthropogenic CO$_2$ and any other passive and conservative tracer from the surface mixed layer into the ocean's interior. This is because oceanic transport and mixing is linear, and up to now, we can assume that ocean circulation has not changed dramatically over the last 200 years. We can therefore use these pulse response functions (also referred to as a Green's function) as a basis for a very simple model that permits us to accurately estimate the uptake of any passive and conservative tracer by the ocean without resorting to simulations with much more complex two and three-dimensional ocean biogeochemical models (see *Joos et al.* [1996] for a complete description of the method).

Let us describe the pulse response function as $r_s(t)$. The surface concentration of anthropogenic *DIC*, $C_{\text{ant}}(t)$ (mmol m^{-3}), where t is any time after the beginning of the anthropocene, t_o, reflects the accumulated air-sea flux of anthropogenic CO$_2$ from the atmosphere, Φ_{as} (mmol m^{-2} yr^{-1}), weighted by how much of this uptake has been transported away into the interior over time. This weighting is is described by the pulse response function, r_s. This gives:

$$C_{\text{ant}}(t) = \frac{1}{h} \int_{t_o}^{t} \Phi_{ant}(t') \, r_s(t - t')dt', \qquad (10.2.13)$$

where h is the depth of the surface mixed layer. As is the case for any gas (see chapter 3, equation 3.3.6), the air-sea flux of anthropogenic CO$_2$ is directly proportional to the air-sea partial pressure difference of anthropogenic CO$_2$ and a gas exchange coefficient, k_g, (mmol m^{-2} yr^{-1} μatm $^{-1}$),

$$\Phi_{ant}(t) = k_g(\delta pCO_2^{atm}(t) - \delta pCO_2^{oc}(t)), \qquad (10.2.14)$$

where δpCO_2 denotes the anthropogenic perturbation to atmospheric and oceanic pCO_2 in μatm. The anthropogenic perturbation of oceanic pCO_2 is linked to $C_{\text{ant}}(t)$, by the buffer factor, γ_{DIC}:

$$\delta pCO_2^{oc}(t) = \frac{\gamma_{DIC}}{\alpha} C_{\text{ant}}(t). \qquad (10.2.15)$$

where α is the DIC/pCO$_2$ ratio (see eq. (10.2.9)).

By combining (10.2.13) with (10.2.14) and (10.2.15), and using a pulse-response function, $r_s(t)$ determined from one of the models, the oceanic uptake of anthropogenic CO$_2$ for any given time trajectory of the atmospheric CO$_2$ perturbation can be computed with great accuracy. The only limiting assumption is that the oceanic circulation has to remain steady. *Joos et al.* [1996] provides accurate formulations for the buffer factor γ over a wide range of atmospheric CO$_2$ perturbations and also functional forms for the pulse response functions, $r_s(t)$ for a range of ocean biogeochemical models.

Buffering by sediment $CaCO_3$

The dynamics of the buffering of anthropogenic CO_2 by seafloor $CaCO_3$ is very slow and takes thousands of years (Figure 10.2.2). This is much slower than the time scale of hundreds of years involved in taking up anthropogenic CO_2 from the atmosphere and transporting it from the surface into the interior of the ocean. An important reason for the slow dynamics of sea-floor $CaCO_3$ buffering is that most of the $CaCO_3$ in the sediments is found at mid-depths of the water column (see Figure 9.1.2). Anthropogenic CO_2 must first reach these depths before it can start to dissolve the $CaCO_3$ in the sediments. In addition, the rate of dissolution induced by anthropogenic CO_2 seems to be relatively small [*Archer et al.*, 1998], a result of both slow diffusion of the bottom water signal into the sediments as well as the slow kinetics of dissolution (see chapter 9). This increases the time-scale for the sea-floor neutralization of anthropogenic CO_2 further.

The exact time scales for the neutralization of the anthropogenic CO_2 with calcium carbonate are associated with quite large uncertainties. Fortunately, these time scales are sufficiently long so that the contribution of calcium carbonate buffering can be neglected when considering anthropogenic CO_2 uptake over the last two centuries and well into the next century. This is supported by the results of *Archer et al.* [1998] who found that the difference between the oceanic uptake of a model with and without calcium carbonate was much less than 1%. In contrast to the anthropogenic CO_2 perturbation, these buffering reactions are of great importance when considering millennial time-scale changes in the global carbon cycle, as they give raise to substantial feedbacks as discussed in association with $CaCO_3$ compensation in chapter 9.

ANTHROPOGENIC CO_2 UPTAKE

So far, we have found that it will take several hundred, if not thousands of years until anthropogenic CO_2 is fully equilibrated between the atmosphere, the ocean and the sediments on the sea-floor. For human societies, however, it is of much more concern to know the current redistribution of anthropogenic carbon in the global carbon cycle and how this may change over the next few decades. This is a topic of intense research and a number of breakthroughs in the past decade have permitted the scientific community to put relatively good constraints on the oceanic uptake of anthropogenic CO_2 (see discussion in *Prentice et al.* [2001], *Sarmiento and Gruber* [2002], and *Sabine et al.* [2004]).

In the global budget of anthropogenic CO_2 (Table 10.2.1), there are only two terms that have been measured directly. One is the emission of CO_2 by burning of fossil fuel and cement manufacture. The other is the increase in the atmospheric CO_2 concentration, which has been directly measured since 1958 at Mauna Loa, Hawaii and the South Pole [*Keeling et al.*, 1989]. These measurements have been extended back in time by measuring CO_2 in ice cores and firn [*Neftel et al.*, 1985, *Etheridge et al.*, 1996]. The remaining two

budgetary terms (ocean uptake, net exchange with the terrestrial biosphere) have to be estimated by less direct means. We focus here on the oceanic uptake only. A good understanding of the magnitude and variability of the oceanic sink for anthropogenic CO$_2$ provides also important constraints for the net exchange of anthropogenic CO$_2$ with the terrestrial biosphere, which is very difficult to measure directly.

This section gives a brief overview of the different approaches proposed so far for estimating the current CO$_2$ uptake by the oceans. We fill first investigate what it takes to estimate this uptake by direct means, i.e. measuring the flux across the air-sea interface, or by measuring the long-term increase of *DIC*. Given our currently limited ability to follow these direct approaches, inventory methods that attempt to separate the small anthropogenic CO$_2$ signal from the large natural background have played a very important role in our deciphering of the anthropogenic CO$_2$ uptake by the ocean. After discussion these inventory methods, we turn to the atmospheric oxygen method, which has given us a lot of insight into the oceanic uptake over the last 10 to 15 years. The reader interested in more detail is referred to the IPCC summaries [*Schimel et al.*, 1994, *Schimel et al.*, 1996, *Prentice et al.*, 2001] and to the overviews by *Siegenthaler and Sarmiento* [1993] and by *Wallace* [1995].

Direct Estimation

The most direct means to estimate the oceanic uptake of anthropogenic CO$_2$ is to measure the increase of *DIC* in the oceans over time, as done for the atmosphere. How large do we expect the signal to be? We can estimate the rate of increase of *DIC* in the surface ocean using the buffer factor, γ_{DIC}, and making the assumption that the inorganic carbon system in the surface ocean stays in equilibrium with the atmospheric perturbation:

$$\frac{dDIC}{dt} = \frac{dDIC}{dpCO_2}\frac{d\,pCO_2^{\mathrm{oc}}}{dt} = \frac{1}{\gamma_{DIC}}\frac{DIC}{pCO_2^{\mathrm{oc}}}\frac{d\,pCO_2^{\mathrm{atm}}}{dt} = \frac{\alpha}{\gamma_{DIC}}\frac{d\,pCO_2^{\mathrm{atm}}}{dt} \qquad (10.2.16)$$

where α is the DIC/pCO_2^{oc} ratio.

The average rate of change of atmospheric pCO_2 from 1975 to 1995 was about 1.5 μatm yr^{-1} [*Keeling and Whorf*, 1998]. Inserting ocean mean surface *DIC* (2026 μmol kg^{-1}, see Table 8.2.4), a buffer factor of 10, and a pCO_2 of 350 μatm results in a predicted *DIC* increase of about 0.9 μmol kg^{-1} yr^{-1}, i.e. a change of 9 μmol kg^{-1} over a ten year period. The change is larger (1.1 μmol kg^{-1} yr^{-1}) in the low latitudes and smaller in the high latitudes (0.8 μmol kg^{-1} yr^{-1}) because of the spatial variation in the buffer factor. Note that this is counter-intuitive, since one would expect the high-latitudes, because of their colder temperature, taking up more anthropogenic CO$_2$ for a given atmospheric pCO_2 perturbation than the warmer low-latitudes. However, in this case, the chemical capacity is the determining factor, and not the solubility. We will discuss this in detail in the following section.

The present measurement precision of DIC is about 1 μmol kg^{-1}, good enough for potentially detecting such a signal over a few years. However, temporal and spatial variability of DIC is large, making such a detection difficult. We have seen, for example, that seasonal variations exceeding 30 μmol kg^{-1} occur at many places. Nevertheless, existing long-term observations of DIC in the surface ocean are in relatively good agreement with the expected increase computed from (10.2.16) (see Figure 10.2.5).

Some of the limitations imposed by spatio-temporal variability can be overcome by fitting the DIC content in seawater at one time with a multiple linear regression model against a number of tracers unaffected by the anthropogenic transient, and then determining the difference between the predicted and the measured DIC at a later time [*Wallace*, 1995]. This approach requires, however, two data sets of high quality separated sufficiently in time. The GEOSECS survey in the 1970s and the WOCE/JGOFS effort of the 1990s provide in principle two such data sets [*Wallace*, 2001], but the high inaccuracy and imprecision of the GEOSECS data (about 10 μmol kg^{-1}) make this approach so far only partially successful [*Sabine et al.*, 1999, *Peng et al.*, 1998, *McNeil et al.*, 2001, *Peng et al.*, 2003]. An ongoing program to resample many of the cruise tracks that were sampled during the WOCE/JGOFS era will vastly expand the opportunities in the future to detect the increase of anthropgenic CO_2 in the ocean over time.

An alternative approach to estimate the uptake of anthropogenic CO_2 by the ocean is to look at the exchange of CO_2 across the air-sea interface (see Figure 8.1.1). Although the flux at any given location represents the superposition of a pre-industrial (i.e. natural) flux and the anthropogenic perturbation flux, the globally integrated air-sea flux should be equal to the total oceanic uptake of anthropogenic CO_2 plus a global net air-sea flux of natural CO_2 associated with the balance between riverine input of organic and inorganic carbon and sea-floor burial [*Sarmiento and Sundquist*, 1992] (see Figure 10.1.1).

We can estimate the level of the observational challenge associated with this approach by computing the partial pressure of CO_2 difference across the air-sea interface associated with the anthropogenic CO_2 uptake. Current estimates of the globally integrated oceanic uptake of anthropogenic CO_2 uptake are about 2 Pg C yr^{-1} or $1.6 \cdot 10^{14}$ mol C yr^{-1} [*Prentice et al.*, 2001]. Dividing this estimate by the ocean area of about $360 \cdot 10^{12}$ m^{-2} gives a mean anthropogenic CO_2 flux, Φ^{ant}, of about 0.5 mol m^{-2} yr^{-1}. Using the air-sea flux equation (3.6.6) and solving it for the partial pressure difference gives:

$$\Delta p\text{CO}_2^{\text{ant}} = \frac{\Phi^{\text{ant}}}{k_g} = \frac{0.5 \text{ mol m}^{-2}\text{yr}^{-1}}{0.065 \text{ mol m}^{-2}\text{yr}^{-1}\mu\text{atm}^{-1}} \approx 8 \ \mu\text{atm}. \qquad (10.2.17)$$

where we used the globally averaged k_g of 0.065 mol m^{-2}yr$^{-1}\mu$atm^{-1} given in Table 3.3.3.

The precision and accuracy of current measurements of oceanic $p\text{CO}_2$ is a few μatm, so this anthropogenic air-sea $p\text{CO}_2$ difference of about 8 ppm is fundamentally amenable to direct observation. However, we have also seen in chapters 3 and 8 (e.g. Figure

3.1.3, 8.1.1 and 8.3.7) that oceanic pCO_2 has spatial and temporal variations that exceed 100 ppm in many places, therefore making the sampling requirements for adequately taking into account the observed spatiotemporal variability extremely high. At the moment, despite the most recent synthesis of more than 1 million ΔpCO_2 observations by *Takahashi et al.* [2002], many key regions of the surface ocean, such as the Southern Ocean, remain strongly undersampled. A further problem of this approach is the large uncertainty associated with estimates of the gas exchange coefficient k_g (see discussion in chapter 3). A final source of uncertainty is the poorly known natural efflux of CO_2 from the ocean as a result of the riverine input of inorganic and organic carbon. Future improvements in the observational coverage as well as our understanding of the factors that control k_g will make this approach, however, substantially more attractive.

Because of the current difficulties of direct detection, the amount of anthropogenic CO_2 taken up by the ocean is estimated often by less direct means. The approach most commonly employed in the past is the use of ocean models designed to take into account not only the thermodynamic capacity of seawater but also air-sea gas exchange and vertical transport. Despite large differences in complexity, most models predict fairly similar uptake rates of about 2.0 ± 0.4 Pg C yr^{-1} [*Prentice et al.*, 2001, *Matsumoto et al.*, 2004]. However, as outlined in table 10.2.3, several additional methods exist to estimate the oceanic uptake of anthropogenic CO_2. We will limit our discussion here to the inventory approach and the atmospheric oxygen method.

Reconstruction of anthropogenic CO_2 inventory

Brewer [1978] and *Chen and Millero* [1979] were the first to point out that the anthropogenic CO_2 can be estimated by correcting the measured DIC in a water sample for the changes that have incurred due to the remineralization of organic matter and the dissolution of carbonates since it last lost contact with the atmosphere, ΔDIC_{bio}, and by subtracting preformed preindustrial DIC, DIC^0_{pi}, i.e.

$$C_{ant} = DIC^{\text{obs}} - \Delta DIC_{\text{bio}} - DIC^0_{\text{pi}}. \tag{10.2.18}$$

where the biological correction is estimated from AOU and the difference between in-situ and preformed Alk, Alk^0:

$$\Delta DIC_{\text{bio}} = -r_{C:O_2} AOU - \tfrac{1}{2} \left(Alk - Alk^0 - r_{N:O_2} AOU \right), \tag{10.2.19}$$

where $r_{C:O_2}$ and $r_{N:O_2}$ are the stoichiometric C:O_2 and N:O_2 ratios during remineralization of organic matter. The first term on the right hand side constitutes the change in DIC due the remineralization of organic matter since the water parcel was last in contact with the atmoshere, and the second term represents the corresponding change in DIC due to the dissolution of $CaCO_3$. The factor $\tfrac{1}{2}$ arises from the fact that the dissolution of $CaCO_3$

changes Alk and DIC in a 2:1 ratio. The AOU term in the carbonate correction term is a result of the influence of the soft-tissue pump on Alk (see chapter 8).

The easiest way of interpreting (10.2.18) is to view it in direct analogy to the computing of preformed properties discussed in chapter 5. The expression $DIC^{\text{obs}} - \Delta DIC_{\text{bio}}$ is directly equivalent to the computation of a preformed concentration, i.e. the biological correction takes a water sample at any given location and moves it back to the surface where it was last in contact with the atmosphere. The anthropogenic CO_2 concentration is then the difference between this preformed DIC concentration and the preformed concentration that existed in pre-industrial times, DIC^0_{pi}.

However, the Brewer and Chen & Millero approach never found general acceptance, since the uncertainties were regarded as too large [*Shiller*, 1981, *Shiller*, 1982, *Broecker et al.*, 1985], particularly because of very large uncertainties associated with the estimation of DIC^0_{pi}. However, *Gruber et al.* [1996] showed that this approach can be significantly improved by taking advantage of the fact that we can estimate water mass ages on the basis of a number of transient tracers (see discussion in chapter 2).

The most relevant change to the original technique by Brewer and Chen & Millero was to separate the DIC^0_{pi} term into a pre-industrial equilibrium term, i.e. the DIC concentration a given water parcel would have had if it had been in equilibrium with pre-industrial atmospheric CO_2 for a given salinity, S, temperature, T, and preformed alkalinity, Alk^0, i.e. $DIC_{\text{eq pi}}$ and a dis-equilibrium term $\Delta DIC_{\text{diseq}}$, i.e.

$$DIC^0_{\text{pi}} = DIC_{\text{eq pi}} + \Delta DIC_{\text{diseq}}. \tag{10.2.20}$$

Inserting (10.2.20 into (10.2.18) gives

$$
\begin{aligned}
C_{\text{ant}} &= DIC^{\text{obs}} - \Delta DIC_{\text{bio}} - DIC_{\text{eq pi}} - \Delta DIC_{\text{diseq}}, &\tag{10.2.21}\\
&= \Delta C^* - \Delta DIC_{\text{diseq}}, &\tag{10.2.22}
\end{aligned}
$$

where we combined the first three terms on the right hand side of (10.2.21) into ΔC^*. The tracer ΔC^* is nearly conservative in the ocean interior and can be calculated on the basis of concurrent observations of DIC, Alk, temperature, salinity, oxygen and nutrients. This tracer is also directly related to the C^* tracer used in chapter 8 for separating the different pump components from the observed variations of DIC. The reader interested in details is referred to *Gruber et al.* [1996] and *Gruber and Sarmiento* [2002].

Therefore, in order to estimate C_{ant}, we are left with the need to estimate the disequilibrium term ΔC_{diseq}. Given an equilibration time-scale of nearly a year for the air-sea exchange of CO_2, this disequilibrium term, which corresponds directly to a $\Delta p CO_2$ at the time a water parcel was last in contact with the atmosphere, can be quite large.

Gruber et al. [1996] made three important assumptions to estimate ΔC_{diseq}: First, they argued that the expected changes of this disequilibrium over time are small, and

therefore assumed it to be constant. Their argument was based on the expectation that the long-term change in this disequilibrium driven by the anthropogenic CO_2 perturbation is on the order of a few μmol kg^{-1} only. As this perturbation of the disequilibrium term is directly equivalent to the anthropogenic perturbation of the air-sea pCO$_2$ difference that we computed in (10.2.17), we can easily confirm their argument. In (10.2.17), we found an anthropogenic change in ΔpCO$_2$ of about 8 μatm, which corresponds to an anthropogenic change of the DIC disequilibrium term of about 4 to 5 μmol kg^{-1}, which is small relative to the observed disequilibria of up to several tens of μmol kg^{-1}. The second assumption is that ocean circulation and mixing occurs predominantly along isopycnal surfaces, consistent with the view adopted in this book. Finally, they assumed that the natural carbon cycle has not changed over the last 250 years in any significant manner, i.e. that it has remained in a dynamic steady-state.

With these assumptions, the estimation of $\Delta DIC_{\text{diseq}}$ is straightforward when examining deep isopycnal surfaces that have regions where it is safe to assume that there is no anthropogenic CO_2 (see Figure 10.2.6a). In such cases C_{ant} in (10.2.22) is zero, and we can estimate the disequilibrium for the water mass, i, that dominates this portion of the isopycnal surface simply by averaging $\Delta DIC_{\text{diseq}}$ in this region:

$$\Delta DIC^i_{\text{diseq}}(\sigma) = \overline{\Delta C^*}\big|_{\sigma=\text{const}} . \tag{10.2.23}$$

This approach fails, however, on isopycnal surfaces that are shallower and well ventilated. Here anthropogenic CO_2 has already affected the entire density surface, and therefore no uncontaminated region can be found. For these density surfaces, *Gruber et al.* [1996] modified their ΔC^* tracer, taking advantage of the availability of age tracers that permit them to estimate the DIC equilibrium concentration at the time a water parcel was last in contact with the atmosphere $(DIC_{\text{eq}}(pCO_2(t_{\text{sample}} - \tau)))$, where τ is the age of the water, and t_{sample} is the time of sampling. Replacing the pre-industrial equilibrium DIC concentration in the definition of ΔC^* with this time-dependent equilibrium DIC gives ΔC^*_t, which is also a measure of the air-sea disequilibrium (see Figure 10.2.6b). Thus, on these shallow isopycnal surfaces, the air-sea disequilibrium of the dominant water mass, i, is estimated from ΔC^*_t:

$$\Delta DIC^i_{\text{diseq}}(\sigma) = \overline{\Delta C^*_t}\big|_{\sigma=\text{const}} . \tag{10.2.24}$$

Once the disequilibria have been determined for all surfaces and n end-members, the amount of anthropogenic CO_2 can finally be calculated from (10.2.22):

$$C_{\text{ant}} = \Delta C^* - \sum_{i=1}^{n} f^i \Delta DIC^i_{\text{diseq}}(\sigma), \tag{10.2.25}$$

where f_i are relative contributions from each end-member.

A number of investigators have applied this technique to various ocean basins [*Gruber*, 1998, *Sabine et al.*, 1999, *Sabine et al.*, 2002, *Lee et al.*, 2003] with *Sabine et al.* [2004] providing a global synthesis. Figure 10.2.6 shows the resulting distribution of C_{ant} along our typical conveyor belt section.

Near-surface concentrations of C_{ant} are highest in subtropical regions and tend to decrease toward the high latitudes. They also tend to be higher in the Atlantic compared to the Pacific. This is surprising since given the higher solubility of CO_2 in colder waters, one might argue, at first thought, that the high latitudes should contain more anthropogenic CO_2. However, integrating (10.2.16) over the anthropocene and assuming that the buffer factor, γ_{DIC}, remained constant, shows that the amount of C_{ant} in the surface ocean expected from equilibrium uptake is inversely proportional to the buffer factor:

$$
\begin{aligned}
C_{ant}(t) &= \int_{t'=pi}^{t'=t} \frac{d[DIC]}{dt} dt' = \frac{\alpha}{\gamma_{DIC}} \int_{t'=pi}^{t'=t} \frac{d\, pCO_2^{atm}}{dt} dt', \\
&= \frac{\alpha}{\gamma_{DIC}} \left(pCO_2^{atm}(t) - pCO_2^{atm}(t=pi) \right).
\end{aligned}
\tag{10.2.26}
$$

As the buffer factor is substantially larger in the high latitudes, and lower in the low latitudes (mainly a consequence of variations in the Alk/DIC ratio, see (10.2.11)), the low latitudes can store substantially more anthropogenic CO_2 than the high latitude for a given atmospheric CO_2 perturbation. The North Atlantic has a particularly low buffer factor, and therefore tends to contain the highest surface concentrations of anthropogenic CO_2. The reconstructed surface concentrations are in quite good agreement with those computed by inserting typical values in (10.2.26) for the early 1990s, when atmospheric pCO_2 was about 360 μatm (see figure 10.1.2). The indication of somewhat lower anthropogenic CO_2 content in the surface waters of the high southern latitudes compared to the expectations indicates that these waters are not able to completely track the atmosphere. This is presumably the result of three factors: the short residence time of these surface waters, substantial dilution of deep and bottom waters by subsurface mixing with old waters, and effective inhibition of air-sea gas exchange by sea ice, especially during winter.

Figure 10.2.7 also reveals substantial meridional differences in vertical penetration of the anthropogenic CO_2 signal. In the tropics, C_{ant} rapidly decreases with depth, whereas the vertical penetration of the signal is much deeper in the subtropical and temperate latitudes. The symmetry breaks down further toward the poles. In the North Atlantic north of 60°N, deep vertical penetration of C_{ant} is found with concentrations above 10 μmol kg^{-1} down to the bottom. In sharp contrast to this only a shallow vertical penetration of anthropogenic CO_2 is found in the Southern Ocean south of 50°S and in the North Pacific north of 50°N. Since anthropogenic CO_2 can be regarded as a conservative tracer, i.e. it is not affected by biological processes, its distribution in the interior is determined by ocean transport only. Can we understand the distribution exhibited by the reconstructed C_{ant}

based on what we have learned about ocean circulation in chapter 2?

The shallow vertical penetration in the tropics and the deeper penetration in the subtropical and temperate zones are primarily reflecting the structure and ventilation of the thermocline. The sharp contrast between the North Atlantic, the Southern Ocean, and the North Pacific requires more discussion. The deep penetration of C_{ant} into the deeper layers of the North Atlantic is clearly a consequence of the formation of Labrador Sea Water and North Atlantic Deep Water and the subsequent transport of these water masses deep into the interior of the North Atlantic. In contrast the absence of any deep water formation in the North Pacific prevents deep penetration of C_{ant} in this region.

But why is the vertical penetration of C_{ant} so low in the Southern Ocean, despite the fact that deep water formation is well known to occur around Antarctica? We have seen already that surface waters in the Southern Ocean are not keeping track with the atmospheric CO_2 increase. This deficit in anthropogenic CO_2 is then aggravated by the fact that the sinking water entrains large amount of old waters containing little or no anthropogenic CO_2, leading to only a small C_{ant} signal in Antarctic Bottom water.

Figure 10.2.8 shows dramatically the resulting differences in column inventories of C_{ant}, i.e. vertically integrated C_{ant}. The highest column inventories are found in the mid-latitudes of the North Atlantic, and at mid-latitudes in the Southern hemisphere. By contrast, the column inventories are smalller in the equatorial regions, and in the high latitude Southern Ocean. Note that this distribution only reflects where anthropogenic CO_2 is currently stored, and not where it actually entered the ocean.

One method to address the question of what the distribution of surface fluxes of anthropogenic CO_2 has to be in order to generate the observed pattern of C_{ant} in the ocean interior is a Green's function inversion method [*Enting*, 2002]. In such an inversion, prescribed fluxes of a dye are released from a number of pre-determined regions in an Ocean General Circulation Model (OGCM) and the model is then integrated forward in time. In the case of anthropogenic CO_2, the fluxes need to be scaled in proportion to the expected increase in uptake over time, i.e. with the magnitude of the atmospheric perturbation, and the model is then integrated forward in time only for the duration of the Anthropocene, i.e. about 250 years [*Gloor et al.*, 2003]. The modeled dye concentrations are then sampled at the locations of the observations, providing a link between concentrations at these locations and fluxes in the various regions. The inversion then attempts to scale the magnitude of the fluxes in the various regions in order to obtain an optimal fit between the estimated resulting concentrations and the actually observed ones.

The results of the first attempts of such an inversion of the reconstructed anthropogenic CO_2 distribution are shown in Figure 10.2.9 [*Gloor et al.*, 2003]. This inversion suggests, for example, that the high storage of C_{ant} in the mid-latitudes of the Southern hemisphere is primarily driven by high uptake of anthropogenic CO_2 at more southerly

latitudes in the Subantarctic Zone and subsequent transport of this C_{ant} into the ocean interior following the paths of Subantarctic Mode Water and Antarctic Intermediate Water [*Gloor et al.*, 2003]. There exists, therefore, a substantial lateral transport of anthropogenic CO_2 in the ocean, which connects uptake at places where deeper waters, generally deficient in anthropogenic CO_2, come to the surface and take up anthropogenic CO_2 from the atmosphere, with storage in the regions of deep thermoclines and net convergence in the mid-latitudes.

The column inventories shown in Figure 10.2.8 sum to a global inventory of anthropogenic CO_2 of 106±17 Pg C for 1994. *Sabine et al.* [2004] showed that an additional 12 Pg C is stored in marginal seas, such as the Arctic Ocean, bringing the total amount of anthropogenic CO_2 taken up by the ocean to 118±19 Pg C. Table 10.2.1 shows that this oceanic sink over the Anthropocene (1800-1994) corresponds to nearly half of the total CO_2 emissions from fossil fuel burning and cement production over the 1800-1994 period (about 244± 20 Pg C). Together with the well known atmospheric CO_2 increase, which corresponds to 165±4 Pg C, this number permits us to constrain the net terrestrial exchange to be a net source to the atmosphere of about 39± 28 Pg C. This net flux is the sum of poorly known emissions from land-use change (about 100 to 180 Pg C), and an inferred net sink of the terrestrial biosphere of 61 to 141 Pg C. Our oceanic sink estimate thus suggests that the ocean has taken up about between 27 and 34% of the total anthropogenic CO_2 emissions, making it the most important sink for anthropogenic CO_2 over the last 200 years.

The atmospheric oxygen method

The anthropogenic CO_2 inventory method permitted us to develop an anthropogenic CO_2 budget for the anthropocene, but we are equally interested in constraining the budget for the last two decades. In the absence of direct measurements of the global oceanic increase in DIC, a very elegant method to constrain the oceanic uptake of anthropogenic CO_2 over the last two decades is based on simultaneous measurements of atmospheric oxygen and CO_2 pioneered by *Keeling and Shertz* [1992].

The method builds upon the fact that O_2 and CO_2 are tightly coupled during the formation and oxidation of organic matter (including the burning of fossil fuels), but that these two gases are exchanged independently between the ocean and atmosphere. If one then assumes that the long-term exchange of O_2 with the ocean is zero or is small and can be estimated from independent sources, one ends up with two balance equations and two unknowns (the exchange of CO_2 with the ocean and land biosphere, respectively), which can be solved.

We begin with the mass balance equations for atmospheric O_2 and CO_2:

$$\frac{dN_{O_2}}{dt} = \Phi_{foss}(O_2) + \Phi_{as}(O_2) + \Phi_{ab}(O_2) \tag{10.2.27}$$

$$\frac{dN_{CO_2}}{dt} = \Phi_{foss}(CO_2) + \Phi_{as}(CO_2) + \Phi_{ab}(CO_2) \tag{10.2.28}$$

where N_{O_2} and N_{CO_2} are the number of moles of atmospheric O_2 and CO_2, respectively, and where Φ_{foss} is the fossil fuel emission of CO_2 and corresponding consumption of O_2, Φ_{as} is the exchange flux between the atmosphere and ocean, and Φ_{ab} is the exchange flux between the atmosphere and land biosphere (all fluxes have units of mol yr^{-1}). In the case of the fossil fuel emissions and the exchange with the land biosphere, the O_2 and CO_2 fluxes are linked stoichiometrically:

$$\Phi_{foss}(O_2) = r_{O_2:C}^{foss}\Phi_{foss}(CO_2) \tag{10.2.29}$$

$$\Phi_{ab}(O_2) = r_{O_2:C}^{terr}\Phi_{foss}(CO_2) \tag{10.2.30}$$

where $r_{O_2:C}^{foss}$ is about -1.4, and $r_{O_2:C}^{terr}$ about -1.1 [*Keeling and Shertz*, 1992, *Keeling et al.*, 1996, *Severinghaus*, 1995].

The concurrent measurements of atmospheric CO_2 and O_2 constrain dN_{O_2}/dt and dN_{CO_2}/dt, and fossil fuel emissions of CO_2 are relatively well known (e.g. [*Marland et al.*, 1998]). If we assume that the natural carbon and oxygen cycles in the ocean have remained in steady-state and have not been perturbed in any substantial manner, the long-term air-sea exchange flux of O_2, $\Phi_{as}(O_2)$ is very small and can be neglected. This assumption is based on the fact that because of much lower solubility of O_2relative to that of CO_2, the perturbation air-sea flux of $O_2$is much smaller than the perturbation flux for CO_2 for the same magnitude of an atmospheric perturbation. If we insert (10.2.30) and (10.2.29) into (10.2.27) and (10.2.28), we thus end up with two equations and two unknowns, $\Phi_{as}(CO_2)$ and $\Phi_{ab}(CO_2)$. Figure 10.2.10 shows a graphical solution to these equations, where the points indicate the observed evolution of atmospheric CO_2 and O_2, and where the direction of the arrows of the different processes are given by their stoichiometric ratios.

Figure 10.2.10 actually includes a small air-sea O_2 flux contribution, $\Phi_{as}(O_2)$. This is because the steady-state assumption of the natural oxygen cycle is not entirely tenable. Long-term observations of oceanic temperatures show that the ocean has warmed significantly over the last 50 years [*Levitus et al.*, 2000]. As the solubility of oxygen is very temperature dependent (see Figure 3.1.2), this must have led to an outgassing of O_2. The warming induced outgassing flux can be directly estimated from (3.4.4) in chapter 3. However, more recent studies indicate that the oxygen outgassing driven by ocean warming is likely amplified by an additional outgassing stemming from warming induced changes in ocean stratification, and that this additional outgassing might increase the purely thermally driven flux by a factor of three or more, requiring an adjustment of up

to 0.6 Pg C yr^{-1} to the original anthropogenic CO_2 budgets [*Keeling and Garcia*, 2002, *Bopp et al.*, 2002, **?**].

The anthropogenic budget for the two decades from 1980 to 1999 as inferred by the oxygen method but adjusted for the ocean warming outgassing are given in Table 10.2.1, both as integrated fluxes and as average fluxes per year. The most remarkable observation from inspection of this table is how strongly the global carbon cycle has been forced over the last 20 years. Almost 50% of the fossil fuel emissions over the anthropocene occured during the period from 1980 to 1999! Similar to the Anthropocene, out of the total anthropogenic CO_2 emissions, the ocean has taken up about 27% over the last two decades. These results and other work suggest that sink strength of the land biosphere has increased in the last two decades. The reasons for this phenomenon are still controversial, but it appears as if much of the land-driven uptake is associated with regrowth of areas that have been clearcut in the past, and have been abandoned or moved to less intensive cultivation [*Pacala et al.*, 2001, *Schimel et al.*, 2001, *Goodale and Davidson*, 2002].

<div align="center">THE ROLE OF BIOLOGY</div>

What is the role of biology in the oceanic uptake of anthropogenic CO_2? This topic has been the source of many misunderstandings and false claims ([*Broecker*, 1991, *Sarmiento*, 1991, *Longhurst*, 1991].

So far in our discussion on anthropogenic CO_2 we have neglected the marine biota. This is somewhat counter-intuitive, because we know that the marine biota is responsible for a large fraction of the surface to deep gradient in DIC (biological pumps). Then why does the biological pump not also transport anthropogenic CO_2 from the surface into the interior of the ocean? The first point to make here is that this downward transport of carbon in organic material is compensated in a steady-state by an equally large upward transport of DIC, resulting in a zero net transport (except for the small fraction that goes into the sediments). Our neglect of the biological pumps is based on the assumption that they had been operating in steady-state before the start of the anthropogenic CO_2 perturbation of the carbon cycle, and that they have continued to do so ever since. There are two lines of evidence that support this hypothesis. First atmospheric CO_2 remained remarkably stable for several thousand years before the 18th century (see Figure 10.1.1), indicating that the fluxes controlling the surface ocean total carbon content were in balance. Second, according to present knowledge, marine phytoplankton is controlled by nutrients (including micronutrients), light and vertical stability of the water column, but not by the CO_2 concentration. Therefore the biological pumps do not sequester anthropogenic carbon, but rather act as a natural background process continuing to work as in pre-industrial times.

The lack of a role of marine biota in the uptake of anthropogenic CO_2 over the last two centuries, is demonstrated by the model study of *Murnane et al.* [1999]   who recently

carried out a simulation of oceanic uptake in two models, one of which contained just the solubility pump and a second combined simulation that included the biological pump. The combined simulation took up 5% less anthropogenic CO$_2$ than the solubility model indicating that adding biology had only a minimal impact on the anthropogenic CO$_2$ uptake. The small reduction in uptake occurs because the biological pump reduces surface alkalinity and hence storage capacity for anthropogenic CO$_2$. If the solubility simulation used the same surface alkalinities as the combined model, then both would take up the same amount of anthropogenic CO$_2$.

One cannot assume, however, that the steady-state operation of the biological pumps will continue forever into the future. Moreover, the above discussion about the possible impact of the observed ocean warming on the oceanic oxygen cycle even suggests that the steady-state assumption for the oceanic carbon cycle over the 20th century may need to be re-evaluated.

Future climate changes associated with the buildup of greenhouse gases in the atmosphere will quite likely modify the biological pump driven fluxes, which could then feed back on the atmospheric composition. Alterations of the biological pumps, for instance, have been proposed as a possible cause for the dramatic changes in atmospheric CO$_2$ between the glacial and interglacial periods. It is difficult at present to to assess how the biological pump will respond to future climate changes and how it will interact with changes in ocean circulation and mixing.

FUTURE CO$_2$ UPTAKE

The primary factor controlling the future uptake of anthropogenic CO$_2$ by the ocean is the atmospheric CO$_2$ burden in excess over the atmospheric CO$_2$ concentration in equilibrium with the total emissions [*Sarmiento et al.*, 1995], as this represents the thermodynamic driving force for the uptake of CO$_2$ from the atmosphere. In the absence of major feedbacks, paradoxically, the higher the future anthropogenic CO$_2$ concentration in the atmosphere, the higher the oceanic sink flux is going to be.

Changes in ocean temperature, salinity, circulation and the ocean's biological pump have, however, the potential to substantially alter this uptake, both by directly impacting the uptake of anthropogenic CO$_2$ and indirectly by altering the air-sea balance of the natural CO$_2$ cycle. Any climate change induced alteration in the future uptake of anthropogenic CO$_2$ by the ocean will lead to feedbacks in the climate system, as the altered atmospheric CO$_2$ concentration will either accelerate (positive feedback) or decelerate (negative feedback) the initial climate change.

It is instructive to first discuss the impact of climate change on the oceanic uptake of anthropogenic CO$_2$, and only thereafter investigate the impact on the natural carbon cycle. A summary of all feedbacks is given in 10.2.4. For more detailed discussions, the reader is referred to *Plattner et al.* [2001] and *Gruber et al.* [2004].

The first feedback to consider is a chemical feedback discussed above, which arises from the decrease in the oceanic buffer capacity as a result of the uptake of anthropogenic CO_2. Figure 10.2.1 shows that this feedback is very substantial and positive in sign. It is also the best understood feedback. A second feedback arises from changes in ocean circulation, as the transport of anthropogenic CO_2 from the surface down into the ocean interior is the primary factor controlling the uptake. Many ocean-atmosphere coupled climate model simulations show a substantial increase in upper ocean stratification, primarily as a result of ocean warming in the low latitudes, and as a result of freshening in the high latitudes [*Cubasch et al.*, 2001]. This leads to a reduction of the vertical exchange and hence to a direct reduction of the uptake of anthropogenic CO_2 [*Sarmiento and LeQuéré*, 1996, *Sarmiento et al.*, 1998, *Joos et al.*, 1999, *Matear and Hirst*, 1999, *Plattner et al.*, 2001] This feedback thus tends to be positive as well.

These temperature, salinity, and circulation changes not only influence the uptake of anthropogenic CO_2, but also affect the natural carbon cycle within the ocean. Ocean warming will reduce the solubility of CO_2 in seawater and lead to a permanent loss of CO_2 from the oceanic reservoir of inorganic carbon. We can estimate the expected outgassing from warming alone on the basis of the temperature sensivity of ocean DIC. This sensitivity can be calculated by combining the temperature sensitivity of pCO_2 with the buffer factor, γ_{DIC}:

$$\frac{\partial DIC}{\partial T} = \frac{\partial DIC}{\partial pCO_2}\frac{\partial pCO_2}{\partial T} = \frac{DIC}{pCO_2^{oc}}\frac{1}{\gamma_{DIC}}0.04\ pCO_2^{oc} = \frac{0.04\ DIC}{\gamma_{DIC}} \tag{10.2.31}$$

Inserting surface ocean mean values for DIC and γ_{DIC} gives a temperature sensitivity of DIC of about 8 μmol kg^{-1} $^\circ$C^{-1}. Dividing this number with the average heat capacity of seawater, $c_p = 4000$ J kg^{-1} $^\circ$C^{-1} gives an estimate of the loss of DIC from the ocean for each Joule of energy taken up from the atmosphere,

$$\frac{\partial DIC}{\partial Q} \approx 2 \cdot 10^{-9} \text{mol J}^{-1} \tag{10.2.32}$$

Levitus et al. [2000] estimated that the ocean heat content increased by about $2 \cdot 10^{23}$ J between the mid 1950 and the mid 1990s, leading to an expected loss of DIC from the ocean of $4 \cdot 10^{14}$ mol, or about 5 Pg C. This is very small relative to the estimated oceanic uptake over the anthropocene of about 118 Pg C (Table 10.2.1), but future ocean warming could strongly accelerate this loss and strenghten this positive feedback.

The increase in vertical stratification and the other circulation changes not only reduce the uptake of anthropogenic CO_2 from the atmosphere, but also affect the natural carbon cycling substantially, even in the absence of any changes in ocean productivity. An important distinction needs to be made between this circulation feedback interacting with the natural carbon cycle and that associated with the anthropogenic CO_2 uptake. The latter

feedback associated with the anthropogenic CO$_2$ uptake affects only the rate at which the atmospheric CO$_2$ perturbation is equilibrated with the ocean and does not change the long-term equilibrium, whereas the former feedback associated with the natural carbon cycle changes the equilibrium distribution of carbon between the ocean and atmosphere.

As it turns out, in the presence of the biological pump, these circulation changes appear to lead to a negative feedback-that is, an increase in the uptake of atmospheric CO$_2$ from the atmosphere. The main reason for this somewhat surprising result is that a slowdown of the surface to deep mixing also reduces the upward transport of remineralized *DIC* (ΔC_{soft}) from the thermocline into the upper ocean, while the downward transport of biologically produced organic carbon remains nearly unchanged. The magnitude of this feedback tends to be coupled to the magnitude of the ocean circulation feedback on the uptake of anthropogenic CO$_2$, as both are driven by the same changes in circulation.

We finally turn to the impact of future changes in ocean biota on the magnitude of the oceanic sink. There are many possible reasons for changes in global marine export production, including changes in surface ocean physical properties, changes in the delivery of nutrients from land by rivers and atmosphere, and internal dynamics of the ocean biota, including complex predator-prey interactions and fisheries-induced pressures on marine predators (see Boyd and Doney 2003 for a comprehensive review). In general, one might expect that an increase in ocean stratification will negatively impact biological productivity in areas that are nutrient limited, such as is the case throughout most of the low and temperate latitudes. By contrast, an increase in vertical stratification actually might lead to an increase in biological productivity in light limited areas, as phytoplankton would tend to spend more time, on average, within the euphotic zone. *Bopp et al.* [2001] investigated these responses in a coupled physical-ecological model and indeed found such a response, with a global change in export production of only a few percent for a doubling of atmospheric CO$_2$, but with regional changes of much larger amplitude.

While this particular simulation has to be viewed as an illustration since very little is known about the sign and magnitude of the changes in marine productivity and export, there is increasing evidence that the calcification rate by coccolithophorids might be significantly reduced in response to a lowering of the surface ocean pH [*Riebesell et al.*, 2000]. As a reduction of calcification leads to an increase in the ocean uptake capacity for atmospheric CO$_2$, this represents a negative feedback for climate change. A lower pH also affects the calcification rates of corals [*Gattuso et al.*, 1996, *Kleypas et al.*, 1999]. This effect, together with the enhanced sea-surface temperatures, poses a significant threat to coral reefs with substantial implications for their ecosystem services, although their impact on atmospheric CO$_2$ likely will be relatively small. A third impact of the invasion on the oceanic CaCO$_3$ cycle is through its lowering of the water column saturation state, possibly affecting the rates of CaCO$_3$ dissolution (cf. *Feely et al.* [2004]). Given the importance of

$CaCO_3$ in transporting organic matter to the deep ocean, a faster dissolution of $CaCO_3$ would reduce the strength of the biological carbon pump, and therefore lead to a positive feedback.

Figure 10.2.10 illustrates the magnitude of a number of these feedbacks and their interaction on the basis of simulations carried out by forcing a coupled ocean-atmosphere model with an interactive ocean carbon cycle with a business as usual emission scenario for CO_2 [*Sarmiento et al.*, 1998]. In the solubility only model, ocean warming and the change in ocean stratification led to a very substantial reduction in the ocean uptake, highlighting the positive signs of these two feedbacks. However, *Sarmiento et al.* [1998] also found that the biological pump has the potential to largely offset this decreased uptake, mainly as a result of a more efficient biological pump. It has to be noted, however, that the representation of the biological pump in this model is very simplistic, and that therefore these simulations have to be regarded as case studies, rather than accurate predictions.

These simulations demonstrate that while the biological pump does not play a significant role for assessing the oceanic uptake of anthropogenic CO_2 in the past and present, these pumps might play an important role for the future uptake. However, very little is known about the possible response of the oceanic biota to climate change. In order to improve these predictions, one has to gain a clear understanding of the processes controlling all important steps of the oceanic biological pumps, e.g. surface production, respiration, export and remineralization. As we have seen during our grand tour through these components of the biological pumps in chapters 4 to 6, there are still considerable gaps in our understanding. However, while we cannot foresee the future, nature has in the past performed several experiments, from which we might learn something about the future. The first set of experiments is the response of the ocean carbon cycle to climate variability on interannual to decadal time scales. The second set of experiments are the large and regular atmospheric CO_2 fluctuations associated with the glacial/inter-glacial cycles.

Tables

Table 10.2.1: Anthropogenic CO_2 budget for the anthropocene (1800-1994) and for the period of the 1980s and 1990s. From *Sabine et al.* [2004].

	1800-1994 Pg C	1980-1999 Pg C	1980-1999 (Avg) Pg C yr^{-1}
Constrained sources and sinks			
(1) Emissions from fossil fuel and cement production	244 ± 20	117 ± 5	5.9 ± 0.3
(2) Storage in the atmosphere	-165 ± 4	-65 ± 1	-3.3 ± 0.1
(3) Ocean uptake	-118 ± 19	-37 ± 7	-1.9 ± 0.4
Inferred Net Terrestrial Balance			
(4) Net terrestrial balance = [-(1)-(2)-(3)]	39 ± 28	-15 ± 9	-0.8 ± 0.5
Terrestrial Balance			
(5) Emissions from changes in land-use	100 - 180	24 ± 12	1.2 ± 0.6
(6) Terrestrial biosphere sink = [-(1)-(2)-(3)]-(5)	-61 to -141	-39 ± 18	-2.0 ± 1.0

Table 10.2.2: Distribution of carbon in a simplified ocean atmosphere carbon system as a function of the size of a perturbation.

	Pre-Industrial	Size of perturbation (Pg C)		
		150	600	1800
Atmosphere	1.5	16.4	17.4	20.8
Ocean	98.5	83.6	82.6	79.2

Note: Totals in all cases are normalized to 100.

Table 10.2.3: Summary of Methods to Estimate the Ocean Uptake of Anthropogenic CO_2.

Method	Present Uncertainty [‡]	Spatial Coverage	Authors
direct observational methods			
Air-sea fluxes of CO_2	L	regional	*Tans et al.* [1990] ; *Takahashi et al.* [2002]
Repeated transects	M	regional	*Peng et al.* [1998]
DIC multi parameter analysis	M	regional	*Wallace* [1995]
Total inventory methods	M-L	regional	*Brewer* [1978]; *Chen and Millero* [1979]
			Gruber et al. [1996]
indirect observational methods			
Atmospheric O_2 and CO_2	M-L	global	*Keeling and Shertz* [1992]
Inversion studies of atm. CO_2	L	regional	*Bolin and Keeling* [1963] ; *Gurney et al.* [2002]
Oceanic change in ^{13}C inventory	L	global	*Quay et al.* [1992]
Air-sea disequilibrium of $\delta^{13}C$	M-L	global	*Tans et al.* [1993] *Gruber and Keeling* [2001]
Dynamic constraints of $\delta^{13}C$	M-L	global	*Heimann and Maier-Reimer* [1996]
tracer analogues (^{14}C, ^{3}H, CCl_4, CFCs)	M-L	regional	*McNeil et al.*[2003]
model based estimates			
tracer calibrated box models	M	global	*Oeschger et al.* [1975] ;
			Siegenthaler and Joos [1992]
dynamic 2-D/3-D models	M	regional	*Maier-Reimer and Hasselman* [1987]
			Sarmiento et al. [1992] ; *Orr et al.* [2001]

‡ : subjectively estimated (M: medium; L: large)

Table 10.2.4: Summary of Marine Carbon Cycle Feedbacks

Process	Sign	Magnitude[‡]	Uncertainty/Understanding
Anthropogenic CO$_2$ uptake feedbacks			
Chemical feedback	Positive	L	Low/high
Circulation feedback (anthropogenic CO$_2$)	Positive	L	Medium/medium
Natural carbon cycle feedbacks			
Temperature/salinity feedback	Positive	M	Low/medium to high
Circulation feedback (constant biota)	Negative	M-L	Medium/medium
Ocean biota feedback (circulation constant)	Positive/ Negative	M	High/low

‡ : subjectively estimated (M: medium; L: large)

Figures

Figure 10.2.1: (a) The global mean instantaneous change in oceanic DIC resulting from a given change in CO_2 concentration for the S450 and S750 scenarios. The large reduction in this ratio through time is a measure of the reduction in the oceanic buffer capacity of surface waters. (b) The annual ocean uptake for the S450 and S750 scenarios. the nonlinear curves have the full oceanic chemistry effect. The linear curves neglect the decrease in the buffer factor. From *Sarmiento et al.* [1995].

Figure 10.2.2: Fractions of anthropogenic CO_2 sequestered by various abiological processes plotted as a function of anthropogenic CO_2 release. The approximate e-folding time scales for each process are given at the right. The fraction remaining in the atmosphere for a given time-scale is the difference between 1 and the level of the cumulative curve. For example, on time-scales of 4,000 years, the fraction remaining in the atmosphere after equilibration is determined by the magnitude sequestered by the ocean by reaction with carbonate and sea-floor $CaCO_3$. For a 4000 Pg C emission, these two processes remove about 87% of it, leaving 13% in the atmosphere. From *Archer et al.* [1997].

Figure 10.2.3: Timeseries of (a) atmospheric pulse response function, and of (b) fractional contributions of four different processes to the sequestration. The four processes are ocean invasion, reaction of the anthropogenic CO_2 with mineral calcium carbonates at the sea floor, reaction with calcium carbonates on land, and sequestration by silicate weathering. Note that the exact shape of the atmospheric pulse response depends on the size of the pulse because of the non-linearity of the oceanic buffer factor. This pulse here has been calculated for a pulse size of 3000 Pg of carbon. Based on results by *Archer et al.* [1997].

Figure 10.2.4: Effective mixed-layer pulse response functions for the Box-Diffusion model, the HILDA model, the 2-D model and the Princeton general circulation model. Inset shows the pulse response functions for the first ten years. Modified from *Joos et al.* [1996].

Figure 10.2.5: Upper ocean timeseries of DIC, Alk, the ^{13}C/^{12}C ratio of DIC, and calculated oceanic pCO$_2$ from HOT and BATS. The DIC and Alk concentrations have been normalized to a constant salinity in order to remove the effect of freshwater fluxes. Clear long-term trends are visible in DIC, oceanic pCO$_2$ and the ^{13}C/^{12}C ratio of DIC, owing to the uptake of anthropogenic CO$_2$ from the atmosphere. Also shown are the atmospheric pCO$_2$ trends, indicating that the oceanic pCO$_2$ are roughly following the atmospheric trends. The oceanic trends are slightly elevated at HOT, likely the result of a combination of climate variability induced changes in rainfall patterns and water mass changes that occured there around 1996/1997 (see *Dore et al.* [2003] and *Keeling et al.* [2004] for discussion). Data are from *Gruber et al.* [2002] and *Keeling et al.* [2004].

Figure 10.2.6: Illustration of the C_{ant} reconstruction method on the basis of ΔC^* and ΔC_t^*. (a) Estimation of C_{ant} on deep isopycnal surfaces, where one can find regions that contain undetectable amounts of anthropogenic CO$_2$. (b) Estimation of C_{ant} on shallow isopycnal surfaces, where anthropogenic CO$_2$ has invaded the entire surface. ADAPT ΔC^* as a function of latitude along two deep isopycnal surface intervals in the Atlantic Ocean: (a) the σ_2 interval 37.03–37.08, which represents the Denmark Strait and Iceland-Scotland Overflow Waters, and (b) the σ_4 interval 45.913–45.938, which lies within the core of the Antarctic Bottom Water. The solid lines depict the average ΔC^* concentration in the regions from 20°S to the equator and from the equator to 20°N which have been used to determine $\Delta DIC_{\mathrm{diseq}}$ for the southern and northern end-member, respectively. In both cases, no difference has been found between these two end-members. The dashed lines are drawn at $\pm$ 5 μmol kg^{-1} from the estimated $\Delta DIC_{\mathrm{diseq}}$. The upward trend near the outcrops in the south and the north is due to the uptake of anthropogenic CO$_2$. (b) ΔC_t^* (triangles) and ΔC^* (circles) versus CFC 11 age along four isopycnal surface intervals in the South Atlantic. These surfaces include (a) the σ_θ interval 26.95-27.25 representing the Subpolar Mode Water, and (b) the σ_θ interval 27.25-27.35 which lies within the upper Antarctic Intermediate Water. The lines for ΔC^* are drawn to emphasize the trend and have been obtained by linear regression. The lines for ΔC_t^* represent the average. From *Gruber* [1998].

Figure 10.2.7: Meridional section of C_{ant} (micromoles per kilogram) from 60°S to 80°N in the western Atlantic Ocean. Reconstruction based on data from the Transient Tracers in the Oceans (TTO) North Atlantic Study (1981), the TTO Tropical Atlantic Study (1982-1983), and the South Atlantic Ventilation Experiment (1989) and refer therefore to different years in the different regions. The uncertainty in the reconstructed C_{ant} has been estimated to be about 9 μmol kg^{-1}. Small circles indicate observations. From *Gruber* [1998].

Figure 10.2.8: Map of the global inventory of anthropogenic CO_2. Data are from *Sabine et al.* [2004].

Figure 10.2.9: Map of inversion results. Based on results of *Gloor et al.* [2003].

Figure 10.2.10: Simulated oceanic uptake of anthropogenic CO_2 by the GFDL/Princeton coupled climate model. (a) Control runs (thin lines) and two scenarios for the biological pump. The thick solid line refers to a simulation where the soft-tissue pump remained constant. The thick broken line corresponds to a scenario where the soft-tissue pump was assumed to change in a manner to keep the surface nutrient concentration constant. (b) Control run and ocean uptake for the solubility model only. In the control runs, the coupled climate model was run in a pre-industrial climate and only atmospheric CO_2 was changed. In the warming scenarios, the climate model was externally forced with a timeseries of effective atmospheric CO_2, constructed from a business as usual scenario (IS92a) including the negative feedback from aerosols. From *Sarmiento et al.* [1998].

10.3 Interannual to decadal time-scale variability

Over the last 50 years, atmospheric CO_2 has been steadily increasing by about 1.5 ppm yr^{-1} (Figure 10.1.2), a direct result of the anthropogenic CO_2 emissions from the burning of fossil fuels and land use changes. However, the atmospheric CO_2 growth rate was not constant, but fluctuated strongly from one year to another (Figure 10.3.1). These variations are not caused by changes in the amount of CO_2 emitted by fossil fuel burning, because they are too small. Rather, these atmospheric CO_2 variations must be caused by variations in the net fluxes between the ocean and atmosphere on one hand and between the terrestrial biosphere and the atmosphere on the other hand. These variations in fluxes are presumably a consequence of interannual variations in weather and climate. Nature has provided us, therefore, with an experiment that permits us to study how the global carbon cycle is responding to changes in the physical climate system. The study of this response provides one of the few means to learn how feedbacks between the physical climate system and the global carbon cycle operate. Only if such feedbacks are well understood, can one make better assessements of what might happen to the global carbon cycle in a future changing climate (see discussion in section 10.3 above).

Bacastow [1976] was first to point out that these atmospheric CO_2 variations are associated with El Niño/Southern Oscillation (ENSO) events. This result has been confirmed in many subsequent studies using longer records [*Bacastow et al.*, 1980, *Keeling and Revelle*, 1985, *Keeling et al.*, 1989, *Keeling et al.*, 1995]. During an El Niño event (positive phase of ENSO), sea surface temperatures in the equatorial Pacific increase and the supply of nutrient and carbon rich water by upwelling ceases, thereby reducing the normally prevailing strong outgassing of CO_2 from this region (see Figures 3.1.3 and 8.1.1). If net air-sea fluxes elsewhere remained constant, this reduction in outgassing would lead to a reduced growth rate in atmospheric CO_2. Figure 10.3.1 shows that the atmospheric CO_2 growth rate is, on average, indeed reduced during the early phases of an El Niño, making the link between ENSO events and atmospheric CO_2 plausible. However, figure 10.3.1 also shows that the late phases of El Niños are usually associated with very high growth rates, which are difficult to explain on the basis of the equatorial Pacific alone.

By measuring the $^{13}C/^{12}C$ ratio of atmospheric CO_2 concurrently with its concentration and employing a simple atmospheric mass balance approach, *Keeling et al.* [1989] and *Keeling et al.* [1995] found that biospheric, as opposed to oceanic, processes are the primary cause of interannual variations in atmospheric CO_2. Nevertheless, C.D. Keeling and coworkers predict also variations in the net air-sea flux of CO_2 of up to $\pm$ 2 Pg C yr^{-1} (Figure 10.3.2b). However, these estimated variations are opposite of what is expected from an oceanic response that is dominated by ENSO related variations in outgassing in the tropical Pacific. *Francey et al.* [1995], *Rayner et al.* [1999], and *Joos et al.* [1999],

using similar techniques, find rather different results. They predict variations in anoma-
lous air-sea fluxes of similar magnitude, albeit slightly smaller, but with a phasing that is
nearly opposite to that of *Keeling et al.* [1995] (Figure 10.3.2b). More recent estimates of
global air-sea CO_2 flux variability by *Bousquet et al.* [2000] and *Roedenbeck et al.* [2003]
on the basis of inversions of atmospheric CO_2 concentrations alone tend to confirm the
latter estimates. Similar conclusions were found by *Battle et al.* [2000] using concurrent
measurements of atmospheric O_2 and CO_2 as a constraint.

Although most recent estimates based on atmospheric constraints point toward a size-
able interannual variability in air-sea CO_2 fluxes, i.e. an amplitude of order of $\pm$ 1 Pg
C yr^{-1}, oceanic observations or oceanic modeling studies tend to suggest a much smaller
oceanic contribution to the observed atmospheric CO_2 variations (Figure 10.3.2a). Esti-
mates that are based on measurements of the variability of pCO_2 in the equatorial Pacific
indicate a maximal interannual amplitude of only about ± 0.5 Pg C yr^{-1}) (see summary in
Feely et al. [1999] and *Chavez et al.* [1999]) (see also Figure 10.3.6). In order to compare
with the atmospheric contraints, which are global, one needs to consider also the contribu-
tion of the the extra-tropical pceanic regions. *Winguth et al.* [1994], *LeQuéré et al.* [2000],
and *McKinley* [2002] found on the basis of global 3-D ocean biogeochemistry models that
interannual variability in air-sea CO_2 fluxes is small in the extra-tropical regions, and that
the global flux is dominated by the equatorial Pacific.

We cannot solve the controversy here, but rather would like to review the evidence
for interannual variations in ocean biogeochemistry and learn the mechanisms that are at
operation. We will focus on the ENSO related variations in the equatorial Pacific because
they are large, and they have been well documented. We will also discuss some recent
research documenting interannual variability in the extratropical ocean carbon cycle.

<div align="center">TROPICAL VARIABILITY</div>

ENSO is the most important mode of SST variability on interannual to decadal time-
scales (see section 2.4). These ENSO related SST anomalies are caused by a combination
of changes in ocean circulation (mainly a change in the strength and source of equatorial
upwelling) and anomalous local air-sea heat exchanges. How does the ocean carbon cycle
respond to these changes? The large positive SST anomalies that are characteristic of
a mature El Niño (Figure 2.5.8) should lead to an increase of oceanic pCO_2. However,
observations show a dramatic decrease of pCO_2, linked to a drop in DIC that more than
compensates for the warming effect (Figure 10.3.3). Is this drop in DIC caused by changes
in circulation, in air-sea gas exchange or in ocean biology?

Before we can address this question we need to understand the mean state of the carbon
system in the equatorial Pacific. The equatorial Pacific is characterized by large positive
ΔpCO_2 (Figure 8.1.1). In fact, it is the region of the most intense outgassing of CO_2 from
the ocean [*Takahashi et al.*, 2002]. During normal and negative phases of ENSO, the loss

of CO$_2$ from the ocean to the atmosphere in the eastern equatorial Pacific (10°S-10°N; 135°W-80°W) was estimated to be around 0.9 ± 0.1 Pg C yr^{-1} [*Feely et al.*, 1995]. What makes this region such a strong source region for atmospheric CO$_2$?

Divergent Ekman transport forced by the trade winds leads to strong upwelling of cold subsurface waters. The main source of the upwelling water is thought to be the Equatorial Undercurrent located at depths of about 100 to 200 m (see Figure 2.4.2). The potential for outgassing can be diagnosed by looking at a quantity referred to as potential pCO$_2$, i.e. the pCO$_2$ that would be achieved if the water at temperature $T^{\text{in situ}}$ were brought to the surface and isochemically warmed to ambient equatorial surfae ocean temperature T^{sfc}. Potential pCO$_2$ can be easily computed by integrating the expression for the temperature sensitivity of pCO$_2$ (i.e. equation (8.3.4)):

$$p\text{CO}_2^{\text{potential}} = p\text{CO}_2^{\text{in situ}} \left(1 + 0.0423°C^{-1}\left(T^{\text{sfc}} - T^{\text{in situ}}\right)\right). \qquad (10.3.1)$$

Figure 10.3.4 shows that the waters of the Equatorial undercurrent have extremely high potential pCO$_2$, leading to a very high potential outgassing of CO$_2$ once these waters come to the surface. The high potential pCO$_2$ in these waters is due to a combination of having cold temperatures and large amounts of remineralized carbon. These very high pressures are, however, greatly reduced at the surface because after the waters arrive in the mixed layer, biological uptake fueled by the high nutrient concentrations removes inorganic carbon from the surface ocean. Additional carbon is lost to the atmosphere by air-sea gas exchange.

It is possible to separate the role of biological CO$_2$ uptake from the CO$_2$ evasion in reducing the supersaturation of the upwelling water through plots of salinity normalized DIC ($sDIC$) versus salinity normalized nitrate [*Broecker and Peng*, 1982]. As can be seen in Figure 10.3.5, samples taken at intermediate depths follow a trend that correspond roughly to the stoichiometry of biological uptake and remineralization [*Anderson and Sarmiento*, 1994]. Samples taken from the surface or near the surface show a marked deviation from this trend by having significantly lower $sDIC$ concentrations than would be expected from their nitrate concentration. Note that this deficiency here is equivalent to the low $\Delta C_{\text{gas ex}}$ concentrations found in the equatorial regions (see Figure 8.4.4). This missing DIC presumably has been lost to the atmosphere. We can obtain a rough estimate of this CO$_2$ loss by multiplying the upwelling rate (about 0.7 m day^{-1} [*Wanninkhof et al.*, 1995]) with the DIC deficit of about 30 μmol kg^{-1}. This yields an outgassing rate of about 8 mol m^{-2} yr^{-1} or 1.3 Pg C yr^{-1} if integrated over the eastern equatorial Pacific (10°S-10°N; 135°W-80°W). This is roughly consistent with estimates based on measurements of the air-sea difference in pCO$_2$. A more sophisticated approach on the basis of the same concept, but using global-scale data and circulation constraints, yields an outgassing estimate of about 0.9 Pg C yr^{-1} [*Gloor et al.*, 2003].

In summary, the strong outgassing of CO_2 in the equatorial Pacific is a result of a combination of strong warming of the cold waters that upwell to the surface and an inefficient biologial pump. The latter means that surface ocean DIC is being replaced faster by upwelling than surface ocean biology can remove it by forming organic matter. This imbalance is manifested also by the existence of residual nutrients (see Figure 10.3.2 and discussion in section 8.5).

During an El Niño, the deepening of the thermocline caused by the eastward propagating Kelvin waves push down the cold, DIC rich waters that typically feed the upwelling. Instead, the upwelling is being fed by much warmer, DIC poor waters. In addition, the weakening of the trade winds leads to a reduction in upwelling rates. These two changes together cause a dramatic reduction in the amount of DIC transported to the surface ocean, resulting in an almost complete removal of the equatorial supersaturation (see Figure 10.3.3). *Feely et al.* [1999] and *Chavez et al.* [1999] estimated that the net ocean to atmosphere CO_2 flux during a strong El Niño event is only about 0.1 to 0.3 Pg C yr^{-1}, hence about 0.5 to 0.9 Pg C yr^{-1} lower than normal (see Figure 10.3.6). Although this decrease is mainly caused by changes in ocean circulation and mixing, surface biology tends to reinforce these changes. This is, at first, counter-intuitive, since the reduced upward supply of nutrients leads to a dramatic decrease in biological productivity in the area. However, it turns out that despite this reduction, the biological pump tends to become more efficient, i.e. the usually present imbalance between upward supply of biologically derived DIC and downward transport of organic matter is shifted toward a balance. This is most clearly expressed in the observed decrease of surface nutrients (Figure 10.3.2). As a result, the anomalous fluxes associated with the changes in the biological pump during El Niños are actually directed into the ocean, i.e. contributing to the observed decrease in ocean outgassing.

Siegenthaler and Wenk [1989] developed a simple four-box model that highlights the relative roles of changes in biological productivity and upwelling (Figure 10.3.7). This model consists of three oceanic boxes (equatorial surface, mid-latitude, and thermocline) overlain by a well mixed atmosphere. Upwelling from the thermocline occurs in the equatorial surface box, from where the water is transported laterally into the mid-latitude box. The large-scale circulation is closed by downwelling in the mid-latitudes. *Siegenthaler and Wenk* [1989] included a simple parameterization of biological productivity depending on nutrient concentration. Figure 10.3.8 shows the response of this four-box model to an idealized El Niño event assumed to last for one year.

Atmospheric CO_2 starts to decrease nearly instantaneously, and the atmospheric CO_2 growth rate remains negative until upwelling resumes at the end of the event. This decrease in atmospheric CO_2 is almost exclusively a result of a dramatic decrease in the $p\text{CO}_2$ of the equatorial surface box, which leads to near cessation of the CO_2 evasion from this region

(Figure 10.3.8d and f). To understand the dynamics underlying this response, it is useful to investigate the carbon fluxes in and out of the equatorial box (Figure 10.3.8f). In normal years, the large-scale transport of water constitutes a source of DIC for the equatorial box, since the upwelling waters have higher DIC concentrations than the waters leaving the box laterally. This net gain is compensated by losses due to gas exchange and by settling particles. When upwelling stops, gas exchange and biological productivity continue for a while, decreasing DIC and nutrient concentrations. This incrementally reduces biological export and the net outgassing of CO$_2$, so that at the end of the El Niño event, all carbon fluxes into or out of the equatorial box are near zero.

It is instructive to compare the model simulated atmospheric growth rates (Figure 10.3.8c) with the observed growth rates over an El Niño event (Figure 10.3.1). The model predicts a minimum in the growth rate towards the end of an El Niño event, whereas atmospheric observations indicate that the minimum growth rates tends to occur early during an El Niño event and are usually followed by a very strong positive anomaly in the growth rates. It therefore appears plausible that the observed initial decline of atmospheric CO$_2$ growth rates may be a consequence of the reduced outgassing in the tropical Pacific. Obviously, a different mechanism must explain the unusually strong atmospheric CO$_2$ growth rates observed afterwards. It has been suggested that changes in extra-tropical waters might be involved. However, model simulations suggest that the response of the extratropical carbon cycle to ENSO variations is relatively small [*Winguth et al.*, 1994, *LeQuéré et al.*, 2000]. If this is correct, then the dominant cause for the ENSO related atmospheric CO$_2$ variations are variations in the net exchange of the terrestrial biosphere.

This is a plausible hypothesis since ENSO events in the tropical Pacific are coupled to large changes in global atmospheric circulation and precipitation patterns. The 1982/83 as well as the 1997/98 El Niños led to severe drought and forest fires in large regions, which resulted in significant release of CO$_2$ from soil respiration and burning of biomass [*der Werf et al.*, 2004]. The global-scale positive temperature anomalies associated with warm ENSO events tend to enhance soil respiration more strongly than photosynthesis. This hypothesis is supported by results from several simulations with prognostic terrestrial carbon cycle model forced with observed variations in temperature and precipitation [*Kindermann et al.*, 1996, *Peylin et al.*, 2004]. These models are able to reproduce successfully the observed atmospheric CO$_2$ growth rate variations primarily on the basis of these processes.

In summary, about two thirds of the observed interannual variations in the atmospheric CO$_2$ growth rates are caused by the terrestrial biosphere, with the remainder being driven by the ocean [*Peylin et al.*, 2004]. There is currently strong consensus between observations, oceanic modeling studies and atmospheric constraints that the equatorial Pacific contributes substantially to global air-sea CO$_2$ variations on interannual time-scales (Fig-

ure 10.3.6).

<center>EXTRA-TROPICAL VARIABILITY</center>

There is little consensus about the magnitude of interannual variations in air-sea CO_2 fluxes in the extra-tropics. Estimates based on atmospheric CO_2 inversions suggest substantial variations in air-sea CO_2 fluxes in the extra-tropical regions of both hemispheres, while currently existing ocean models suggest a very small contribution from these regions [*Peylin et al.*, 2004]. One possibility to resolve this discrepancy is to analyze observations from as many oceanic regions as possible. However, very few sites exist where the inorganic carbon system has been observed regularly enough to establish interannual variability. The two longest such records come from the subtropical gyres (see also Figure 10.2.5) and will be discussed below.

Before we start investigating the subtropical records, it is instructive to discuss first the processes that could lead to interannual variations in air-sea CO_2 fluxes. A good starting point is the seasonal cycle, since interannual variations in the extra-tropics can be viewed as perturbations of the seasonal cycle. We have seen in chapter 8 that the seasonal cycle of oceanic pCO_2 is primarily controlled by the interplay of antagonistic tendencies between SST and surface DIC variations, where surface DIC is controlled by net community production, air-sea gas exchange, vertical entrainment, i.e. the input of thermocline DIC into the surface mixed layer whenever it deepens, and lateral exchange.

In the subtropical gyres, we found that the influence on pCO_2 of the seasonal warming and cooling dominates over the seasonal DIC changes, leading to a positive correlation between SST and DIC (Figure 8.3.7). In contrast, the influence of the seasonal DIC drawdown on oceanic pCO_2 outweighs the seasonal warming in higher latitudes, leading to a negative correlation between DIC and SST. Therefore, if the analogy with the seasonal cycle is correct, we expect that interannual anomalies in SST tend to dominate interannual variations in pCO_2 in the subtropical gyres, while interannual anomalies in DIC are expected to control pCO_2 anomalies at higher latitudes.

In order to get a sense of where interannual variability in oceanic pCO_2, and consequently air-sea CO_2 fluxes might be expected to be large, we show in Figure 10.3.9 maps of the variance of three factors that might drive such variability, SST, mixed layer depth, and export production. These maps were produced from satellite observations by first deasonalizing the data and then calculating the variance of the residuals (for details see *LeQuéré and Gruber* [2004]). While the SST anomalies are clearly the largest in the equatorial Pacific, the maps also suggest that there are large variations in these three driving forces in the extratropical regions, potentially giving rise to substantial interannual variations in oceanic pCO_2 there. Whether or not these extratropical variations lead to pCO_2 changes depends in part on possible correlations between the different driving factors.

For example, interannual variations in SST and DIC may correlate, as colder than

normal SSTs are usually associated with anomalously deep surface mixed layers (both a forcing and a result of the entrainment of cold thermocline waters), which enhances the entrainment of DIC. This would tend to lead to a negative correlation between SST and DIC anomalies, suppressing the variability of oceanic pCO$_2$, as the reduced SST tends to decrease pCO$_2$, while the positive DIC anomalies tend to increase pCO$_2$. Anomalously strong entrainment also enhances the input of nutrients into the surface layer, which, in nutrient limited ecosystems, can increase biological productivity and hence lower DIC. This would tend to lead to a positive correlation between DIC and SST, as colder than normal conditions would be associated with anomalously low DIC. In such a case, these two driving factors would enhance the variability of oceanic pCO$_2$. The resulting relationship between SST and DIC therefore pCO$_2$ depends then critically on the magnitude of the biological response. In contrast, in light-limited ecosystems, deeper mixed layers would tend to reduce biological production, therefore enhancing the negative correlation between SST and DIC. In these regions, oceanic pCO$_2$ variability is determined by the relative magnitude of the SST and DIC changes. Given these sometimes synergistic and sometimes antagonistic driving factors, it is very difficult to predict the overall response of the oceanic pCO$_2$ to changes, but it is useful to keep these general principles in mind as we next look at the observations from the subtropical gyres.

Figure 10.3.10a shows seasonally and long-term mean detrended time-series of temperature, salinity normalized DIC, $sDIC$, the reduced ^{13}C/^{12}C isotopic ratio of DIC and calculated pCO$_2$ from Station "S"/BATS in the Sargasso Sea near Bermuda. Figure 10.3.10b shows the respective records from the HOT program near Hawaii. The concentrations of DIC and Alk are normalized to a constant salinity in order to remove the effect of freshwater fluxes at the surface, denoted as $sDIC$ and sAlk. These anomalies were computed by removing the mean seasonal cycles shown in Figures 8.3.8 and 8.3.9 from the time-series records shown in Figure 10.2.5. The long-term trend, primarily the result of the uptake of isotopically light anthropogenic CO$_2$ from the atmosphere, was taken into account by fitting a linear function of time to the data (see *Gruber et al.* [2002] and *Brix et al.* [2004] for details).

At both sites, the resulting interannual anomaly time-series show substantial variations, with considerable correlations between the different variables. In particular, anomalously cold years tend to coincide with increased $sDIC$ concentrations and a slight tendency for negative anomalies in the ^{13}C/^{12}C ratio. As a result of the anti-correlated SST and $sDIC$ anomalies, variations in oceanic pCO$_2$ tend to be suppressed, i.e. whenever warmer than normal conditions increase oceanic pCO$_2$, the concurrent negative DIC anomalies tend to cause a decrease of pCO$_2$. Overall, SST anomalies tend to prevail, causing a positive correlation between oceanic pCO$_2$ and SST, consistent with our hypothesis put forward on the basis of the analogy with the seasonal cycle.

What are the processes causing these co-variations between SST, DIC, and the ^{13}C/^{12}C ratio? *Gruber et al.* [2002] and *Brix et al.* [2004] investigated the processes causing the observed variations at the two sites in detail, taking advantage of the concurrently observed ^{13}C/^{12}C ratio variations. These data, together with a large number of other observations, such as mixed layer depth and wind speed, permitted them to estimate the interannual variability of the contribution from each of the five processes that are controlling the surface ocean $sDIC$ balance: Air-sea gas exchange, net community production, vertical entrainment, vertical diffusion, and lateral transport (see also section 8.3). Figure 10.3.11 shows that at both sites, air-sea gas exchange and net community production represent two of the three important contributors to the observed interannual variability. The two sites differ, however, with regard to the third process. Near Bermuda, it is vertical entrainment, while it is lateral tranport near Hawaii. It thus appears that variations in convection are the dominant driving factor near Bermuda, while these variations tend to be unimportant near Hawaii. This is not entirely surprising, since mixed layer variations near Bermuda are large and play an important role for the seasonal cycle, whereas, near Hawaii, mixed layer variations are small and therefore unimportant on seasonal time-scales.

It is instructive to stratify the different years into two modes depending on the state of the most important external factor believed to drive interannual variations in the upper ocean carbon cycle. Variations in winter-time convection clearly emerge as the main factor near Bermuda, while SST variations appear to be the leading external forcing at the Hawaiian time-series station. Figure 10.3.12 depicts idealized seasonal cycles of the upper ocean carbon cycle at the two sites in the respective modes.

Near Bermuda, years with intense winter time convection start their seasonal cycle with positive $sDIC$ anomalies because of the anomalously large entrainment of $sDIC$ from the thermocline. SSTs tend to be colder during these years. These colder temperatures outweigh the pCO_2 increasing effect of the positive $sDIC$ anomalies, leading to negative oceanic pCO_2 anomalies. Coupled with the higher-than-normal winds, this leads to a substantially larger uptake of CO_2 from the atmosphere during these years. Biological productivity is also inferred to be higher, presumably a consequence of the higher nutrient input from below. These two factors lead to an enhanced seasonal cycle of $sDIC$, but with an overall positive $sDIC$ anomaly. Years with anomalously shallow winter-time convection tend to follow the reverse pattern. The differences between the two modes are quite substantial and amount to up to 50% variations of the annual mean fluxes.

Near Hawaii, differences between the two modes are somewhat less marked, but still significant. In warmer than normal years, net community production tends to be reduced, which should lead to a positive anomaly in $sDIC$. This is outweighed by weaker uptake of CO_2 from the atmosphere caused by SST induced positive pCO_2 anomalies and weaker winds, and a weaker than normal addition of DIC by lateral transport. These two factors

lead to the observed negative $sDIC$ anomalies in warm years.

The data from the subtropical gyres thus indicate a substantial sensitivity of the upper ocean carbon cycle to variations in meteorological forcing. The main driving forces are similar at the two sites, heat fluxes and wind, but their impact on the upper ocean carbon cycle takes different routes. Near Bermuda, the influence of these two forces on the upper ocean carbon cycle is primarily expressed through changes in the amount of $sDIC$ and nutrients that are entrained in the surface mixed layer, while near Hawaii, the impact is more direct by primarily changing air-sea gas exchange, and secondly by altering lateral transport.

Since interannual variations in wind and heat fluxes tend to vary in concert over large spatial-scales, it is conceivable that the observed local variations near Bermuda and Hawaii are representative over larger regions. For example, an extrapolation of the air-sea flux anomalies observed near Bermuda to the entire subtropical gyre of the North Atlantic yields air-sea flux anomalies of the order of $\pm$ 0.3 Pg C yr^{-1} [*Gruber et al.*, 2002]. A similar extrapolation of the Hawaii record gives integrated air-sea flux anomalies for the southern subtropical gyre of the Pacific of similar magnitude [*Brix et al.*, 2004]. It thus appears as if the extratropical ocean may be more variable than suggested by current oceanic modeling studies. However, more direct comparisons of these models with the in situ constraints near Bermuda and Hawaii suggest that the models are relatively successful in capturing these variations, but that they tend to simulate air-sea CO$_2$ flux variations at higher latitudes that tend to be opposite in phase to those at lower latitudes, thus suppressing the variability when fluxes are integrated over entire ocean basins.

Too many things are still unknown or ill constrained in order to make a final assessment of what the role of the ocean is in generating the observed interannual variability in atmospheric CO$_2$. One can expect, however, rapid progress over the next years, as the number of sites where interannual variability can be investigated will increase dramatically. But, irrespective of the uncertainties associated with the current assessment, it is clear that the oceanic carbon cycle responds sensitively to changes in meteorological forcing. On short time-scales the impact of these changes on atmospheric CO$_2$ will be suppressed because of the long equilibration time-scale associated with the exchange of CO$_2$ across the air-sea interface. On time-scales of decades and longer, this constraint is substantially less important. Furthermore, the reservoir of DIC in the ocean that can exchange with the atmosphere increases as the time-scale of the variations of interest increases. On time-scales of several hundreds of years, the entire oceanic reservoir of DIC is available for exchange, which, given the fact that this reservoir is 60 times larger than that of the atmosphere, makes the ocean the primary factor controlling atmospheric CO$_2$ on centennial and longer time-scales. In the next section, we will investigate the most prominent example of such variations, the glacial-interglacial change in atmospheric CO$_2$.

Figures

Figure 10.3.1: Plot of variations in growth rates of atmospheric CO$_2$, fossil fuel emissions, and inferred net carbon sinks. Arrows indicate the occurrence of El Niño events in the equatorial Pacific. Such events are usually accompanied by an initial decrease in the growth rates followed by a strong increase. The annual growth rates have been calculated from the annual mean atmospheric CO$_2$ concentrations and are plotted in the forward year. Data are from the Mauna Loa observatory, Hawaii (MLO) and from the South Pole Station, Antarctica (SPO). Adapted from *Sarmiento and Gruber* [2002].

Figure 10.3.2: Time series of interannual sea-to-air flux of CO$_2$ as estimated by different studies. Estimates in the top panel are based on ocean observations and models, whereas those in the bottom panel are from atmospheric observations and models. The oceanic observations in the top panel are based on pCO$_2$ measurements in the equatorial Pacific only [*Feely et al.*, 1997] and are represented as deviations from a mean of 0.5 Pg C yr^{-1}. Shown are estimates from *LeQuéré et al.* [2000], *Winguth et al.* [1994], *Lee et al.* [1998], *Keeling et al.* [1995], *Francey et al.* [1995], *Joos et al.* [1999], *Rayner et al.* [1999]. Adapted from *LeQuéré et al.* [2000].

Figure 10.3.3: Surface distribution of properties during non-El Niño (left column) and during El Niño (right column) conditions in the eastern equatorial Pacfic. (a) and (b) pCO$_2$ difference between the surface ocean and the atmosphere; (c) and (d) estimated sea-to-air CO$_2$ flux; (e) anf (f) surface nitrate concentrations; and (g) and (h) surface chlorophyll. From [*Chavez et al.*, 1999].

Figure 10.3.4: Vertical section of potential pCO$_2$ in the equatorial Pacific. Potential pCO$_2$ is the CO$_2$ pressure a sample would achieve if it were isochemically depressurized (to 1 atm) and warmed (to 25°C) (see text). From *Broecker and Peng* [1982].

Figure 10.3.5: Salinity normalized *DIC* versus nitrate in the upper 200 m between the equator and 5°S along (a) 110°W; (b) 125°W; and (c) 140°W, during boreal spring. The deviation of the surface values (dashed line) from the trend in the thermocline (solid line) is attributed to the loss of *DIC* by outgassing. From [*Wanninkhof et al.*, 1995].

Figure 10.3.6: Time-series of air-to-sea CO_2 flux anomalies for the eastern equatorial Pacific. From *Peylin et al.* [2004]. The black line and the grey band are estimates based on an inversion of atmospheric CO_2 [*Bousquet et al.*, 2000]. The green and blue-dashed curves represents the model based estimatea of *McKinley* [2002] *LeQuéré et al.* [2000], respectively. The symbols represent estimates based on a compilation of oceanic data [*Feely et al.*, 1999]. The Southern Oscillation Index (SOI) index is also shown as a Reference (right axis). From *Peylin et al.* [2004].

Figure 10.3.7: Schematic structure of the 4-box model used by *Siegenthaler and Wenk* [1989] for simulating ENSO events. A: atmosphere, E: equatorial Pacific surface water, M: mid-latitude Pacific surface water, T: thermocline. F_u and F_{mu}: water fluxes, P_T and P_M: biological particle fluxes. From [*Siegenthaler and Wenk*, 1989].

Figure 10.3.8: Simulated response of the 4-box model to a simulated El Niño event starting at the beginning of model year 15 and lasting one year. (a) prescribed time evolution of the upwelling flux F_u; (b) predicted atmospheric CO_2 concentration; (c) simulated atmospheric CO_2 growth rate variations; (d) simulated variations in pCO_2 of equatorial surface waters; (e) simulated variations in temperature of equatorial surface waters; and (f) carbon fluxes into and out of the equatorial surface water box. From [*Siegenthaler and Wenk*, 1989].

Figure 10.3.9: Maps of satellite based estimates of interannual variance of key drivers for the ocean carbon cycle: (a) Sea-surface temperature, (b) mixed layer depth, and (c) Export production. Sea-surface temperature is based on AVHRR, mixed layer depth has been deduced from Topex/Poseidon's measurements of sea surface height and AVHRR, and export production has been estimated based on SeaWiFS. See *LeQuéré and Gruber* [2004] for details.

Figure 10.3.10: Timeseries of anomalies in (a) SST, (b) salinity normalized *DIC*, (c) ^{13}C/^{12}C ratio of *DIC* (c) calculated pCO$_2$ at stations "S"/BATS near Bermuda and at station ALOHA near Hawaii. Anomalies have been computed by removing the average seasonal cycle and a linear long-term trend. Data are from *Gruber et al.* [2002] and *Brix et al.* [2004].

Figure 10.3.11: Observed and diagnosed interannual variability at Station "S"/BATS near Bermuda and Station ALOHA near Hawaii. Shown are the anomalies of all properties after the mean seasonal cycle has been removed (a) winter-time mixed layer (b) air-sea gas exchange, (c) entrainment, (d) net community production, (e) SST anomalies, (f) air-sea gas exchange, (g) horizontal transport, and (h) net community production. The lines in (b-d) and (f-h) represent $+/-$ one standard deviation uncertainty estimates from Monte Carlo experiments. From *Gruber et al.* [2002] and *Brix et al.* [2004].

Figure 10.3.12: Schematic illustration of the seasonal carbon cycle at Station "S"/BATS near Bermuda and at Station ALOHA near Hawaii and its interannual modulations. The main physical forcing mechanism near Bermuda is winter mixed layer depth variations, while it is SST variations near Hawaii. Modified from *Gruber et al.* [2002] and *Brix et al.* [2004].

10.4   Glacial-interglacial atmospheric CO_2 changes

The largest variations in atmospheric CO_2 in the past occured in connection with the glacial-interglacial cycles that characterized earth's climate over the past million years (Figure 10.1.2). During full glacial conditions, such as prevailed on the Earth about 20,000 years ago, the atmospheric mixing ratio CO_2 was about 80 ppm lower than the pre-anthropogenic interglacial value of about 280 ppm. Recent backward extensions of atmospheric CO_2 records from ice cores showed that the 80 ppm rise that occured at the close of the last glaciation also characterized the close of the preceeding three glaciations [*Fischer et al.*, 1999, *Petit et al.*, 1999]. The tight connection between variations in atmospheric CO_2 and temperature becomes even more evident in Figure 10.4.1, where the atmospheric CO_2 record over the last 420,000 years from an Antarctic ice-core drilled at Vostok is plotted together with a temperature reconstruction on the basis of isotopic variations contained in the ice. Also shown is a proxy record of ice volume, which demonstrates that not only did temperatures in Antarctica get colder during the ice-ages, but also likely the whole earth system, leading to the formation of massive ice-sheets on land. Model simulations suggest that the 80 ppm change in atmospheric CO_2 accounts for more than half of the necessary change in radiative forcing in order to drive earth's climate from interglacial to glacial conditions [*Weaver et al.*, 1998, *Webb et al.*, 1997]. Less clear is whether CO_2 is a primary driver or a secondary amplifier of the glacial cycles.

Despite the clear importance of atmospheric CO_2 as an amplifier or even as a driver of glacial cycles, the mechanisms responsible for the glacial/interglacial CO_2 changes have remained unresolved ever since these changes were first observed about 25 years ago [*Berner et al.*, 1979, *Delmas et al.*, 1980, *Neftel et al.*, 1982]. Our inability to clearly decipher the mechanisms that led to these large changes in atmospheric CO_2 in the past clearly indicates that there are important aspects of the carbon cycle we do not understand, and that my hinder our ability to predict how the global carbon cycle may respond to future climate change. One of the few things that are well established, is that the cause for these changes must lie in the ocean [*Broecker*, 1982]. The $CaCO_3$ rocks on land, which contain by far the largest fraction of inorganic carbon, are interacting too slowly with the rest of the global carbon cycle to account for changes over glacial cycles [*Berner et al.*, 1983]. The terrestrial biosphere could absorb additional CO_2 from the atmosphere on these time scales, but any such change would be quickly dampened by the interaction with the ocean's huge carbon reservoir (see Figure 10.1.1). Furthermore, carbon-13 isotope data from the deep ocean indicate that the terrestrial biosphere actually released CO_2 during glacial times [*Shackelton*, 1977], making the need for an oceanic sink even larger.

Therefore the search for an explanation of the glacial/interglacial atmospheric CO_2 variations must focus on the factors controlling the pCO_2 in the ocean surface water. Since

surface ocean pCO$_2$ is controlled by temperature, salinity, DIC, and Alk, changes in any of these properties alone or in conjunction could do the job. Over the last two decades many hypotheses have been proposed to explain the glacial-interglacial CO$_2$ variations in the atmosphere (see summary in Table 10.4.1). But so far, each of them has failed in turn to conform to the increasing number of constraints placed on the glacial carbon cycle from paleoceanographic and paleoclimate records.

We will first begin with a discussion of the processes whose impact is relatively well known, such as temperature and salinity changes, but also the loss of carbon from the terrestrial biosphere, which needs to be compensated by the ocean. We will see that these three processes lead to nearly no change in atmospheric CO$_2$, because the cooling effect is nearly offset by the atmospheric CO$_2$ increase stemming from the loss of carbon from the terrestrial biosphere and the increase in oceanic pCO$_2$ resulting from the increase in salinity. This means that changes in the surface ocean DIC and Alk must be the primary means of reducing atmospheric CO$_2$. These concentrations are primarily controlled by the soft-tissue and the carbonate pumps, interacting with ocean circulation. We will guide our search for the causes of these changes in these two pumps by first reviewing the evidence that this search should focus on the high-latitudes, particularly the Southern Ocean. This Southern Ocean focus is a result of the fact that this region is the primary region that connects the surface ocean with the deep ocean reservoir that contains most of the carbon in the combined atmosphere-ocean system. This focus is also justified by the observation that changes in the low-latitudes appear to have substantially less influence on atmospheric CO$_2$. If this is correct, it would greatly narrow the number of candidate processes that need to be investigated, but we will see that the high-latitude dominance is likely somewhat less strong than previously thought. Nevertheless, Southern Ocean based hypotheses are still the primary candidates for explaining the lower atmospheric CO$_2$ concentrations, and we will therefore discuss these hypotheses in detail, including their evaluation with paleoceanographic constraints. Low-latitude based hypotheses have mostly been rejected, but scenarios that invoke a change in the export of CaCO$_3$ relative to that of organic matter on a global scale can lead to large changes in atmospheric CO$_2$ through a process called CaCO$_3$ compensation (see Chapter 9) and therefore need to be considered as well. We end with a possible synthesis scenario that combines several elements and appears to be consistent with most constraints. The reader interested in more detail is referred to the excellent review by *Sigman and Boyle* [2000], and the papers by *Broecker and Peng* [1998] and [*Archer et al.*, 2000]. *Broecker* [1995] and *Imbrie and Imbrie* [1986] provide more general overviews of the climate changes associated with glacial/interglacial cycles.

SETTING THE SCENE

Terrestrial biosphere carbon loss

During the last glacial maximum (LGM), about 20,000 years ago, ice-sheets extended in the Northern hemisphere as far south as 40°N, covering most of Alaska and Canada on the North American continent, and covering all of Scandinavia and northern Russia and Siberia on the Eurasian continent [*Peltier*, 1994]. This resulted in a substantial loss of land available for vegetation to grow, which was only partially compensated by the increase in land due to the lower sea-level stand. In addition, cooler temperatures prevailed over much of earth, with most estimates indicating a cooling of several °C, even in the tropics (e.g. *Stute et al.* [1995]), associated with a significant slowdown of the hydrological cycle (e.g. *Yung et al.* [1996]). This led to cooler and drier conditions over much of the land surface, except in a few areas such as the southwestern U.S., where the presence of large inland lakes suggest wetter conditions during the LGM. These changes over land impacted global biogeochemical cycles in two major ways. First, the substantial reduction of areas suitable for ecosystems that store substantial amounts of carbon led to the loss of substantial amounts of carbon from the terrestrial biosphere. Second, the generally drier conditions and the existence of extensive desert-like areas caused an increase in the mobilization of dust, which presumably increased the transport and deposition of it over the ocean [*Mahowald et al.*, 1999].

Shackelton [1977] estimated the magnitude of the carbon release by the terrestrial biosphere by looking at oceanic changes in the ^{13}C/^{12}C ratio of *DIC*. Since terrestrial CO$_2$ has a much lower ^{13}C/^{12}C ratio than ocean *DIC*, the oceanic uptake of terrestrially derived CO$_2$ would lead to a whole ocean change in the ^{13}C/^{12}C ratio of *DIC*, whose magnitude is proportional to the ^{13}C/^{12}C ratio of terrestrial biosphere and the magnitude of the release. Using calcite shells of foraminifera that either dwelled in near surface waters or in the surface sediments, he reconstructed the oceanic ^{13}C/^{12}C ratios of *DIC* in both near surface and near bottom waters, thereby eliminating changes that are due to ocean internal redistributions of carbon. He arrived at a terrestrial biosphere loss of about 500 Pg C. More recent reconstructions put the loss in the range of 300 to 700 Pg C [*Curry et al.*, 1988, *Bird et al.*, 1994, *Bird et al.*, 1996, *Beerling*, 1999]. This represents up to nearly 30% lower carbon storage in the terrestrial biosphere compared to the amount of carbon stored in the terrestrial biosphere today, which is about 2300 Pg C (see Figure 10.1.1).

An even smaller terrestrial biosphere is estimated for the LGM by biome reconstructions on the basis of terrestrial pollen data [Harrison et al., 1998; Jolly et al., 1998; Prentice et al., 2000]. These data suggest a terrestrial biospheric carbon loss of 700-1400 GtC [Adams and Faure, 1998], but these estimates need to be viewed with greater caution

than those based on the C-13 mass balance, due to large gaps in the data considered, and assumptions about the average carbon density of different biomes.

In order to evaluate the impact of this reduction in the carbon storage of the terrestrial biosphere, we need to consider how much of this biospheric loss actually remained in the atmosphere. This problem is directly analogous to our discussion of the anthropogenic CO$_2$ uptake by the ocean, except that for the glacial-interglacial changes considered here, the relevant time-scales are several thousand years. On such time-scales, we can assume that the equilibration of the atmospheric perturbation with the oceanic reservoir of *DIC* is complete, and that the buffering by the dissolution of oceanic CaCO$_3$ is nearly complete as well. However, buffering with CaCO$_3$ on land, and silicious rocks are too slow to represent important sinks for atmospheric CO$_2$ on these timescales. We infer from Figure 10.2.2 that the fraction remaining in the atmosphere after equilibration with the ocean and seafloor CaCO$_3$ is about 8% for a release of the order of 1000 Pg C or less. If we adopt a terrestrial release estimate of 500 Pg C, about 40 Pg C will remain in the atmosphere even after reaction with seafloor CaCO$_3$, leading to an atmospheric CO$_2$ increase of about 18 ppm. Therefore, rather than explaining a 80 ppm G-IG difference by an oceanic mechanisms, we now need to explain a nearly 100 ppm difference!

It is instructive to consider how exactly the oceanic carbon cycle buffered this terrestrial release. As is the case for anthropogenic CO$_2$, the primary buffering by the ocean occurs by the chemical reaction of the excess CO$_2$ with the CO$_3^{2-}$ ion, leading to a substantial reduction in the oceanic mean CO$_3^{2-}$ concentration. As a result, the mean depth of the CaCO$_3$ saturation horizon shifted upward, exposing a larger fraction of the seafloor sediments to waters undersaturated with regard to CaCO$_3$ (see Figure 10.4.2). Since the CaCO$_3$ saturation horizon is the primary factor controlling CaCO$_3$ dissolution in marine sediments, this upward movement led to increasing CaCO$_3$ dissolution. This process continues until the oceanic mean Alk concentration has increased to the level that the oceanic mean CO$_3^{2-}$ ion concentration is the same as before the perturbation. This is because at this point, the CaCO$_3$ saturation horizon has returned to its original position, ensuring again a balance between the Alk input by rivers and Alk loss by burial (Figure 10.4.2c). The oceanic CaCO$_3$ system responds therefore as a "homeostat", buffering the atmospheric CO$_2$ perturbation. Its response requires a temporary upward excursion of the CaCO$_3$ saturation horizon and presumably the ocean's lysocline. The opposite occurs during the buildup of the terrestrial biosphere carbon reservoir [*Broecker et al.*, 2001], leading to a preservation event in the ocean's sediments. The slow time-scale associated with this "reverse" CaCO$_3$ compensation has been proposed as a mechanism to explain post-glacial variations in atmospheric CO$_2$ during the present warm period, i.e. the holocene [*Broecker et al.*, 2001], although this effect seems to be too small [*Joos et al.*, 2004].

Salinity changes

During the last glacial maximum, the ocean surface was both cooler and saltier than today's ocean surface. The salinification of the ocean was a consequence of the buildup of huge continental ice sheets that locked large amounts of fresh water on land away from the ocean. The cooling and salinification of the surface ocean have opposing effects on its pCO$_2$, and hence on atmospheric CO_2. We know from (8.3.4) that surface ocean pCO$_2$ drops by about 10-12 μatm per $^\circ$C of cooling. However, we cannot simply take the salinity sensitivity of pCO$_2$ as given in (8.3.5), because this sensitivity only takes the impact of salinity on the dissociation into account (the so-called salting out effect), but disregards the fact that the total concentrations of DIC and Alk in the ocean were higher as a result of removing freshwater with zero Alk and near-zero DIC from the ocean. We can estimate the total change in oceanic pCO$_2$ that results from salinification by considering the total derivative of pCO$_2$ with regard to changes in salinity, DIC, and Alk while keeping temperature constant.

$$\Delta p\text{CO}_2 = \Delta S \left.\frac{\partial p\text{CO}_2}{\partial S}\right|_{DIC,Alk=\text{const}} + \Delta DIC \left.\frac{\partial p\text{CO}_2}{\partial DIC}\right|_{Alk,S=\text{const}} + \Delta Alk \left.\frac{\partial p\text{CO}_2}{\partial Alk}\right|_{DIC,S=\text{const}},$$
$$(10.4.1)$$

where ΔDIC, and ΔAlk are the salinity induced changes in DIC and Alk. A simple mass balance shows that these latter two changes are proportional to the salinity changes, ΔS, with the proportionality given by the respective mean concentrations, i.e. $\Delta DIC = (DIC/S)\Delta S$, and $\Delta Alk = (Alk/S)\Delta S$. Inserting these proportionalities into 10.4.1, and using the definitions of the buffer factor, γ_{DIC} (8.3.14), the alkalinity factor γ_{Alk} (8.3.15) and the salinity dependence, $\gamma_S = (S/p\text{CO}_2)(\partial p\text{CO}_2/\partial S)$ (8.3.5), we obtain

$$\Delta p\text{CO}_2 = \Delta S \frac{p\text{CO}_2}{S} \left(\gamma_S + \gamma_{DIC} + \gamma_{Alk}\right) \approx \Delta S \frac{350\ \mu\text{atm}}{35} \left(1 + 10 - 9.4\right) \approx 16\ \mu\text{atm}\ \Delta S,$$
$$(10.4.2)$$

where we used global mean values for the different γ's (see chapter 8). Therefore, the salinity induced changes in DIC and Alk increase the oceanic pCO$_2$ lead to an approximately 16 μatm change per unit change of salinity, instead of just a 10 μatm change if DIC and Alk were held constant.

We next need to know the magnitude of the salinity change. During peak glacial times, sea-level is believed to have been about 120 to 140 m lower than it is today [*Bard et al.*, 1996, *Adkins et al.*, 2002]. This is roughly equivalent to the removal of about 3% of today's volume of the ocean. Since the amount of salt remained the same, mean ocean salinity must have changed by about $0.03 \cdot 35 = 1.1$ salinity units. As this change occured uniformly over the entire ocean, we can directly estimate from 10.4.2 that this change led to an atmospheric CO_2 increase of about 18 ppm.

Temperature changes

Sea-surface temperatures during the LGM are thought to be on average about 2 to 4°C colder than today. The exact magnitude and distribution of these changes is still intensively debated [*Broecker*, 1996]. The original findings of the CLIMAP program [*CLIMAP Project members*, 1981] on the basis of a detailed analysis of foraminiferal assemblages suggested 2-4°C colder temperatures in the mid to high-latitudes of the Southern hemisphere and in the North Pacific, 4-8°C cooling in the North Atlantic, and virtually no change in the tropics and temperate regions. Reconstructions based on oxygen isotopes preserved in pelagic foraminifera [*Broecker*, 1986, *Birchfield*, 1987] generally support such little cooling in the tropics. However, these findings, particularly the small cooling in the tropics, have become seriously challenged over the last few years. The first indication of substantially colder temperatures in the tropics came from measurements of the strontium to calcium ratios in marine corals [*Guilderson et al.*, 1994, *Beck et al.*, 1997] that suggest tropical cooling of up to 6°C. Additionally, *Schrag et al.* [1996] showed that the temperature change based on the oxygen isotopes might have been substantially underestimated by assuming a too small change in oxygen-18 in seawater from the growth of ice-sheets on land.

Cooler tropical SSTs are also in good agreement with terrestrial temperature proxies, including snow line elevations, noble gases in groundwater and pollen records (e.g. *Stute et al.* [1995]). On the other hand, temperature proxy records on the basis of marine alkenones, chain-like organic molecules manufactured by marine plants [*Bard et al.*, 1997], show that the tropical cooling was likely not more than 2°C. It is presently unclear whether the disagreement between the different proxies reflect regional differences in the extent of cooling, or whether neglected or underestimated effects are affecting one proxy group or the other [*Broecker*, 1996]. We need to worry about this unresolved puzzle in our quest to understand the causes of the glacial-interglacial CO$_2$ variations. Temperature would appear to explain a significant fraction of the atmospheric CO$_2$ change if the ocean indeed cooled by 6°C over a large fraction of its surface, including the high-latitudes. This is because under isochemical conditions, a 6°C change causes a pCO$_2$ change of about 60-70 μatm.

However, two caveats greatly diminish the importance of temperature as a possible driver for glacial-interglacial changes. The first one is that temperature changes in the high-latitudes were quite certainly smaller than 6 °C. Since most of these waters are already close to the freezing point, it is more likely that temperature changes in the high-latitude regions were only around 1 to 2°C. The second caveat is that changes in the low-latitudes tend to have a smaller effect on atmospheric CO$_2$ compared to the high latitudes, despite the fact that the low latitudes cover approximately 80% of the total surface ocean area. The primary reason for the greater importance of the high latitudes is the fact that they

are the primary conduit for the exchange of water and carbon between the surface ocean and the large reservoir of the deep ocean. We will discuss this issue in detail below. The most current estimates of the impact of cooling suggest an atmospheric CO_2 decrease of the order of 30 ppm [*Sigman and Boyle*, 2000].

In summary, it appears that the three relatively well constrained processes, i.e. loss of carbon from the terrestrial biosphere, increase in ocean salinity, and ocean cooling, are unable to explain the 80 ppm drawdown in atmospheric CO_2 that occured during glacial maxima. More specifically, if we take the 18 ppm increase from terrestrial biosphere carbon release, the 18 ppm increase from salinity change, and the 30 ppm decrease from cooling together, we arrive at a near zero change in atmospheric CO_2. Clearly other processes must be at work.

<div align="center">FUNDAMENTAL MECHANISMS</div>

Since changes in the solubility of CO_2 forced by changes in salinity and temperature can be ruled out as a cause for the glacial drawdown of atmospheric CO_2, the drawdown must be caused by processes that affect the oceanic distribution of DIC and Alk. A useful framework to start the discussion is equation (8.3.3), which links changes in DIC and Alk to pCO_2 changes:

$$pCO_2 \approx \frac{K_2}{K_0 \, K_1} \frac{(2DIC - Alk)^2}{Alk - DIC} \qquad (10.4.3)$$

This approxmiation shows that in order to decrease surface ocean pCO_2 and hence atmospheric pCO_2, the processes must cause either a decrease of surface ocean DIC, an increase in surface ocean Alk, or a combination of these two effects.

Fundamentally, changes in any of the three carbon pumps discussed in chapter 8, i.e. the soft-tissue pump, carbonate pump, and gas exchange pump, can contribute to the decrease in surface DIC. In thinking about the action of these pumps, it is also important to recall that the surface to deep gradient, $DIC_s - DIC_d$, generated by the biological pumps in a simplified one-dimensional framework not only depends on the magnitude of the downward transport of organic matter $\Pi^{C_{org}}$ and $CaCO_3$, Π^{CaCO3_3}, but also on the magnitude of vertical transport and mixing, ν, (see equation (1.2.3)), thus

$$DIC_s = DIC_d + \frac{\Pi^{C_{org}} + \Pi^{CaCO3_3}}{\nu}. \qquad (10.4.4)$$

Therefore, the surface ocean concentration, DIC_s, can be reduced not only by an increase in the export of carbon, but also by a reduction in vertical transport and mixing, ν. Undeniably, both cases need to be considered. A reduction in C_d, reflecting essentially a reduction in whole ocean DIC could also be invoked, but we are unaware of a mechanism that could have caused such a decrease. In fact, the whole ocean DIC must have been higher during the LGM than it is today, because of the decrease in ocean volume, because

of the uptake of the carbon lost from the terrestrial biosphere, and because of the additional uptake of CO_2 from the atmosphere required to lower atmospheric CO_2.

Analogous to DIC, the surface ocean Alk concentration, Alk_s is governed by the deep concentration, Alk_d, and the balance between the export of $CaCO_3$ and organic carbon, and the re-supply by mixing and transport:

$$Alk_s = Alk_d + \frac{2\Pi^{CaCO_3} - r_{N:C}\Pi^{C_{org}}}{\nu}, \qquad (10.4.5)$$

where $r_{N:C}$ is the nitrogen to carbon ratio of the organic matter exported from the surface coean. We can therefore increase the surface concentration of Alk by decreasing the strength of the carbonate pump, by increasing the strength of the soft-tissue pump, or by increasing the deep concentration Alk_d. The latter change can be accomplished by dissolving $CaCO_3$ sediments, or increasing the Alk input into the ocean by rivers.

We thus have to consider changes in ocean circulation, in surface ocean production of organic matter and $CaCO_3$ and their subsequent export and remineralization, in river input, and in the interaction with the $CaCO_3$ in the sediments as possible candidate processes driving the glacial/interglacial changes in atmospheric CO_2. We also have to consider changes in air-sea gas exchange, as changes in the kinetics of the exchange of CO_2 across the air-sea interface can lead to changes in surface DIC as well (see discussion about the gas exchange pump in chapter 8). Given this myriad of possible processes, our search for a cause of the glacial CO_2 drawdown would be greatly aided if we had some guidance as to which region and which processes we need to focus on.

Southern Ocean Dominance

It was recognized early on that not all regions of the world's ocean exert an equal influence on atmospheric CO_2. A series of seminal papers in the early 1980s pointed out that the high-latitude oceans, despite their limited area, dictate the atmospheric CO_2 content to a large extent [*Knox and McElroy*, 1984, *Sarmiento and Toggweiler*, 1984, *Siegenthaler and Wenk*, 1984]. Since these independent studies were done at Harvard, Princeton, and Bern (Switzerland) respectively, *Broecker and Peng* [1998] coined the expression Harvardton-Bears to refer them as a group. This concept of high-latitude dominance has been extremely influential in shaping the discussion about the causes for the glacial/interglacial changes in atmospheric CO_2.

The dominance of the high-latitude regions is a consequence of the direct connection that exists between the high-latitude ocean and the deep ocean through deep water formation and isopycnal ventilation, pinning the chemistry of the high-latitude surface ocean very close to that of the deep ocean. By contrast, the link between the cold and dense waters of the deep ocean (cold water sphere) and the warm and light waters of the low-latitudes (warm water sphere) is much weaker, a direct consequence of ocean interior flow occuring along isopycnal surfaces. An additional reason for the high-latitude dominance

stems from the fact that the transport of CO_2 via the atmosphere between the low-latitude and high-latitude regions is sufficiently rapid to bring the pCO_2 of the low-latitude surface ocean close to that of the high-latitudes. As a result, any anomalous CO_2 created in the low-latitudes will escape into the atmosphere, and tend to be taken up by the high-latitude oceans and ultimately buffered in the deep ocean, leading to only a small net change in atmospheric pCO_2. In order to illustrate this contraint, we use the three-box model introduced in chapter 1 (Figure 10.4.3) and perturb either the high-latitudes or low-latitudes with a warming of 2°C. Figure 10.4.4 shows that in the new steady-state, the 2°C warming in the high-latitudes causes an atmospheric CO_2 change of 15 ppm, whereas the same warming in the low-latitudes causes an atmospheric CO_2 change that is 5 times smaller, i.e. only 3 ppm. In the latter case, most of the CO_2 that is expelled from the low-latitudes is taken up by the high-latitudes and buffered by the deep ocean reservoir. We term this process *equilibration*.

<div align="center">*Equilibration of low-latitude changes*</div>

What determines the magnitude of this low-latitude equilibration effect, i.e. the substantial reduction in the impact of low-latitude changes on atmospheric CO_2? It turns out that the degree of equilibration depends on the relative magnitude of air-sea gas exchange versus the magnitude of the exchange between the surface and deep ocean. If air-sea gas exchange is efficient in equilibrating the atmosphere and surface ocean, atmospheric pCO_2 will be almost entirely determined by the high latitudes and will not respond to low-latitude changes. Conversely, if air-sea gas exchange is slow relative to the exchange between the cold and warm water spheres, changes in low latitude chemistry and temperature can lead to substantial changes in atmospheric CO_2.

Given the importance of this equilibration constraint, it behooves us to investigate it further. We return to the three-box model (Figure 10.4.3) since it captures the relevant processes, while being simple enough to understand it straightforwardly. The defining characteristics of this model are (i) separation of ocean surface into a low-latitude box and a high-latitude box, (ii) a deep box, whose volume comprises nearly 97% of the total volume of the ocean, rendering its chemistry nearly immutable to internal redistributions of carbon, but not to external perturbations, such as associated with the dissolution of $CaCO_3$, (iii) an exchange term that couples the high-latitude box very closely to the deep ocean, and (iv) an overturning term, which represents sinking in high-latitudes and upwelling in low-latitudes. While various shortcomings of this model have been noted, such as the fact that there is little upwelling of deep waters directly in the warm low-latitudes (see discussion in chapter 7 and [*Toggweiler*, 1999]), this model is nevertheless very instructive. Temperatures of this model are set to 21.5°C for the low-latitude box and 2°C for the high-latitude box. By design, the deep box will have the same temperature as the high-latitude box, i.e. 2°C.

We investigate the equilibration effect in this model by initializing it with homogeneous DIC and Alk and by then determining how the carbon is redistributed within the system depending on the relative rates of air-sea exchange and ocean mixing (see Figure 10.4.5). As the equilibration effect is primarily determined by physical processes, it is sufficient to neglect biology and consider only an abiotic ocean. Alkalinity is set to 2340 μmol kg^{-1} in all boxes and DIC is initialized to 2150 μmol kg^{-1}, yielding an initial pCO_2 of 280 μatm at the surface of the high-latitude box and an initial pCO_2 of 630 μatm at the surface of the low-latitude box. The model is then run forward in time until it reaches a steady-state.

We first investigate a case where the transport of DIC between the surface and deep ocean is far more rapid than the transport of CO_2 from the warm surface reservoir via atmosphere to the cold surface reservoir (Figure 10.4.5c). This is accomplished by reducing the gas exchange coefficient to a very small number. No equilibration will occur in this case as the DIC concentration in the low-latitude surface box will remain relatively close to the mean concentration of the deep box. As some carbon will be lost to the atmosphere, the mean oceanic DIC concentration drops somewhat to about 2130 μmol kg^{-1}, yielding a low-latitude pCO_2 of 561 μatm, and a high-latitude pCO_2 of 247 μatm. Given the slow exchange of CO_2 between the ocean and atmosphere, the atmospheric pCO_2 is in this case simply equal to the area weighted means (0.20 x 247 μatm + 0.80 * 561 μatm = 514 μatm). The other extreme is a case, where the rate of CO_2 transfer between atmosphere and ocean far outstrips the rate of water circulation and mixing (Figure 10.4.5b). In this case, full equilibration will occur, and the pCO_2 in all surface boxes would be equal to that of the atmosphere. Integration of the model gives a value of 281 μatm. If the model parameters are set to "realistic" values of 20 Sv for the transport of water around the thermohaline circuit, to 60 Sv for the high-latitude to deep ocean mixing term, and to 13 cm h^{-1} for the piston velocity of CO_2, atmospheric pCO_2 stabilizes at 303 μatm.

Broecker et al. [1999] attempted to capture the degree of this deep ocean equilibration effect of low-latitude changes by the Harvardton-Bear Equilibration Index (HBEI). They defined this index in such a way that it describes how close the realistic case is to the full equilibration case weighted by the difference between the two extreme cases of full and no equilibration:

$$\text{HBEI} \quad = \quad \frac{pCO_2^{\text{atm}}\big|_{\text{realistic}} - pCO_2^{\text{atm}}\big|_{\text{full equil}}}{pCO_2^{\text{atm}}\big|_{\text{no equil}} - pCO_2^{\text{atm}}\big|_{\text{full equil}}}, \quad\quad (10.4.6)$$

$$= \quad \frac{303 - 281}{514 - 281} = 0.09. \quad\quad (10.4.7)$$

The value of the HBEI can be interpreted as an approximate measure of how effective a given change in the low latitudes is in changing atmospheric CO_2. An HBEI value of 1 means that no equilibration with the deep ocean occurs and therefore atmospheric CO_2 will respond proportionally to any change in low-latitude pCO_2. A value of 0 means

that full equilibration occurs, i.e. changes in low-latitude pCO_2 would have no impact on atmospheric CO_2, since atmospheric CO_2 is clamped by the high-latitudes in connection with the deep ocean reservoir. Note that the HBEI index is only an approximation of the degree of equilibration and atmospheric effectiveness, as the exact values depends on the magnitude of the perturbation because of the associated changes in the buffer factor.

The low HBEI value of 0.09 found by this simple three box model implies that for a given change in low-latitude pCO_2, only approximately 9% of this change multiplied with the fractional area of the low-latitudes, i.e. 0.85*0.9 = 0.08, would show up as a change in atmospheric CO_2. If this value of HBEI is correct, we can immediately rule out any low-latitude based hypothesis. For example, the discussion about the exact magnitude of low-latitude cooling would be largely irrelevant, since even a very large cooling of 6°C, leading to a low latitude pCO_2 reduction of 70 μatm, would cause only a 6 μatm reduction in atmospheric CO_2. However, before we can have any confidence in ruling out low-latitude based hypotheses, we need to ensure that this extremely low sensitivity of low-latitude changes is real and not just a peculiarity of this simple three-box model.

Broecker et al. [1999] computed the HBEI of a wide spectrum of models, ranging from simple box models to three-dimensional ocean biogeochemistry models (Figure 10.4.7). They found that three-dimensional coupled ocean circulation/biogeochemistry models show a substantially larger influence of the low-latitudes (HBEI indices up to 0.4) than the box models. It is presently not clear how large the HBEI of the real ocean is, but it is instructive to consider which processes determine its magnitude (see also *Archer et al.* [2000, *Ito and Follows* [2003, *Follows et al.* [2002]). Since the HBEI is a measure of the degree of equilibration between CO_2 anomalies in the low-latitudes and the deep ocean via exchange with the high-latitudes, any process that affects this equilibration changes the HBEI. Possible candidates are variations in the rate of CO_2 exchange across the air-sea interface, the magnitude and location of the mass exchange between the warm and cold water spheres and the reservoir sizes of these two spheres.

For example, as pointed out by *Toggweiler et al.* [2003], the exchange of CO_2 between the atmosphere and the high-latitude surface ocean is kinetically unconstrained in this three-box model, while this exchange experiences strong kinetic limitation in three-dimensional ocean models. This is primarily a result of the fact that the high-latitudes in the three box model were assigned a fractional area of 15%, while a census of the surface area of the ocean that has surface densities equal or denser than the deep ocean in a typical three-dimensional ocean model gives fractional areas of only a few percent. Restricting the high-latitude area so that the slowness of air-sea gas exchange becomes limiting for the exchange between the atmosphere and high-latitude box will work against equilibration, and therefore increase the HBEI. Figure 10.4.6a shows that if the high-latitude surface area in the three-box model is set to 3%, similar to what it is in three-dimensional ocean

circulation models, the HBEI index goes up to above 0.3. The effective surface area of the high-latitudes can also be decreased by increasing the fraction that is covered by sea-ice, leading to a similar increase in the HBEI index (Figure 10.4.7).

The magnitude of the exchange between the warm and cold water spheres and their relation to their reservoir sizes represents a second set of factors controlling the HBEI. Any increase in the exchange between the two reservoirs, e.g. by adding a low-latitude deep-ocean exchange (Figure 10.4.7c) would diminish the atmospheric equilibration pathway, and therefore increase HBEI. *Archer et al.* [2000] proposed that this mechanims is the primary factor explaining the large difference between the low HBEI of the original Harvardton-Bear box models, and the high HBEI of the three-dimensional ocean circulation models that participated in the comparison study of *Broecker et al.* [1999]. *Archer et al.* [2000] argued that because of their relatively coarse vertical resolution, these three-dimensional models tend to be overly diffusive vertically, therefore overestimating the HBEI index. On the other hand, *Follows et al.* [2002] pointed out that these three-dimensional models represent the warm-water sphere much more realistically than the Harvardton-Bear box models, as the warm-water sphere in the real ocean includes much of the upper and mid thermocline, whereas the Harvardton-Bear box models restrict it to a very thin surface layer. As a consequence, the warm-water sphere has almost no capacity in the Harvardton-Bear box models, while it may comprise more than 20% of the total ocean volume in the real ocean. Figure 10.4.7d shows that the HBEI increases as the volume of the warm-water sphere increases. In fact, expanding the volume of the low-latitude box and increasing the exchange between the low-latitude and deep boxes are structurally analogous, as both of them tend to increase the effective carbon reservoir size associated with the low-latitude surface, making equilibration with the deep ocean more difficult.

A last process to consider is the magnitude of the meridional overturning circulation, which is not captured in the Harvardton-Bear box models, but included in some of the 4 to 7 box models (e.g. [*Toggweiler*, 1999, *Lane et al.*, 2004]. For example, *Lane et al.* [2004] pointed out recently that the inclusion of a dynamic feedback of the changes in ocean temperature and salinity on the meridional overturning circulation during the last glacial led to a substantial increase in the sensitivity of atmospheric CO₂ to changes in the low latitudes. This suggests a note of caution when interpreting HBEI's computed for current interglacial conditions, as these values might be considerably different during glacial conditions.

In summary, it appears that the Harvardton-Bear box models likely underestimate the HBEI, and therefore underestimate the possible role of low-latitude changes. However, given the fact that the reservoir associated with the low latitudes is much smaller than the high-latitude surface and deep ocean reservoir, the equilibration of a change in the

low latitude surface ocean with the deep ocean is always going to be larger than the equilibration of a change in the high latitude surface ocean with the low latitude reservoir. Therefore, the low-latitudes are always going to be less effective in changing atmospheric CO_2 than the high-latitudes. In addition, substantial leverage exists in the high-latitudes to change surface ocean pCO_2 there, making the high-latitudes the primary region of focus for explaining the large atmospheric CO_2 changes associated with G/IG transitions. We therefore will first focus our discussion on this region.

<div align="center">CLOSING THE SOUTHERN OCEAN WINDOW</div>

We have seen in chapter 8 that the Southern Ocean represents an area of strong biologically driven outgassing of CO_2 (Figure 8.5.1). This outgassing is primarily a consequence of upwelling bringing waters with high concentrations of respired DIC (ΔC_{soft}) to the surface near the Southern Ocean Polar Front. Since biological productivity in these regions is too slow to fix all this excess CO_2, a substantial fraction of it escapes to the atmosphere. We highlighted in chapter 8 also that the existence of residual nutrients at the surface is a good indicator of this biologically induced CO_2 leak into the atmosphere. In steady-state the CO_2 lost to the atmosphere in the Southern Ocean is taken up elsewhere, particularly in those regions where the residual nutrients are taken up and used to fuel photosynthesis. The strength of the Southern Ocean leak is directly controlled by the balance between the upward supply of ΔC_{soft} and the downward export of organic matter. A reduction in the upward supply of DIC, while keeping organic matter export the same, will reduce surface ocean DIC, close the window and pull down atmospheric CO_2. Another option to close the window is to strengthen export production, while keeping the upward supply of DIC and nutrients the same. As the Southern Ocean represents the main window of the surface ocean to the deep ocean DIC reservoir, the closure of this window has a large impact on atmospheric CO_2.

We investigate this Southern Ocean window and its impact on atmospheric CO_2 with the same three-box model that we used above for the discussion of the HBEI index. In this case, we have to consider biological production and export, which we tie to phosphate. It is assumed that all phosphate is consumed in the low-latitude box, linking its biological export directly to the rate of supply of phosphate. In contrast, only a fraction of the phosphate is used in the high-latitudes. This leaves the biological production in the high-latitudes a free parameter and makes the high-latitude phosphate concentration, $[PO_4]_h$ a key diagnostic of the model. The full set of equations and a solution method is given by *Toggweiler and Sarmiento* [1985]. A steady-state solution for the high-latitude ocean DIC, DIC_h can be obtained in a manner analogous to that we have used for O_2 (see equation (1.2.11)):

$$DIC_h = DIC_d - r_{\text{C:PO}_4} \left([PO_4]_d - [PO_4]_h \right), \qquad (10.4.8)$$

The high latitude PO$_4^{3-}$ concentration is controlled by the balance between the rate of supply from the deep ocean and the rate of biological removal by high latitude export of organic phosphorus, Π_h^P:

$$[\text{PO}_4]_h = \frac{[\text{PO}_4]_d \, f_{hd} - \Pi_h^P}{f_{hd} + T}. \tag{10.4.9}$$

where f_{hd} is the high-latitude/deep-ocean mixing term, and T the overturning term (see also Figure 10.4.3). Inserting (10.4.9) into (10.4.8) gives:

$$DIC_h = DIC_d - r_{\text{C:PO}_4} \frac{[\text{PO}_4]_d \, T - \Pi_h^P}{T + f_{hd}}. \tag{10.4.10}$$

Thus any reduction in the mixing term, f_{hd}, or increase in biological export, Π_h^P or overturning circulation, T, will lead to a decrease in high-latitude DIC. Note that in the case of $T=0$, this equation is directly analogous to equation (10.4.4), except that the mixing term here is called $f_h d$ instead of ν. In order to determine atmospheric CO$_2$, one also would need to specify the changes in the low-latitude box. However, we have seen above that changes in the low-latitudes are much less effective in changing atmospheric CO$_2$, since changes in this reservoir tend to be compensated by equilibration with the deep ocean. This is not the case for high-latitude changes, so that any change in high-latitude pCO$_2$ leads to nearly corresponding changes in atmospheric CO$_2$. We thus have a very effective way of changing atmospheric CO$_2$ with the high-latitude surface concentration of PO$_4^{3-}$ being a good indicator of the Southern Ocean window.

This "high-latitude dominance" and the role of the Southern Ocean window is illustrated in Figure 10.4.8). Today, the Southern Ocean window is semi-open, as diagnosed by the fact that high-latitude surface ocean PO$_4^{3-}$ is below that of the deep ocean. If the window were completely opened, e.g. by setting Π_h^P to zero and making f_{hd} very large, atmospheric CO$_2$ would shoot up by nearly 150 ppm. Closing the Southern Ocean window by setting $[\text{PO}_4]_d \, f_{hd}$ equal to Π_h^P, i.e. setting high latitude PO$_4^{3-}$ to zero, lowers atmospheric CO$_2$ by about 120 ppm. We thus have a mechanism with a very high leverage on atmospheric CO$_2$.

Figure 10.4.9 shows that glacial levels in atmospheric CO$_2$ can be attained in the three-box model by reducing the mixing between the deep ocean and the high-latitude ocean from about 60 Sv to about 19 Sv without any change in biological productivity, or by increasing biological productivity about six-fold from about 1 mol C m^{-2} yr^{-1} to about 6.3 mol C m^{-2} yr^{-1} without changing mixing. However, these estimates are based only on the "closed system" responses, and therefore do not include the "open system" effects associated with CaCO$_3$ compensation (see chapter 9), which tends to amplify initial changes. We therefore need to review CaCO$_3$ compensation in the context of the G/IG problem before moving on to a discussion of how the Southern Ocean window can be closed.

We have seen in chapter 9 that any change in the ocean's biological pumps, either by changing the downward transport of organic matter or $CaCO_3$, or by changing ocean circulation will lead to imbalances between the input of Alk by rivers and the removal of Alk by carbonate burial on the seafloor. On the timescale of several thousand years as considered for the G/IG CO_2 problem, the oceanic $CaCO_3$ cycle will respond to this perturbation and restore the balance by altering the depth of the lysocline either temporarily or permanently and by changing ocean mean Alk. These "open system" changes impact the ocean-atmosphere balance of CO_2 and are therefore of great importance for thinking about G/IG variations in atmospheric CO_2.

The two possibilities mentionned so far to close the Southern Ocean window, i.e. increasing Southern Ocean stratification and/or increasing biological productivity are equivalent in their impact on the vertical distribution of DIC, as both tend to increase the vertical gradient. If we assume that the strength of the $CaCO_3$ pump remains the same, the vertical gradient of Alk will change only minimally in the changing productivity case, and increase in the stratification case, but these changes are much smaller than those of DIC. As a result, the concentration of the CO_3^{2-} ion, approximately given by $[CO_3^{2-} = Alk - DIC$, will decrease in the ocean's interior. This will induce an upward shift of the $CaCO_3$ saturation horizon, causing anomalous $CaCO_3$ dissolution. The resulting excess of Alk input by rivers over Alk loss by $CaCO_3$ burial will increase oceanic Alk until the carb ion concentration is restored to its original concentration, and the $CaCO_3$ saturation horizon restored to its original position. As a result of a net dissolution of $CaCO_3$ on the seafloor, this open system response increases the mean ocean Alk twice as strongly as it increases mean ocean DIC, therefore enhancing the initial perturbation as shown in Figure 9.5.2. In the case of the Southern Ocean window closure and using the three-box model, the enhancement turns out to be relatively small, only of the order of a few %. This is primarily because the CO_3^{2-} ion changes in the deep reservoir of the three-box model are very small, simply a result of the large volume of this reservoir. We will see below, however, that in the case of changes of the $CaCO_3$ pump, the open system response can be quite large. Another way to enhance the $CaCO_3$ compensation effect is to reduce the volume of the deep reservoir, so that its chemistry changes are larger (an effect used by *Toggweiler* [1999], see below).

Physical mechanisms

We have learned so far that there are two fundamentally different mechanisms to close the Southern Ocean window and reduce atmospheric CO_2 (Figure 10.4.9). One is physically driven by reducing the exchange between the high-latitude surface box and the deep box, while the other is biologically driven and requires a substantial increase in biological fixation of CO_2 in the surface ocean and subsequent export. A third possibility exists in the form of increased sea-ice coverage, which would close the Southern Ocean

window by simply impeding the physical exchange of CO$_2$ across the air-sea interface [*Stephens and Keeling*, 2000]. The three-box model permits us to investigate the ramnifi-cations of these changes, but it does not give us insight into the possible processes leading to these changes. We focus first on the physical mechanisms.

The exchange between the high-latitude surface box and the deep ocean can be reduced by reducing the mixing in the Southern Ocean in response to, for example, an increase in vertical stratification there. An alternative mechanism is to separate the deep ocean vertically into several reservoirs, and add a finite amount of mixing between them. In this latter case, vertical stratification is added to the entire deep ocean, but the net effect is essentially the same, in that it reduces the amount of mixing between the surface ocean of the high-latitudes and the deep ocean reservoir of DIC. The real world analog is the separation between the cool, fresh Antarctic Bottom Water (AABW) and the warm, salty North Atlantic Deep Water (NADW).

Toggweiler [1999] made use of the latter strategy and proposed that deep ocean strat-ification between NADW and AABW was substantially larger during the LGM, resulting in a "chemical" divide that reduces the upwelling of ΔC_{soft} rich waters in the Southern Ocean and prevent them from letting CO$_2$ escape into the atmosphere. Supporting ev-idence that this occured comes from chlorinity and δ^{18}O measurements of pore fluids, which suggest that AABW was close to the freezing point and much more salty relative to the rest of the ocean during the LGM in comparison to today [*Adkins et al.*, 2002]. At the same time, although NADW appears to have been somewhat cooler than today, its increase in density was likely smaller than that of AABW, leading to a stronger density contrast between Southern Ocean source waters occupying the bottom ocean, and the deep waters lying above. By extending the classical Harvardton-Bears three-box models to seven boxes, *Toggweiler* [1999] attempted to capture this physical separation between waters of southern and waters of northern high-latitude origin. Of particular relevance for this model is not only the physical separation, but also the fact that the chemical composition of northern and southern source waters is very different. We have seen in chapter 8 that North Atlantic Deep Water has a very low ΔC_{soft} concentration for its temperature (Figure 8.4.7), while the ΔC_{soft} concentration of Southern Ocean source wa-ters is very high. By increasing vertical stratification in the deep ocean, one also separates also waters with a high potential for inducing outgassing from those with a much smaller potential. *Toggweiler* [1999] demonstrated with this model that a decrease in the venti-lation of the bottom waters together with CaCO$_3$ compensation can cause a nearly 60 ppm drawdown in atmospheric CO$_2$ (21 ppm from ventilation and 36 ppm from CaCO$_3$ compensation). This model has a much larger enhancing effect from CaCO$_3$ compensa-tion than the Harvardton-Bear models, because most of the chemical changes occur in the intermediate size bottom water box in this 7-box model, leading to substantial changes

in *DIC* and Alk. This requires a substantially larger amount of CaCO$_3$ dissolution to restore the ocean's CO$_3^{2-}$ ion concentration, thereby enhancing the CO$_2$ drawdown in the atmosphere to a much larger extent. Although successful in creating a large drawdown in atmospheric CO$_2$, *Toggweiler* [1999] did not provide a physical mechanisms to explain what might have caused the reduction in bottom ocean water ventilation.

Stephens and Keeling [2000] suggested instead that extended sea-ice coverage closed the Southern Ocean window. Their hypothesis is based on the arguments that the glacial Southern Ocean was much colder than today, and that the warm layer derived from NADW sitting underneath the surface, which tends to prevent sea-ice from growing too rapidly in the present ocean [*Gordon*, 1981], was likely absent. Both factors would have led to a substantial increase in sea-ice coverage in the Southern Ocean. Their argument is hampered by the fact that in order for this mechanism to be effective, sea-ice needs to cover nearly the entire Southern Ocean. In their model, a substantial reduction was only achieved if sea-ice covered 99% of the entire Southern Ocean, for which there is only limited evidence [*Crosta et al.*, 1998].

The sea-ice extent and deep-ocean stratification mechanisms were combined and put into a unified framework by *Gildor and Tziperman* [2001a] and *Gildor et al.* [2002]. They used a meridional box model of the ocean, atmosphere, land-ice and sea-ice climate system, and combined it with a relatively simple representation of the oceanic carbon cycle. With present-day seasonal forcing from the sun, the physical part of the climate model develops 100,000 year time-scale variations that mimic the glacial-interglacial cycles observed in ice-cores (see Figure 10.4.1). As explained by *Gildor and Tziperman* [2001b], these oscillation emerge from a combination of feedbacks between temperature and precipitation, and temperature and albedo [*Ghil et al.*, 1987, *Ghil*, 1994], but are modified by a sea-ice feedback in the northern hemisphere, which influences the growth and retreat of the continental ice-sheets. When run with Milankovitch forcing, i.e. the small variations in solar forcing that result from slight, but regular changes in earth's orbit around the sun (eccentricity, time-scale about 100,000 years), in the tilt of earth's axis of rotation relative to the plane of earth's orbit around the sun (obliquity, 41,000 years), and in the absolute direction of this tilt (precession, 23,000 years), the model's main periodicity locks in with eccentricity, as observed.

Gildor and Tziperman [2001] propose that the physical changes in the Southern Ocean needed to draw down atmospheric CO$_2$ during glacial periods emerge naturally from the physical model and are driven by changes in the Northern hemisphere. They suggest that NADW becomes cooler during the buildup stage of Northern Hemisphere ice sheets, and that it maintains this property as it moves along its journey to the Southern Ocean. This results in a cooling of the Circumpolar Deep Waters, making the stratification in the Southern Ocean more stable during glacial maxima. *Gildor and Tziperman* [2001a] then

use simple formalisms linking the stratification to vertical mixing, thereby generating the mechanism needed to draw down atmospheric CO$_2$ according to the hypothesis of *Toggweiler* [1999]. The reduced vertical mixing and the lower deep water temperature result in a larger sea ice extension during cold periods. This, in turn, can again reduce atmospheric CO$_2$ according to the mechanism of *Stephens and Keeling* [2000].

Although compelling and successful in explaining the atmospheric CO$_2$ drawdown, it is not possible yet to evaluate whether the mechanism proposed by *Gildor and Tziperman* [2001a] and *Gildor et al.* [2002] is correct. Their results need to be scrutinized more carefully with various paleoclimatological constraints and investigated in greater detail with models of higher complexity. We will discuss paleoclimatological constraints below, but note that the success of the hypotheses by *Toggweiler* [1999], *Stephens and Keeling* [2000], and *Gildor and Tziperman* [2001a] in explaining the glacial drawdown in atmospheric CO$_2$ critically depends on the existence of a strong high-latitude dominance. *Archer et al.* [2003] examined this high-latitude dominance with a particular emphasis on the sea-ice mechanism, and found that atmospheric CO$_2$ in spatially more resolving models, such as two-dimensional and three-dimensional ocean circulation models shows virtually no response to an increase in sea-ice coverage in the Southern Ocean. This finding is consistent with our discussion above of these models having a higher low-latitude sensitivity, i.e. higher HBEI index. Given that we do not know the high versus low latitude sensitivity of the real ocean, *Archer et al.* [2003] concluded that until these sensitivities can be resolved, glacial CO$_2$ hypotheses based on Southern Ocean barrier mechanisms are "walking on thin ice".

Biological mechanims

An alternative set of mechanisms to close the Southern Ocean window is to increase biological productivity and carbon export by taking advantage of the large unused nutrient pool in this HNLC region as first suggested by the Harvardton-Bears [*Knox and McElroy*, 1984, *Sarmiento and Toggweiler*, 1984, *Siegenthaler and Wenk*, 1984]. We have seen already that in order to decrease atmospheric CO$_2$ to glacial levels in the Harvardton-Bear three-box model, high-latitude productivity has to increase about sixfold (Figure 10.4.9). While the Harvardton-Bears did not know how such a large increase in biological productivity could have happened, the discovery that iron might be the factor limiting phytoplankton in this region (see discussion in chapter 4), provided *Martin* [1990] the basis for proposing that the higher dust levels during the glacial periods (see Figure 10.4.10) fertilized the Southern Ocean with the necessary iron to increase biological export. *Watson et al.* [2000] investigated this hypothesis in a multi-box model of the ocean carbon cycle, and found that iron fertilization on the basis of the observed variations of dust flux in the Vostok ice-core could explain a drawdown of about 40 ppm in atmospheric CO$_2$. By contrast, *Bopp et al.* [2002], using a three-dimensional coupled ocean circulation/ecosystem model and using the LGM dust flux reconstruction of *Mahowald et al.* [1999] found a maximum

effect of only 15 ppm. These results need to be viewed tentatively since uncertainties with regard to iron availibility and the magnitude of the iron fluxes during the LGM are very large. However, some of the differences can also be explained by differences in the high-latitude sensitivity of these two models. *Watson et al.* [2000] used a model with a low HBEI, whereas *Bopp et al.* [2002] employed a model with a high HBEI, thereby having, by design, a lower effectiveness of high-latitude changes in export production.

<div align="center">Paleoceanographic constraints</div>

Each hypothesis attempting to explain the observed G/IG variations in atmospheric CO_2 needs to be carefully evaluated against available paleoceanographic constraints. However, these evaluations are seldom very straightforward, since very few constraints come from direct measurements of the property of interest, e.g. temperature, but rather are derived from another, related property, e.g. the $\delta^{18}O$ of $CaCO_3$. The relationship of these proxy properties with the property of interest are sometimes very tight and well understood, but often based only on empirical relationships or made more complicated by other interfering factors. In the case of temperature, for example, the $\delta^{18}O$ of CO_3^{2-} in water and hence in $CaCO_3$ is also influenced by the magnitude of the continental icesheets, requiring this contribution to be well determined before the $\delta^{18}O$ of $CaCO_3$ can be used to infer water temperature. Keeping these limitations in mind, we investigate next how the hypotheses centered around the closure of the Southern Ocean compare to these constraints. A critical prediction of the Southern Ocean vertical stratification and productivity hypotheses is that the surface to deep gradient of PO_4^{3-} has to increase substantially. This is because high-latitude PO_4^{3-} decreases (see Figure 10.4.9b), while the deep ocean PO_4^{3-} remains about the same.

An important proxy is the $^{13}C/^{12}C$ ratio of seawater DIC recorded by planktonic and benthic foraminifera. During the photosynthetic uptake of CO_2, marine plants discriminates against the heavy isotope ^{13}C by about 20‰, whereas respiration and remineralization is associated with only a very small fractionation. Because phosphate is controlled by photosynthesis and respiration/remineralization as well, a relatively good correlation exists between the $^{13}C/^{12}C$ isotopic ratio of surface water DIC and phosphate. Deviations in the correlation are a consequence of fractionations occuring during the air-sea gas exchange of CO_2 and due to variations in the biological fractionation. Nevertheless, to first approximation, the $^{13}C/^{12}C$ ratio of DIC can be regarded as a good proxy for phosphate. Any increase in the phosphate gradient between the surface waters and the deep ocean should therefore lead to an increase in the surface to deep gradient in the $^{13}C/^{12}C$ ratio of DIC. However, the existing data show little change in the surface to deep difference in this region [*Charles and Fairbanks*, 1990].

The conclusion based on the marine $^{13}C/^{12}C$ ratios are also supported by measurements of the cadmium content recorded in foraminifera. No significant change is found in pelagic

and benthic foraminifera from the Southern ocean [*Boyle*, 1992]. As there exists a very tight correlation between cadmium and phosphate in the modern ocean, this again suggests that nutrient concentrations in the Southern Ocean have not dropped significantly during glacial time.

A third constraint, albeit less strong, is the ^{13}C/^{12}C ratio change in atmospheric CO$_2$ [*Leuenberger et al.*, 1992, *Marino et al.*, 1992]. The closing of the high-latitude window makes the ^{13}C/^{12}C ratio of the surface waters more heavy and along with it the ^{13}C/^{12}C ratio of atmospheric CO$_2$. For example, the three-box model predicts an increase of about 1‰ in the ^{13}C/^{12}C of atmospheric CO$_2$. In sharp contrast, the reconstructions suggest that the ^{13}C/^{12}C ratios of atmospheric CO$_2$ were lower by about 0.3-0.7‰ during the last glacial [*Leuenberger et al.*, 1992, *Marino et al.*, 1992]. However, there are several additional processes to consider that ease the constraint [*Broecker and Henderson*, 1998]. First, we have to take into account the whole ocean isotopic shift of about 0.4‰ that is usually interpreted as resulting from the transfer of isotopically light carbon from the terrestrial biosphere into the ocean during glacial periods [*Shackelton*, 1977, *Curry et al.*, 1988]. In addition, a recently discovered pH artifact in foraminifera [*Spero et al.*, 1997] and variations in the biological fractionation conspire together with the decrease from the isotopically light carbon from the terrestrial biosphere to reduce the ^{13}C/^{12}C ratio of atmospheric CO$_2$ by about 0.9‰ [*Broecker and Henderson*, 1998]. Hence, the corrected model predicted increase in the ^{13}C/^{12}C ratio of atmospheric CO$_2$ is only 0.1‰ , making the discrepancy with the observations relatively small.

Toggweiler [1999] demonstrated that these constraints may not be as strong as they appear at first. In particular, he pointed out that the representation of the entire deep ocean as one large box in the Harvardton-Bear three-box models neglects the possible existence of a chemical divide in the ocean. In his model, most of the changes needed to drive down atmospheric CO$_2$ come from the Southern Ocean bottom water box, which is much smaller in volume than the large deep box in the Harvardton-Bear three-box models. It therefore depends critically on where certain constraints are coming from in order to establish their strength. For example, *Toggweiler* [1999] shows that he can fit the atmospheric ^{13}C/^{12}C ratio changes, while at the same time fitting the oceanic ^{13}C/^{12}C DIC changes.

The need for consideration of the spatial nature of the constraints becomes even more evident when considering how export production might have changed relative to today. Figure 10.4.11 shows a map of changes in export production inferred from a large number of paleo-productivity proxies. With regard to the Southern Ocean, a relatively clear pattern emerges with the region south of the Polar Front (the Antarctic zone) generally showing a decrease in export production, while the the region between the Polar Front and the sub-Antarctic Front (the sub-Antarctic Zone), showing an increase (see chapter 7 for a

discussion of these fronts and Figures 7.3.3 for illustration of the zonal mean meridional circulation in the Southern Ocean). How do these observations compare to the Southern Ocean window closure hypotheses? The consideration of changes in export production alone is insufficient to answer this question, as the closing of the window requires an increase in the efficiency of the biological pump, i.e. an increase in the downward transport of organic matter relative to the upward supply. We have seen above that a good proxy for this balance, i.e. the degree of nutrient utilization, is the surface concentration of macro-nutrients.

It turns out that the ratio of ^{15}N to ^{14}N measured in organic matter deposited on the seafloor is a good recorder for the degree of nutrient utilization in the overlying surface ocean [*Francois et al.*, 1997]. Due to an isotopic fractionation during the photosynthetic uptake of nitrate, the ^{15}N content of near surface organic nitrogen exhibits in the modern ocean a very strong correlation with the concentration of nitrate [*Altabet and Francois*, 1994, *Sigman et al.*, 1999]. As this signal gets transmitted and incorporated into the sediments, bulk-sediment ^{15}N/^{14}N provides a good proxy of the degree of nitrate utilization in the overlying surface waters, i.e. the balance between upward physical supply of nitrogen and downward export of organic nitrogen [*Sigman et al.*, 1999, *Sigman et al.*, 2000].

Observations of the ^{15}N/^{14}N ratio in the Southern Ocean reveal a substantial increase in the nitrate utilization south of the modern Polar Front, i.e. in the Antarctic [*Francois et al.*, 1997, *Sigman et al.*, 1999] whereas little change in nitrate utilization was found north of the modern Polar Front. The former change is very consistent with the Southern Ocean window closure hypothesis, as an increase in nutrient utilization reduces the outgassing of biologically derived CO_2. Combining the increased nutrient utilization in the Antarctic with the lower biological export in this area (Figure 10.4.11) suggests that the primary mechanism responsible for the closure is a reduced supply of nutrients, probably due to an increase in vertical stratification, in agreement with the hypothesis by *Toggweiler* [1999]. The increase in biological export in the sub-Antarctic Zone coupled with a nearly unchanged nutrient utilization suggests that the supply of nutrients to this zone increased, but had little influence on the evasion of CO_2 since the increase in supply was compensated by an increase in the downward export of organic matter.

In summary, the available paleoceanographic constraints indicate a spatially inhomogeneous picture, which paleoceanographers are still grappling to fully understand. Most recent constraints suggest that the Southern Ocean experienced substantial changes during the LGM, with a distinct difference between the Antarctic and the Sub-antarctic Zones. While the available constraints tend to indicate changes that are consistent with the Southern Ocean window being more closed during the LGM in comparison to today, the changes they permit seem insufficient to explain the entire drawdown of atmospheric

CO_2. As we will see below, however, an important argument in favor of the Southern Ocean playing an important role is the strong connection between Southern hemisphere climate changes and atmospheric CO_2.

A ROLE FOR THE REGIONS OUTSIDE THE SOUTHERN OCEAN?

With paleoceanographic constraints limiting the contribution of the Southern Ocean, many researchers have given increased attention to mechanisms outside the Southern Ocean. We review the most important hypotheses in the next subsections, organized into whether the hypotheses invoke primarily changes in ocean circulation, the soft-tissue pump, or the carbonate pump. We will discuss their strengths and weaknesses at the same time. A summary of these hypotheses is given in Table 10.4.1. We will see that few of these hypotheses are consistent with existing constraints, while still large enough to explain a substantial drawdown of atmospheric CO_2, except those that invoke a modest change in the carbonate to organic carbon rain ratio. In a following section, we will develop a synthesis scenario that combines elements from the Southern Ocean hypotheses with some of those discussed next.

Circulation scenarios

We have so far neglected changes in circulation outside the Southern Ocean, in particular also the possibility of changes in the meridional overturning circulation associated with NADW. Although there is abundant evidence that the meridional overturning circulation in the Atlantic underwent large changes between glacial and interglacial conditions, with substantial variability in between [*Alley et al.*, 2003], it turns out that these changes appear to have had a relatively small impact on atmospheric CO_2. *Archer et al.* [2000] found a reduction of only 6 ppm for the LGM, based on a three-dimensional ocean biogeochemistry model whose circulation was optimized by an adjoint method to reflect paleoceanographic constraints for the glacial ocean [*Winguth et al.*, 1999]. However, given the relatively small number of paleoceanographic constraints, it is possible that this adjoint model underestimates the changes that occured between glacial and interglacial periods. This is indeed suggested by the recent six-box modeling study of *Lane et al.* [2004], who obtained a very strong drawdown of atmospheric CO_2 when they permitted their meridional overturning circulation to adjust dynamically to the changed boundary conditions. In particular, they found that the data constraint for the glacial ocean asked for an moderate reduction in the overturning circulation associated with NADW from about 16 Sv to 12 Sv, and a very strong reduction from about 17 Sv to 9 Sv in the formation of abyssal waters in the Southern Ocean. They did not provide a separation into how much of the atmospheric CO_2 drawdown was driven by the Southern Ocean pathway versus the North Atlantic pathway, but if it turns out that the majority of the drawdown is driven by the Southern Ocean, their explanation would belong to the category of physical mechanisms closing the

Southern Ocean window (as do *Toggweiler* [1999] and *Gildor and Tziperman* [2001a]). As mentioned before, an important point noted by *Lane et al.* [2004] was their finding that the reduction in ocean circulation not only reduced atmospheric CO_2 by capturing it in the interior ocean through a more efficient biological pump, but also because these ocean circulation changes also made atmospheric CO_2 responding much more sensitively to the low-latitude cooling.

A substantial change in the oceanic circulation was indeed needed if the nutrient redistribution hypothesis of *Boyle* [1988] were correct. His argument was based on the observation that the reorganisation of the Atlantic conveyor circulation during glacial periods shifted nutrients and metabolic CO_2 from intermediate waters to deeper waters. This causes a substantial $CaCO_3$ compensation response, which would be mainly responsible for the atmospheric CO_2 drawdown. *Boyle* [1988] argued that this mechanism can explain at least half of the 80 ppm difference between glacial and interglacial periods. However, there is one strong argument that speaks against this hypothesis. *Sigman et al.* [1998] showed that such a nutrient redistribution associated with $CaCO_3$ compensation would lead to a significant steady-state deepening of the lysocline (see chapter 9). Such a deepending was observed in the Pacific and the Indian ocean, whereas the opposite was the case in the Atlantic ocean, resulting in an overall deepening of the lysocline during the LGM of only a few hundred meters [*Catubig et al.*, 1998].

<center>*Soft-tissue pump scenarios*</center>

If circulation changes are unable to explain the glacial CO_2 drawdown, maybe changes in the strength of biological export outside the Southern Ocean could represent the key mechanism. In fact, initial attempts to solve the mystery of reduced atmospheric CO_2 focused from the very beginning on the role of the soft-tissue pump. This is not surprising, given the importance of this pump in generating the surface to deep gradients in DIC (see Figure 8.4.2) and the many ways how this pump could respond to changes in environmental factors. As the level of nutrients in the surface waters constitute one of the primary factors controlling the biological productivity, many scenarios have been developed that are coupled to changes in nutrients (see Table 10.4.1). The primary idea behind most of these hypotheses is to increase ocean productivity throughout the ocean by increasing the total ocean nutrient inventory. This can be accomplished by a reduction of the fraction of nutrients that are buried in the shelf sediments [*Broecker*, 1982] or in the case of nitrogen by changing the balance between nitrogen fixation and denitrification [*McElroy*, 1983, *Broecker and Henderson*, 1998] or changing stoichiometry.

We can immediately exclude the shelf-nutrient hypothesis of [*Broecker*, 1982] because it is tied to sea-level change, which clearly occured after the rise in atmospheric CO_2 [*Broecker and Henderson*, 1998]. By contrast, the recent proposal of *Broecker and Henderson* [1998] that iron controlled imbalances between nitrogen fixation and denitrification can lead to

drastic changes in the fixed nitrogen inventory in the ocean is in agreement with the sequence of events as the Earth's climate went from glacial conditions into interglacial ones. During glacial periods, high dust fluxes bearing large amounts of iron are thought to fuel intense nitrogen fixation in the subtropical gyres [*Falkowski*, 1997], leading to a gradual buildup of the ocean inventory of fixed nitrogen. Such a nitrogen buildup could alternatively be caused by lower denitrification in the glacial ocean as proposed by *Ganeshram et al.* [1995]. If we neglect the limiting role of phosphate and other (micro)nutrients for the moment, this increase in fixed nitrogen would support higher biological production, leading to higher export production and hence lower pCO$_2$. After the abrupt cessation of the dust flux, nitrogen fixation would sharply drop as well, and the fixed nitrogen inventory would start to decrease with a time-scale of approximately 3000 years [*Gruber and Sarmiento*, 1997], consistent with the observed slow increase of atmospheric CO$_2$ over about 8000 years. Though this scenario is in agreement with the sequence of events during deglaciation, its feasibility hinges also on the magnitude of the necessary changes in nutrient inventory to cause a significant drop of atmospheric CO$_2$.

In order to reduce atmospheric CO$_2$ by 80 ppm in the three-box model, the limiting nutrient in this model has to increase by more than 70%. As it turns out, this low sensitivity is again a consequence of the low HBEI exhibited by the three-box model. We mentioned above that three-dimensional models have a substantially larger HBEI, opening the possibility that smaller changes in nutrient inventories could suffice to change atmospheric CO$_2$ dramatically. However, we still have to consider the role of other limiting nutrients, especially phosphate (see review by *Gruber* [2004].

In strong contrast to the fixed nitrogen inventory, the phosphate inventory of the ocean cannot be changed directly by biological processes. This inventory is controlled by river input and burial, which set the residence time to about 50,000 years [*Delaney*, 1998]. Thus, for the timescale of interest here, the phosphate inventory can be viewed as being constant. Therefore, unless we accept that the stoichiometric ratios between phosphate and nitrate uptake during photosynthesis have changed from the standard 1:16 relationship, ocean productivity can only change within rather tight limits as a function of the fixed nitrogen inventory before phosphate becomes limiting. There exists some leeway, because the phosphate inventory is about 10% larger than expected from the nitrate inventory. We have already encountered this phosphate excess as the non-zero intercept of the nitrate versus phosphate plot in Figure 5.1.10. This excess also shows up also as a positive constant in the definition of N^* in equation (6.3.8). It is therefore possible to increase the ocean fixed nitrogen inventory by about 10% without running into a phosphate limitation. Changing the nutrient inventory in the three-box model by this amount decreases atmospheric CO$_2$ by only 10 ppm. However, if the 'true' HBEI was four times bigger than that of the three-box model, atmospheric CO$_2$ would decrease by about 40 ppm!

We used observations of the ^{13}C/^{12}C ratio in the ocean and atmosphere before as an argument against the proposal that changes in high-latitude ventilation have reduced atmospheric CO$_2$. Any increase in surface productivity enriches the *DIC* remaining in the surface waters in ^{13}C and hence also enriches atmospheric CO$_2$, quite contrary to the observations which suggest a reduction in the ^{13}C/^{12}C ratio of atmospheric CO$_2$ and little change in the ^{13}C/^{12}C ratio of planktonic foraminifera [*Broecker and Peng*, 1998]. However, we have also seen, above, that the input of isotopically light carbon from the terrestrial biosphere, a *p*H related artifact and a decrease in the photosynthetic fractionation work together to more than offset the increase in the ^{13}C/^{12}C ratio of atmospheric CO$_2$ caused by the higher productivity. Thus, the proposal that a significant increase in the nutrient inventory was at the core of the processes that reduced atmospheric CO$_2$ to glacial levels, is not inconsistent with the ^{13}C/^{12}C records of atmospheric CO$_2$ and surface ocean *DIC*.

There exists, however, at least one serious caveat. *Sigman et al.* [1998] and *Archer et al.* [2000] show that CaCO$_3$ compensation could strongly offset any atmospheric CO$_2$ drawdown caused by an increase in the nutrient inventory. This compensation has to do with the fact that an increase in the surface ocean productivity tends to enhance also the formation of CaCO$_3$ shells, thus increasing the flux of CaCO$_3$ to the sea floor. This is equivalent to saying that the CaCO$_3$ to organic matter rain ratio remains constant. In addition to an increase in CaCO$_3$ rain to the seafloor, the increased oxygen demand in the sediments shift much of the sedimentary respiration from oxic chemistry, which promotes CaCO$_3$ dissolution, to anoxic reactions which have a much lesser influence on porewater pH. The sum of these effects is to sharply increase the rate of CaCO$_3$ burial in the ocean, throwing off the balance with the Alk input. In order to restablish the equilibrium between input and burial, the ocean has to dissolve more CaCO$_3$ which is accomplished by a reduction of the oceanic CO$_3^{2-}$ ion content permitting a much more shallow lysocline. A lower CO$_3^{2-}$ ion content increases the mean ocean buffer factor, which reduces the ocean's ability to hold CO$_2$ and therefore increases atmospheric CO$_2$. This strongly offsets the inital response of the ocean carbon cycle to the increase in the nutrient inventory. *Sigman et al.* [1998] find that a 30% increase of the nutrient inventory draws atmospheric CO$_2$ initially down by 34 ppm, but that the compensation response increases *p*CO$_2$ of the atmosphere back up to a change of only 18 ppm. Similar results are found by *Archer et al.* [2000]. If the negative feedback by CaCO$_3$ compensation is indeed as strong as suggested by these studies, the nutrient inventory scenario can be rejected as a possible driver for the low glacial atmospheric CO$_2$ concentration. However, if the formation of CaCO$_3$ is uncoupled with general biological productivity, nutrient inventory changes could play some role.

Alkalinity and carbonate pump scenarios

We have seen in the last example, how changes in the ocean's carbonate pump can have substantial influence on atmospheric CO$_2$, particularly in the presence of CaCO$_3$ compensation feedbacks. Alternative mechanisms affecting the ocean's alkalinity balance include changes in river input and burial independent of carbonate pump changes. Given the high sensitivity of atmospheric CO$_2$ to changes in the ocean's alkalinity balance, alkalinty based mechanisms were among the first to be proposed (e.g. *Berger* [1982], *Opdyke and Walker* [1992], and *Milliman* [1993], see Table 10.4.1). All of these intial hypotheses are linked to sea-level change, permitting us to reject them immediately since atmospheric CO$_2$ started to rise several thousand years before sea-level started to rise significantly during the last two deglaciations [*Broecker and Henderson*, 1998].

The sea-level constraint does not affect any scenario that calls for a reduction in the carbonate pump. Everything else being the same, this would at first drastically reduce the burial of CaCO$_3$ at the sea floor. In order to compensate, the lysocline has to deepen to suppress dissolution until a new steady-state between burial and alkalinity input has been achieved (see Figure 9.5.2). As we noted previously, such a change in the lyscocline depth has not been observed. However, the situation may be more complex since factors other than the deep ocean CO$_3^{2-}$ content can control deep ocean dissolution of CaCO$_3$. We discussed in chapter 9 that the lysocline is only poorly related to the magnitude of the dissolution flux, particularly in cases where the flux of organic matter reaching the sediments is larger than the flux of CaCO$_3$. Respiratory enhanced dissolution of CaCO$_3$ in the sediments provides a means how the dissolution of CaCO$_3$ in the sediments can be decoupled from the CO$_3^{2-}$ content of the overlying waters.

Archer and Maier-Reimer [1994] argued that if the rain rate of organic matter to the sediment was higher during glacial times, the CO$_3^{2-}$ concentration in the deep ocean could increase without a large change in the lysocline and the depth of the transition zone. Their proposed sequence is a follows: the increased flux of organic matter leads to intensified respiratory driven dissolution, which if not complete, reduces the CO$_3^{2-}$ content of the overlying waters driving the lysocline temporarily to shallower depths. This increased dissolution of CaCO$_3$ and the smaller downward flux of CaCO$_3$ both lead to dramatically smaller deposition of CaCO$_3$ on the sea floor, thus resulting in a large alkalinity imbalance with the input. In order to compensate, the deep ocean CO$_3^{2-}$ concentration has to increase until the additional bottom water CO$_3^{2-}$ content balances the respiration induced deficit of CO$_3^{2-}$ in the upper sediments. The lysocline would then move back to its original position as observed. This would lead to a situation where the depth of the saturation horizon is strongly separated from the depth of the lysocline.

Support for the rain ratio scenario is provided by paleo-reconstructions of ocean pH with the help of boron isotopes [*Sanyal et al.*, 1995]. Boron pH values from the glacial deep

Pacific and Atlantic seem to show an increase of about 0.1 to 0.3 pH units, which would correspond to an increase in the CO_3^{2-} concentration of about 40-100 μmol kg^{-1}, consistent with the rain ratio hypothesis. However, according to *Sigman et al.* [1998] the predicted strong separation between the saturation horizon and the lysocline cannot be sustained under such circumstances. When *Sigman et al.* [1998] halved the $CaCO_3$ rain in the low-latitudes, the lysocline in their box-model deepened by 1,000-1,500 m, thus drastically increasing the area of high $CaCO_3$ sediments. This has not been observed in the sediment cores, thus putting the rain ratio scenario in doubt. However, *Archer et al.* [2000] argues on the basis of their 3-D biogeochemistry model that the deepening of the lysocline is much smaller than modeled by *Sigman et al.* [1998] and not at odds with the observations. If the lysocline constraint by *Sigman et al.* [1998] is indeed not as strong as they suggested, then the rain ratio hypothesis emerges as one of the likely candidate drivers for explaining the low glacial CO_2 concentrations. However, many questions are still unanswered and it is too early to either accept or reject this scenario. For instance, what are the reasons for the shift in the organic matter to $CaCO_3$ rain ratio? *Archer et al.* [2000] shows that such a change could occur as a consequence of a drastic increase in the input of $Si(OH)_4$ from weathering which would promote the growth of diatoms at the expense of coccolithoporids, hence reducing the $CaCO_3$ formation rate in the surface ocean.

Brzezinski et al. [2002] recently proposed another plausible scenario for how a shift in the $CaCO_3$ to organic matter export ratio could have occured, building on the premise that given extra $Si(OH)_4$, diatoms would tend to outcompete coccolithoporids. In this case, however, the extra $Si(OH)_4$ comes from the Southern Ocean as a result of a leakage of the normally existing Southern Ocean trap for $Si(OH)_4$ (see chapter 7). Under present-day conditions, $Si(OH)_4$, in the Southern Ocean is tighly confined to the Antarctic continent (see Figure 7.1.1), since it gets drawn down very quickly once it is upwelled south of the Polar Front and pushed equatorward by Ekman drift (see Figure 7.3.3). In contrast, the region of high NO_3^- in the Southern ocean extends much further north (Figure 7.1.1). When these waters reach the latitudes where Antarctic Intermediate Water (AAIW) and Sub-antarctic Mode Water (SAMW) are formed, $Si(OH)_4$ concentrations are essentially zero, while NO_3^- cocentrations are still elevated. We have seen in chapter 7 that $Si^* = Si(OH)_4$ - NO_3^- is a useful indicator of this strong deficiency of $Si(OH)_4$ relative to NO_3^- (Figure 7.3.4). We also found that the resulting low Si^* waters, indicative of high concentrations of pre-formed NO_3^-, but containing no pre-formed $Si(OH)_4$, can be traced throughout the Southern hemisphere thermocline, and even into the thermocline of the North Atlantic (Figure 7.3.5). This extraordinary reach coupled with the fact that diapycnal mixing in the ocean tends to be small, has provided the foundation for the proposal that changes in the source region of AAIW and SAMW could lead to substantial alterations of the nutrient distribution in the thermocline of the world's ocean, ultimately affecting biological produc-

tivity throughout the low-latitudes [*Sarmiento et al.*, 2004]. To illustrate the importance of this pathway for providing nutrients to the low-latitudes, *Sarmiento et al.* [2004] set all nutrients entering this pathway to zero, and found productivity north of 30°S dropped by about 75%.

We discussed in chapter 7 that the trapping of $Si(OH)_4$ in the Southern Ocean, while substantial amounts of NO_3^- get exported into the low-latitudes, is likely the result of iron limitation of diatom growth in the Southern Ocean, as diatoms are known to silicify much more heavily under such conditions. This opens the possibility that an increase in the availability of iron in the Southern Ocean through higher aeolian deposition during the LGM could have relieved the diatoms from their iron stress. Since diatoms tend to take up NO_3^- and $Si(OH)_4$ in a 1:1 ratio under iron replete conditions, and since the $Si(OH)_4$ concentration of the water upwelled into the Southern Ocean is much higher than this ratio (see Figure 7.2.4), this could have led to a situation where the surface waters feeding AAIW and SAMW were replete in both $Si(OH)_4$ and NO_3^-. Thus, the Southern Ocean trap for $Si(OH)_4$ would have turned into a region of $Si(OH)_4$ export, enriching the thermocline of the low-latitudes with $Si(OH)_4$. When these waters make it the surface in the low-latitudes, they tend to stimulate the growth of diatoms at the cost of coccolithophorids, leading to a reduction in the export of $CaCO_3$ from the surface ocean. Through $CaCO_3$ compensation, this would lead to a substantial drawdown of atmospheric CO_2 [*Brzezinski et al.*, 2002]. Therefore, without changing biological productivity, an iron induced change in diatom physiology in the Southern Ocean could lead to a change in phytoplankton community composition "downstream" in the low-latitudes with global carbon cycle implications.

Matsumoto et al. [2002] investigated the magnitude of this effect in a multi-box model and concluded that it could explain an atmospheric CO_2 drawdown of about 30 to 40 ppm. They noted, however, given the much higher low-latitude sensitivity or higher HBEI, that three-dimensional models could generate a much larger drawndown, perhaps as large as 100 ppm. Evidence in support of this hypothesis comes from the observation that sediment records in the Antarctic region of the Southern Ocean show an anti-phasing of $\delta^{30}Si$ and $\delta^{15}N$ (see Figure 10.4.13). Since variations of $\delta^{30}Si$ are primarily reflecting the degree of Si utilization, i.e. directly analogous to $\delta^{15}N$ for N, this anti-phasing has puzzled researchers for a long time, since $\delta^{30}Si$ showed a lower degree of nutrient utilization, while $\delta^{15}N$ showed a higher degree of nutrient utilization during the LGM [*Rocha et al.*, 1998]. The hypothesis of *Brzezinski et al.* [2002] provides now a good explanation for this puzzle, because it exactly predicts this antiphasing in the nutrient utilization of these two nutrients in the Antarctic Zone.

The present debate about the role of the $CaCO_3$ pump as a driver for low glacial atmospheric CO_2 concentration is still associated with many uncertainties at even relatively fundamental levels. This is reflected in the fact that small changes in the formulation

of how CaCO$_3$ compensation operates can make drastic changes in the model results [*Sigman et al.*, 1998]. Much progress can be expected in the next years, as more and more quantitative information about CaCO$_3$ cycling in the sediments becomes available, thus drastically reducing the number of uncertainties in the model parameterizations.

A SYNTHESIS SCENARIO

The causes for the 80 ppm variations in atmospheric CO$_2$ associated with glacial/interglacial cycles remain elusive and represent one of the largest unsolved puzzles of the ocean carbon cycle. We have reviewed many hypothesis, rejected many of them because they are not in accordance with paleoceanographic evidence and identified a few that look promising. It's important to note that we focused largely on single mechanisms to explain the entire glacial/interglacial change or at least a good fraction of it. However, it seems likely that no single mechanism caused the atmospheric CO$_2$ change, but that the glacial CO$_2$ reduction was the consequence of the interaction of many small changes. However, the remarkable degree of coupling between Earth's temperature and atmospheric CO$_2$ and the regularity of the global carbon cycle response to physical climate changes, suggest that these mechanisms must be linked to each other in a predictible manner. In addition, mechanisms centered or connected with Southern Ocean changes remain at the forefront. Not only do they tend to have much more impact on atmospheric CO$_2$ changes, but they would also explain the near synchroneity between Antarctic temperature and atmospheric CO$_2$ during the LGM-holocene transition, which does not exist for northern hemisphere high-latitude temperature (Figure 10.4.12).

Following these leads, *Sigman and Boyle* [2000] suggested a synthesis scenario centered around the Southern Ocean, which combines several proposed scenarios into a single framework. We extend this synthesis scenario with the Si leakage mechanism of *Brzezinski et al.* [2002]. Figure 10.4.14a shows the condition during interglacial conditions, while Figure 10.4.14b depicts the proposed conditions during the LGM. *Sigman and Boyle* [2000] suggest that the cooler conditions during the LGM caused a northward shift of the westerly wind belt, causing a decrease in upwelling of deep water in the Antarctic. In response, this region was more likely to develop a cold, but fresh stable surface layer with frequent substantial ice-coverage. This would further reduce the ventilation of deep waters. In response, biological productivity appears to have gone down in the Antarctic, but the utilzation of nitrate went up, indicating that the decrease in the upward supply was larger than the reduction in biological export. The higher dust input from the atmosphere is not strong enough to overcome the physically induced reduction in phytoplankton reduction in the Antarctic, but likely is large enough to alleviate diatoms from iron stress. This leads to a lower Si utilization in this region. The glacial subantarctic appears to be more productive, perhaps also because of an increased supply of iron from dust. Subantarctic utilization of nitrate and phosphate have not changed much, possibly because of an in-

creased nutrient supply from the thermocline below the subantarctic surface offsetting the effect on the observed increase in productivity. These changes suggest a combined physically and biologically induced closure of the Southern Ocean window, thereby reducing atmospheric CO$_2$. In this scenario, the effect is dominated by the Antarctic.

The changes in the Southern Ocean are linked with changes throughout the rest of the ocean. One is a consequence of the fact that changes in the nutrient concentrations of the Subantarctic have a disproportionally large impact on low-latitude productivity. In particular, we propose that the alleviation of iron stress of diatoms leads to a leakage of the Southern Ocean Si trap, providing Si to the low-latitude. This is suggested to have altered the balance from coccolithophorids to diatoms, thereby reducing the export of CaCO$_3$ from the surface, and affecting atmospheric CO$_2$ through CaCO$_3$ compensation. Figure 10.4.14b also suggests that stronger vertical separation of DIC and nutrients occured during the LGM, with the mid-depth ocean loosing DIC and nutrients, while the bottom ocean waters gained them. This would have brought changes of opposite sign to ocean interior O$_2$. This vertical separation would have caused a CaCO$_3$ dissolution event in the abyssal ocean at the onset of ice ages, further reducing atmospheric CO$_2$.

This synthesis hypothesis is consistent with many paleoproxies, but far from being validated. Clearly, one of the major obstacles in the evaluation of this and other hypotheses is the uncertainty and ambiguities associated with the interpretation of proxy data. However, as more proxies are developed and the existing ones are expanded, these uncertainties will become smaller, permitting us to give more scrutiny to this hypothesis and the many others. For example, the information contained in the sequence of events during the initiation of glaciations or during the deglaciations have only began to be used. Without doubt, the quest for the causes of the low glacial atmospheric CO$_2$ concentrations will remain an exciting research topic for the future.

Tables

Table 10.4.1: Summary of scenarios that attempt to explain the lower CO_2 content of the atmosphere during glacial periods.

hypothesis	problems	author
Hypotheses calling for a closure of the Southern Ocean window		
Sea-ice coverage	coverage	[*Stephens and Keeling*, 2000]
Deep-ocean stratification	mechanism	[*Toggweiler*, 1999]
NADW driven stratification and sea-ice coverage		[*Gildor and Tziperman*, 2001]
Polar dominance	S. Ocean Productivity	[*Sarmiento and Toggweiler*, 1984; *Siegenthaler and Wenk*, 1984]
Iron Fertilization	S. Ocean Productivity	[*Martin*, 1990]
S. Ocean Synthesis Scenario		[*Sigman and Boyle*, 2000]
Hypothesis outside the Southern Ocean driven by physical changes		
Cooler North Atlantic	timing	[*Keir*, 1993]
Cooler Subtropics	magnitude	[*Bacastow*, 1996]
Vertical redistribution	lysocline, $\delta^{13}C$	[*Boyle*, 1988; *Keir*, 1991]
Ocean Circulation changes	magnitude	[*Archer et al.*, 2000]
Hypothesis outside the Southern Ocean driven by changes in the soft-tissue pump		
Shelf hypothesis	sea-level	[*Broecker*, 1992]
Iron deposition and N_2 fixation		[*Falkowski*, 1997; *Broecker and Henderson*, 1998]
Denitrification		[*McElroy*, 1983; *Altabet et al.*, 1995; *Ganeshram et al.*, 1995]
Hypothesis outside the Southern Ocean driven by changes in the soft-tissue pump		
Shallow $CaCO_3$	sea-level	[*Berger*, 1982; *Opdyke and Walker*, 1992]
Rain ratio	lysocline	[*Archer and Maier-Reimer*, 1994]
Polar alkalinity	SO Prod.	[*Broecker and Peng*, 1989]
Iron deposition and diatoms		[*Brzezinski et al.*, 2002; *Matsumoto et al.*, 2002]

Figures

Figure 10.4.1: Plot of the covariations of atmospheric CO$_2$ and local air-temperature at Vostok, Antarctica over the last 450 kyr. Local air-temperature has been estimted on the basis of the deuterium excess. Also shown is an estimate of ice-volume, derived from benthic foraminiferal oxygen isotope data from deep-sea sediment cores. During peak glacial periods, atmospheric CO$_2$ is 80 to 100 p.p.m.v. lower than during peak interglacial periods, with upper and lower limits that are reproduced in each of the 100-kyr cycles. Ice core records, including the Vostok record shown here, indicate that atmospheric CO$_2$ was among the early parameters to change at the termination of glacial maxima, roughly in step with Southern Hemisphere warming and preceding the decline in Northern Hemisphere ice volume. From *Sigman and Boyle* [2000].

Figure 10.4.2: Mechanism of oceanic CaCO$_3$ compensation of the loss of carbon from the terrestrial biosphere. Adapted from [*Broecker and Peng*, 1998]

Figure 10.4.3: Schematics of the high-latitude outcrop three box model developed by the Harvardton-Bears, i.e *Sarmiento and Toggweiler* [1984], *Knox and McElroy* [1984], and *Siegenthaler and Wenk* [1984].

Figure 10.4.4: Variational impact of a 2°C warming in the low- and high-latitudes on atmospheric CO_2. The changes were computed using the standard configuration of the Harvardton-Bear three-box model shown in 10.4.3.

Figure 10.4.5: Schematic illustration of the Harvardton-Bear Equilibration Index in an abiotic version of the three-box model shown in Figure 10.4.3. Hence, differences in CO_2 chemistry are entirely driven by the solubility pump. If the air-sea gas exchange is much more rapid than the transport of DIC around the thermohaline circuit, CO_2 in the atmosphere will be the same as the pCO_2 of the high- and low-latitude boxes. At the other extreme, if the transport of CO_2 through the atmosphere from the low-latitude to the high-latitudes is much slower than the transport of DIC between the reservoirs by the thermohaline circulation, the DIC concentrations in all reservoirs would be equal and the pCO_2 variations in the two surface boxes determined by temperature only. In this case atmospheric CO_2 equilibrates at the weighted average of 514 ppm. Hence in this simple model, atmospheric CO_2 depends on the ratio of the rate of air-sea gas exchange over the rate of thermohaline circulation. Using a "realistic" parameters, the model gives an atmospheric CO_2 of 303 ppm. The Harvardton-Bear Equilibration index is now a measure of how much the transport of CO_2 through the atmosphere is able to remove a signal in the low-latitudes and buffer it in the deep ocean. It can be calculated from the ratio of the difference between the "realistic case" and the "full equilibration" and the difference between the "no equilibration" and the the "full equilibration" cases, hence (303-281)/(514-281) = 0.09. Adapted from [*Broecker et al.*, 1999].

Figure 10.4.6: Comparison of estimates of HBEI from a range of models. From [*Broecker et al.*, 1999].

Figure 10.4.7: Sensitivity of HBEI in the Harvardton-Bear 3-box model to changes in (a) fractional area of high-latitudes, (b) fractional ice-cover of high-latitude box, (c) low-latitude/deep ocean mixing, and (d) depth of the low-latitude box. All simulations were done following the protocols of *Broecker et al.* [1999].

Figure 10.4.8: Illustration of sensitivity of the atmospheric CO_2 concentration to the high-latitudes. In (a) the high-latitude window is open, high-latitude PO_4^{3-} high, and atmospheric pCO_2 attains concentrations of 425 ppm. (b) represents the pre-industrial ocean, where the window is half-open, PO_4^{3-} in the high-latitudes is at intermediate levels and atmospheric CO_2 is 280 ppm. In (c) the high-latitude window is closed, high-latitude PO_4^{3-} is low, and atmospheric pCO_2 decreases to about 160 ppm.

Figure 10.4.9: Contour plot of atmospheric CO$_2$ in ppm as computed by the three-box model depicted in Figure 10.4.3. Atmospheric CO$_2$ is contoured over a parameter space defined by variations in the high-latitude-deep box exchange term, f_{hd}, and the high-latitude productivity, P_h. Note that the axis are plotted logarithmically. From *Toggweiler* [1999].

Figure 10.4.10: Time-series of atmospheric CO$_2$ and dust from Vostok. Data are from *Petit et al.* [1999].

Figure 10.4.11: Map of differences of marine biological productivity between the present interglacial and the LGM. From *Bopp et al.* [2002].

Figure 10.4.12: Events surrounding the end of the last glaciation. (a) δ^{18}O of ice as a proxy for temperature from GRIP Greenland) [*Johnsen et al.*, 1997]. (b) δ^2H of ice as a proxy for temperature from Dome C (Antarctica) [*Jouzel et al.*, 2001]. (c) Dust flux (inverted scale) at Dome C site as reconstructed from the sea-salt corrected Ca^{2+} and the accumulation rate [*Roethlisberger et al.*, 2002]. (d) Atmospheric CO$_2$ as recorded in air bubbles from various Antarctic ice cores [*Indermühle et al.*, 1999, 2000; *Flückiger et al.*, 2002; *Monnin et al.*, 2002]. (e) Atmospheric N$_2$O as recorded in air bubbles from various Antarctic and Greenland ice cores. The filled triangles denote data from the GISP icecore drilled in Greenland [*Sowers et al.*, 2003], the open circles are from the Taylor Dome [*Sowers et al.*, 2003], the solid line with the crosses denote data from the GRIP icecore [*Flückiger et al.*, 1999], and the solid line with the circles are from Dome C [*Flückiger et al.*, 2002]. The data are plotted versus age before the year 1950, using age-scales of the respective records. ACR denotes Antarctic Cold Rerversal, DO1 stands for Dansgaard-Oeschger event 1. ADD sealevel or something similar

Figure 10.4.13: Time-evolution of δ^{18}O (N. pachyderma) [Charles et al., 1991], opal content [Charles et al., 1991], d30Si of diatom opal and d15N of bulk sediment [Rau and Froelich, 1993] from a sediment core taken in the Antarctic zone of the South Atlantic (core RC13-259 (53°53'S; 4°56'W; 2,677 m.). Numbers indicate oxygen isotope stages 1-10. The precision of the isotope analyses is 0.13 and 0.20 ‰ ($\pm$1 s.d.) for d30Si and d15N measurements, respectively. From *Brzezinski et al.* [2002].

Figure 10.4.14: The modern ocean (a, b) and a Southern Ocean-based synthesis hypothesis for reduced levels of atmospheric CO_2 during glacial times (c, d). The figure shows a generalized depth section running from north to south (a, c) with an expanded view of the Southern Ocean (b, d). The meridional components of ocean circulation are shown as lines, while the intensity of circulation is depicted by the shading, with the lighter shade representing more vigorous circulation. This illustrates the hypothesis that ice-age circulation was less vigorous in the cold, dense, deep ocean but more vigorous in the warmer, less dense, upper ocean. In the modern ocean (a, b), circulation of the interior can be characterized as follows. New deep water forms in the high-latitude North Atlantic (North Atlantic Deep Water, NADW). NADW flows south and mixes with other deep waters (including Antarctic Bottom Water, AABW) to generate Circumpolar Deep Water (CDW). Eastward winds (a circled cross) over the Polar Frontal Zone (PFZ) drive upwelling of CDW into the Antarctic surface, releasing deep-sequestered CO_2 to the atmosphere (upward arrow in a). Antarctic surface water flows northward to the PFZ, where it sinks into the subsurface as Antarctic Intermediate Water (AAIW) or mixes with subantarctic surface water, some of which forms Subantarctic Mode Water (SAMW). The biological production and export of organic matter (arrows) extracts nutrients and inorganic carbon from surface waters. AAIW and SAMW ventilate the mid-depth ocean and supply nutrients to the lower-latitude surface. This nutrient supply fuels biological export production, the degradation of which causes a subsurface deficit in dissolved oxygen which is most intense at intermediate depths (the O2 minimum in a). The hypothetical ice-age Southern Ocean described in the text includes the following changes (c, d). Upwelling into the Antarctic surface decreased, possibly due to an equatorward shift in the belt of eastward winds, and/or a freshening of the surface ('salinity-stratification') related to an increase in sea ice. In the Subantarctic, the winds may have driven the upwelling of intermediate-depth waters, which formed in the North Atlantic and/or North Pacific. The supply of iron from dust was high (downward arrows and stippling). Organic carbon export was higher in the Subantarctic but lower in the Antarctic (arrows). Possibly due to the greater supply of dust-borne iron, the degree of nitrate utilization was higher in both regions, leading to lower surface nitrate and less nutrient transport to the lower latitudes. This pattern of nutrient supply and export production caused the O_2 minimum to migrate into the abyssal ocean and reduced the release of CO_2 from the Southern Ocean. ADD SI EXPORT. Modified from *Sigman and Boyle* [2000].

Bibliography

Adkins, J. F., K. McIntyre, and D. P. Schrag, The salinity, temperature and $\delta^{18}O$ content of the glacial deep ocean, *Science, 298*, 1769–1773, 2002.

Alley, R. B., J. Marotzke, W. D. Nordhaus, J. T. Overpeck, D. M. Peteet, R. A. Pielke, R. T. Pierrehumbert, P. B. Rhines, T. F. Stocker, L. D. Talley, and J. M. Wallace, Abrupt climate change, *Science, 299*, 2005–2010, 2003.

Altabet, M. A., and R. Francois, Sedimentary nitrogen isotopic ratio as a recorder for surface nitrate utilization, *Global Biogeochem. Cycles, 8*(1), 103–116, 1994.

Anderson, L. A., and J. L. Sarmiento, Redfield ratios of remineralization determined by nutrient data analysis, *Global Biogeochem. Cycles, 8*(1), 65–80, 1994.

Archer, D., H. Kheshgi, and E. Maier-Reimer, Multiple time-scales for neutralization of fossil fuel CO_2, *Geophys. Res. Lett., 24*(4), 405–408, 1997.

Archer, D., H. Kheshgi, and E. Maier-Reimer, Dynamics of fossil fuel CO_2 neutralization by marine $CaCO_3$, *Global Biogeochem. Cycles, 12*(2), 259–276, 1998.

Archer, D., and E. Maier-Reimer, Effect of deep-sea sedimentary calcite preservation on atmospheric CO_2 concentration, *Nature, 367*, 260–263, 1994.

Archer, D. E., G. Eshel, A. Winguth, and W. Broecker, Atmospheric CO_2 sensitivity to the biological pump in the ocean, *Global Biogeochem. Cycles, 14*, 1219–1230, 2000.

Archer, D. E., P. A. Martin, J. Milovich, V. Brovkin, G.-K. Plattner, and C. Ashendel, Model sensitivity in the effect of antarctic sea ice and stratification on atmospheric pCO_2. paleoceanography, 18(1), , 2003., *Paleoceanogr., 18*(s), 1012, doi:10.1029/2002PA000760, 2003.

Archer, D. E., A. Winguth, D. Lea, and N. Mahowald, What caused the glacial/interglacial atmospheric pCO_2 cycles?, *Rev. Geophys., 38*(2), 159–189, 2000.

Bacastow, R. B., Modulation of atmospheric carbon dioxide by the Southern Oscillation, *Nature, 261*, 116–118, 1976.

Bacastow, R. B., J. A. Adams, C. D. Keeling, D. J. Moss, T. P. Whorf, and C. S. Wong, Atmospheric carbon dioxide, the Southern Oscillation and the weak 1975 El Niño, *Science, 210*, 66–68, 1980.

Bard, E., B. Hamelin, M. Arnold, L. Motaggioni, G. Cabioch, G. Faure, and F. Rougerie, Deglacial sea-level record from tahiti corals and the timing of global meltwater discharge, *Nature, 382*, 241–244, 1996.

Bard, E., R. Rostek, and C. Sonzogni, Interhemispheric synchrony of the last deglaciation inferred from alkenone paleothermometry, *Nature, 385*, 707–710, 1997.

Battle, M., M. Bender, P. P. Tans, J. W. C. White, J. T. Ellis, T. Conway, and R. J. Francey, Global carbon sinks and their variability, inferred from atmospheric O_2 and $\delta^{13}C$, *Science, 287*, 2467–2470, 2000.

Beck, J. W., J. Rcy, F. Taylor, R. L. Edwards, and G. Cabioch, Abrupt changes in early holocene tropical sea surface temperature derived from coral records, *Nature, 385*, 705–707, 1997.

Beerling, D. J., New estimates of carbon transfer to terrestrial ecosystems between the last glacial maximum and the holocene, *Terra Nova, 11*(4), 162–167, 1999.

Berger, W. H., Increase of carbon dioxide in the atmosphere during deglaciation: The coral reef hypothesis, *Naturwissenschaften, 69*, 87–88, 1982.

Berner, R. A., A. C. Lasage, and R. M. Garrels, The carbonate-silicate geochemical cycle and its effect on atmospheric carbon dioxide over the past 100 million years, *Am. J. Sci., 283*, 641–683, 1983.

Berner, W., B. Stauffer, and H. Oeschger, Past atmospheric composition and climate, gas parameters measured on ice cores, *Nature, 275*, 53–55, 1979.

Betts, R. A., Offset of the potential carbon sink from boreal forestation by decreases in surface albedo, *Nature, 408*, 187–190, 2000.

Birchfield, G. E., Changes in deep-ocean water $\delta^{18}O$ and temperature from the last glacial maximum to the present, *Paleoceanogr., 2*(4), 431–442, 1987.

Bird, M. I., J. Lloyd, and G. D. Farquhar, Terrestrial carbon storage at the last glacial maximum, *Nature, 371*, 566, 1994.

Bird, M. I., J. Lloyd, and G. D. Farquhar, Terrestrial carbon storage from the last glacial maximum to the present, *chemosphere, 33*, 1675–1685, 1996.

Bolin, B., and C. D. Keeling, Large-scale atmospheric mixing as deduced from the seasonal and meridional variations of carbon dioxide, *J. Geophys. Res., 68*, 3899–3920, 1963.

Bopp, L., K. E. Kohfeld, C. L. Quéré, and O. Aumont, Dust impact on marine biota and atmospheric CO_2 during glacial periods, *paloce, 18*(2), 2002, doi: 10.1029/2002PA000810.

Bopp, L., C. LeQuéré, M. Heimann, A. Manning, and P. Monfray, Climate-induced oceanic oxygen fluxes: Implications for the contemporary carbon budget, *Global Biogeochem. Cycles, 16*(2), doi:10.1029/2001GB001445, 2002.

Bopp, L., P. Monfray, O. Aumont, J.-L. Dufresne, H. L. Treut, G. Madec, L. Terray, and J. C. Orr, Potential impact of climate change on marine export production, *Global Biogeochem. Cycles, 15*(1), 81–99, 2001.

Bousquet, P., P. Peylin, P. Ciais, C. LeQuéré, P. Friedlingstein, and P. P. Tans, Regional changes in carbon dioxide fluxes of land and oceans since 1980, *Science, 290*, 1342–1346, 2000.

Boyle, E. A., Vertical oceanic nutrient fractionation and glacial/interglacial CO_2 cycles, *Nature, 331*, 55–56, 1988.

Boyle, E. A., Cadmium and $\delta^{13}C$ paleochemical distributions during the stage 2 glacial maximum, *Annual Review of Earth Planetary Science, 20*, 245–287, 1992.

Brewer, P. G., Direct observation of the oceanic CO_2 increase, *Geophys. Res. Lett., 5*(12), 997–1000, 1978.

Brix, H., N. Gruber, and C. D. Keeling, Interannual variability of the upper ocean carbon cycle at station ALOHA near Hawaii, *Global Biogeochem. Cycles*, in press, 2004.

Broecker, W. S., Glacial to interglacial changes in ocean chemistry, *Progr. Oceanogr., 11*, 151–197, 1982.

Broecker, W. S., xx, *Quat. Res., 0*(0), 0, 1986.

Broecker, W. S., Keeping global change honest, *Global Biogeochem. Cycles, 5*(3), 191–192, 1991.

Broecker, W. S., *The glacial world according to Wally*, Eldigio Press, Lamont Doherty Earth Observatory of Columbia University, Palisades, NY, 1995.

Broecker, W. S., Glacial climate in the tropics, *Science, 272*, 1902–1904, 1996.

Broecker, W. S., and G. M. Henderson, The sequence of events surrounding Termination II and their implications for the cause of glacial-interglacial CO_2 changes, *Paleoceanogr., 13*(4), 352–364, 1998.

Broecker, W. S., J. Lynch-Stieglitz, D. Archer, M. Hofmann, E. Maier-Reimer, O. Marchal, T. F. Stocker, and N. Gruber, How strong is the Harvardton-Bear constraint?, *Global Biogeochem. Cycles, 13*(4), 817–820, 1999.

Broecker, W. S., J. Lynch-Stieglitz, E. Clark, I. Hajdas, and G. Bonani, What caused the atmosphere's CO_2 content to rise during the last 8000 years?, *Geochem., Geophys., Geosys.*, doi: 10.1029/2001GC00177, 2001.

Broecker, W. S., and T.-H. Peng, *Tracers in the Sea*, Eldigio Press, Lamont-Doherty Geological Observatory, Palisades, NY, 1982.

Broecker, W. S., and T. H. Peng, *Greenhouse Puzzles, 2nd edition*, Eldigio Press, Lamont Doherty Earth Observatory of Columbia University, Palisades, NY, 1998.

Broecker, W. S., and T. Takahashi, Neutralization of fossil fuel CO$_2$ by marine calcium carbonate, in *The fate of fossil fuel CO$_2$ in the Oceans*, edited by N. Andersen and A. Malahoff, pp. 213, Plenum Press, New York, 1977.

Broecker, W. S., T. Takahashi, and T.-H. Peng, Reconstruction of past atmospheric CO$_2$ from the chemistry of the contemporary ocean: An evaluation, *U.S. Dep. of Energy, Washington, D.C., Tech. Rep. TRO 20*, 1985.

Brzezinski, M. A., J. L. Sarmiento, K. Matsumoto, C. J. Pride, D. M. Sigman, N. Gruber, G. H. Rau, and K. H. Coale, A switch from Si(OH)$_4$ to NO$_3^-$ depletion in the glacial Southern Ocean, *Geophys. Res. Lett., 29*(12), 5.1 – 5.4, doi: 10.1029/2001GL014349, 2002.

Catubig, N. R., D. E. Archer, R. Francois, P. deMenocal, W. Howard, and E.-F. Yu, Global deep-sea burial rate of calcium carbonate during the last glacial maximum, *Paleoceanogr., 13*(3), 298–310, 1998.

Charles, C. D., and R. G. Fairbanks, Glacial to interglacial ^{13}C change in benthic and planctonic foraminifera from the Southern Oceans, in *Geological History of the Polar oceans: Arctic versus Antarctic*, edited by U. Bleil and J. Thiede, pp. 512–538, Kluwer Acad. Publ., Dordrecht, 1990.

Chavez, F. P., P. G. Strutton, G. E. Friederich, R. A. Feely, G. C. Feldman, D. G. Foley, and M. J. McPhaden, Biological and chemical response of the Equatorial Pacific ocean to the 1997-98 El Niño, *Science, 286*, 2126–2131, 1999.

Chen, C.-T. A., and F. J. Millero, Gradual increase of oceanic CO$_2$, *Nature, 277*, 205–206, 1979.

CLIMAP Project members, Seasonal reconstruction of the earth's surface at the last glacial maximum, *Geol. Soc. Am., Tech. Rep. Map and Chart Ser., MC 36*, Boulder, Colorado, 1981.

Crosta, X., J. Pichon, and L. Burckle, Application of modern analog technique to marine antarctic diatoms: Reconstruction of maximum sea ice extent at the last glacial maximum, *Paleoceanogr., 13*, 284–297, 1998.

Crutzen, P. J., and E. F. Stoermer, The anthropocene, *IGBP Newsletter, 41*, 12–13, 2000.

Cubasch, U., G. A. Meehl, G. J. Boer, R. J. Stouffer, M. Dix, A. Noda, C. A. Senior, S. Raper, and K. S. Yap, Projections of future climate change, in *Climate Change 2001: The Scientific Basis. Contribution of Working Group I to the Third Assessment Report of the Intergovernmental Panel on Climate Change*, edited by J. T. Houghton, Y. Ding, D. J. Griggs, M. Noguer, P. van der Linden, X. Dai, K. Maskell, and C. A. Johnson, Chapter 10, pp. 527–585, Cambridge University Press, Cambridge, 2001.

Curry, W. B., J. C. Duplessy, L. D. Labeyrie, and N. J. Shackelton, Changes in the distribution of δ^{13}C of deep water TCO$_2$ between the last glaciation and the holocene, *Paleoceanogr., 3*(3), 317–341, 1988.

Delaney, M. L., Phosphorus accumulation in marine sediments and the oceanic phosphorus cycle, *Global Biogeochem. Cycles, 12*(4), 563–572, 1998.

Delmas, R. J., J.-M. Ascencio, and M. Legrand, Polar ice evidence that atmospheric CO$_2$ 29,000 BP was 50% of present, *Nature, 284*, 155–157, 1980.

der Werf, G. R. V., J. Randerson, G. J. Collatz, L. Giglio, P. Kasibhatla, A. Arellano, S. Olsen, and E. Kasischke, Continental-scale partitioning of fire emissions during the 1997 to 2001 El Niño/La Niña period, *Science, 303*, 73–76, 2004.

Dickinson, R. E., and R. J. Cicerone, Future global warming from atmospheric trace gases, *Nature, 319*, 109–115, 1986.

Dore, J. E., R. Lukas, D. W. Sadler, and D. M. Karl, Climate-driven changes to the atmospheric CO$_2$ sink in the subtropical North Pacific Ocean, *Nature, 424*, 754–757, 2003.

Enting, I. G., *Inverse Problems in atmospheric constituent transport*, Cambridge Atmospheric and Spae Science Series, Cambridge University Press, Cambridge, 2002.

Etheridge, D. M., L. P. Steele, R. L. Langenfelds, R. J. Francey, J.-M. Barnola, and V. I. Morgan, Natural and anthropogenic changes in atmospheric CO$_2$ over the last 1000 years from air in Antarctic ice and firn, *J. Geophys. Res., 101*, 4115–4128, 1996.

Falkowski, P. G., Evolution of the nitrogen cycle and its influence on the biological sequestration of CO$_2$ in the ocean, *Nature, 387*, 272–275, 1997.

Feely, R. A., C. L. Sabine, K. Lee, W. Berelson, J. Kleypas, V. J. Fabry, and F. J. Millero, Impact of anthropogenic CO$_2$ on the CaCO$_3$ system in the oceans, *Science, 305*, 362–366, 2004.

Feely, R. A., R. Wanninkhof, C. E. Cosca, P. P. Murphy, M. F. Lamb, and M. D. Steckley, CO$_2$ distributions in the equatorial Pacific during the 1991-1992 ENSO event, *Deep Sea Res. II, 42*(2-3), 365–386, 1995.

Feely, R. A., R. Wanninkhof, C. Goyet, D. E. Archer, and T. Takahashi, Variability of CO$_2$ distributions and sea-air fluxes in the central and eastern equatorial Pacific during the 1991-1994 El Niño, *Deep Sea Res. II, 44*(9-10), 1851–1867, 1997.

Feely, R. A., R. Wanninkhof, T. Takahashi, and P. Tans, Influence of El Niño on the equatorial Pacific contribution to atmospheric CO$_2$ accumulation, *Nature, 398*, 597–601, 1999.

Fischer, H., M. Wahlen, J. Smith, D. Mastroianni, and B. Deck, Ice core records of atmospheric CO$_2$ around the last three glacial terminations, *Science, 283*, 1712–1714, 1999.

Flückiger, J., A. Dällenbach, T. Blunier, B. Stauffer, T. F. Stocker, D. Raynaud, and J.-M. Barnola, Variations in atmospheric N$_2$O concentration during abrupt climate changes, *Science, 285*, 227–230, 1999.

Flückiger, J., E. Monnin, B. Stauffer, J. Schwander, T. F. Stocker, J. C. D. Raynaud, and J.-M. Barnola, High-resolution holocene N$_2$O ice core record and its relationship with CH$_4$ and CO$_2$, *Global Biogeochem. Cycles, 16*(1), doi: 10.29/2001GB001417, 2002.

Follows, M. J., T. Ito, and J. Marotzke, The wind-driven, subtropical gyres and the solubility pump of CO$_2$, *Global Biogeochem. Cycles, 16*(4), 1113, doi:10.1029/2001GB001786, 2002.

Francey, R. J., P. P. Tans, C. E. Allison, I. G. Enting, J. W. C. White, and M. Troller, Changes in oceanic and terrestrial carbon uptake since 1982, *Nature, 373*, 326–330, 1995.

Francois, R., M. A. Altabet, E.-F. Y, D. M. Sigman, M. P. Bacon, M. Frank, G. Bohrmann, G. Bareille, and L. D. Labeyrie, Contribution of southern ocean surface-water stratification to low atmospheric CO$_2$ concentrations during the last glacial period, *Nature, 389*, 929–933, 1997.

Ganeshram, R. S., T. F. Pedersen, S. E. Calvert, and J. W. Murray, Large changes in oceanic nutrient inventories from glacial to interglacial periods, *Nature, 376*, 755–758, 1995.

Gattuso, J.-P., M. Frankignoulle, S. V. Smith, J. R. Ware, and R. Wollast, Coral reefs and carbon dioxide, *Science, 271*, 1298–1300, 1996.

Ghil, M., Cryothermodynamics: The chaotic dynamics of paleoclimate, *Physica D, 77*, 130–159, 1994.

Ghil, M., A. Mullhaupt, and P. Pestiaux, Deep water formation and quaternary glaciations, *Clim. Dyn., 2*, 1–10, 1987.

Gildor, H., and E. Tziperman, Physical mechanisms behind biogeochemical glacial-interglacial CO$_2$ variations, *Geophys. Res. Lett., 28*, 2421–2424, 2001a.

Gildor, H., and E. Tziperman, A sea ice climate switch mechanism for the 100-kyr glacial cycles, *J. Geophys. Res., 106*, 9117–9133, 2001b.

Gildor, H., E. Tziperman, and J.R.Toggweiler, Sea ice switch mechanism and glacial-interglacial CO$_2$ variations, *Global Biogeochem. Cycles, 16*, doi: 10.1029/2001GB001446, 2002.

Gloor, M., N. Gruber, J. L. Sarmiento, C. L. Sabine, R. A. Feely, and C. Roedenbeck, A first estimate of present and pre-industrial air-sea CO$_2$ fluxes patterns based on ocean interior carbon measurements and models, *Geophys. Res. Lett., 30*, 1–4, doi:10.1029/2002GL015594, 2003.

Goodale, C. L., and E. A. Davidson, Uncertain sinks in the shrubs, *Nature, 418*, 593–594, 2002.

Gordon, A. L., Seasonality of Southern Ocean sea ice, *J. Geophys. Res., 86*, 4193–4197, 1981.

Gruber, N., Anthropogenic CO$_2$ in the Atlantic Ocean, *Global Biogeochem. Cycles, 12*(1), 165–191, 1998.

Gruber, N., The dynamics of the marine nitrogen cycle and atmospheric CO$_2$, in *Carbon Climate interactions*, edited by T. Oguz and M. Follows, Kluwer Academic, Rotterdam, in press, 2004.

Gruber, N., N. Bates, and C. D. Keeling, Interannual variability in the North Atlantic carbon sink, *Science, 298*, 2374–2378, 2002.

Gruber, N., P. Friedlingstein, C. B. Field, R. Valentini, M. Heimann, J. E. Richey, P. Romero-Lankao, D. Schulze, and C. Chen, The vulnerability of the carbon cycle in the 21st century: An assessment of carbon-climate-human interactions, in *Toward CO$_2$ stabilization: Issues, Strategies, and Consequences*, edited by C. B. Field and M. R. Raupach, Chapter 2, pp. 45–76, Island Press, Washington, D.C., 2004.

Gruber, N., and C. D. Keeling, An improved estimate of the isotopic air-sea disequilibrium of CO$_2$: Implications for the oceanic uptake of anthropogenic CO$_2$, *Geophys. Res. Lett., 28*(3), 555–558, 2001.

Gruber, N., and J. L. Sarmiento, Global patterns of marine nitrogen fixation and denitrification, *Global Biogeochem. Cycles, 11*(2), 235–266, 1997.

Gruber, N., and J. L. Sarmiento, Biogeochemical/physical interactions in elemental cycles, in *THE SEA: Biological-Physical Interactions in the Oceans*, edited by A. R. Robinson, J. J. McCarthy, and B. J. Rothschild, vol. 12, pp. 337–399, John Wiley and Sons,, New York, 2002.

Gruber, N., J. L. Sarmiento, and T. F. Stocker, An improved method for detecting anthropogenic CO$_2$ in the oceans, *Global Biogeochem. Cycles, 10*(4), 809–837, 1996.

Guilderson, R. P., R. G. Fairbanks, and J. L. Rubinstone, Tropical temperature variations since 20,000 years ago: modulating interhemispheric climate change, *Science, 263*, 663–665, 1994.

Gurney, K. R., R. M. Law, A. S. Denning, P. J. Rayner, D. Baker, P. Bousquet, L. Bruhwiler, Y.-H. Chen, P. Ciais, S. Fan, I. Y. F. M. Gloor, M. Heimann, K. Higuchi, J. John, T. Maki, S. Maksyutov, K. Masarie, P. Peylin, M. Prather, B. C. Pak, J. Randerson, J. Sarmiento, S. Taguchi, T. Takahashi, and C.-W. Yuen, Towards robust regional estimates of CO$_2$ sources and sinks using atmospheric transport models, *Nature, 415*, 626–630, 2002.

Heimann, M., and E. Maier-Reimer, On the relations between the oceanic uptake of CO$_2$ and its carbon isotopes, *Global Biogeochem. Cycles, 10*(1), 89–110, 1996.

Houghton, J. T., Y. Ding, D. J. Griggs, M. Noguer, P. van der Linden, X. Dai, K. Maskell, and C. A. Johnson, *Climate Change 2001: The Scientific Basis*, Cambridge University Press, New York, 2001.

Houghton, J. T., G. J. Jenkins, and J. J. Ephraums, *Climate Change, The IPCC Scientific Assessment*, Cambridge University Press, New York, 1990.

Imbrie, J., and Imbrie, *xx*, yy, 1986.

Indermuehle, A., E. Monnin, B. Stauffer, T. F. Stocker, and M. Wahlen, Atmospheric CO$_2$ concentration from 60 to 20 kyr BP from the the Taylor Dome ice core, Antarctica, *Geophys. Res. Lett., 27*(5), 735–738, 2000.

Indermühle, A., T. F. Stocker, F. Joos, H. Fischer, H. J. Smith, M. Wahlen, B. Deck, D. Mastroianni, J. Tschumi, T. Blunier, R. Meyer, and B. Stauffer, Holocene carbon-cycle dynamics based on CO$_2$ trapped in ice at Taylor Dome, Antarctica, *Nature, 398*, 121–126, 1999.

Ito, T., and M. Follows, Upper ocean control on the solubility pump of co2, *J. Mar. Res., 61*, 465–489, 2003.

Johnsen, S. J., H. Clausen, W. Dansgaard, N. Gundestrup, C. Hammer, U. Andersen, K. Andersen, C. Hvidberg, D. Dahl-Jensen, J. Steffensen, H. Shoji, A. Sveinbjrnsdttir, J. White, J. Jouzel, , and D. Fisher, The δ^{18}O record along the Greenland Ice Core Project deep ice core and the problem of possible Eemian climatic instability, *J. Geophys. Res., 102*, 26397–26410, 1997.

Jones, P. D., and A. Moberg, Hemispheric and large-scale surface air temperature variations: An extensive revision and an update to 2001, *J. Clim., 16*, 206–223, 2003.

Joos, F., M. Bruno, R. Fink, U. Siegenthaler, T. F. Stocker, C.LeQuere, and J. L. Sarmiento, An efficient and accurate representation of complex oceanic and biospheric models of anthropogenic carbon uptake, *Tellus, 48B*, 397–417, 1996.

Joos, F., S. Gerber, I. C. Prentice, B. L. Otto-Bliesner, and P. J. Valdes, Transient simulations of holocene atmospheric carbon dioxide and terrestrial carbon since the last glacial maximum, *Global Biogeochem. Cycles, 18*(2), doi:10.1029/2003GB002156, 2004.

Joos, F., R. Meyer, M. Bruno, and M. Leuenberger, The variability in the carbon sinks as reconstructed for the last 1000 years, *Geophys. Res. Lett., 26*, 1437–1441, 1999.

Joos, F., G.-K. Plattner, T. F. Stocker, O. Marchal, and A. Schmittner, Global warming and marine carbon cycle feedbacks on future atmospheric CO_2, *Science, 284*, 464–467, 1999.

Jouzel, J., V. Masson, O. Cattani, S. Falourd, M. Stievenard, B. Stenni, A. Longinelli, S. Johnsen, J. Steffensen, J. Petit, J. Schwander, R. Souchez, , and N. Barkov, A new 27 ky high resolution east antarctic climate record, *Geophys. Res. Lett., 28*(16), 3199–3202, 2001.

Keeling, C., H. Brix, and N.Gruber, Seasonal and long-term dynamics of the upper ocean carbon cycle at station ALOHA near Hawaii, *Global Biogeochem. Cycles*, in press, 2004.

Keeling, C. D., R. B. Bacastow, A. F. Carter, S. C. Piper, T. P. Whorf, M. Heimann, W. G. Mook, and H. Roeloffzen, A three dimensional model of atmospheric CO_2 transport based on observed winds: 1. analysis of observational data, in *Aspects of Climate Variability in the Pacific and the Western Americas*, edited by D. H. Peterson, Geophys. Monogr. Ser., 55, pp. 165–237, AGU, Washington, D.C., 1989.

Keeling, C. D., and R. Revelle, Effects of El Niño/Southern Oscillation on the atmospheirc content of carbon dioxide, *Meteoritics, 20*(2), 437–450, 1985.

Keeling, C. D., and T. P. Whorf, Atmospheric CO_2 concentration – Mauna Loa Observatory, Hawaii, 1958 - 1997 (revised August 1998), *Carbon Dioxide Inf. Anal. Cent., Data Report, ORNL NDP-001*, Oak Ridge Natl. Lab., Oak Ridge, Tenn., 1998.

Keeling, C. D., T. P. Whorf, M. Wahlen, and J. v. d. Plicht, Interannual extremes in the rate of atmospheric carbon dioxide since 1980, *Nature, 375*, 666–670, 1995.

Keeling, R., S. C. Piper, and M. Heimann, Global and hemispheric CO_2 sinks deduced from changes in atmospheric O_2 concentration, *Nature, 381*, 218–221, 1996.

Keeling, R. F., and H. E. Garcia, The change in oceanic O_2 inventory associated with recent global warming, *Proceedings of the National Academy of Sciences, 99*(12), 7848–7853, 2002.

Keeling, R. F., and S. R. Shertz, Seasonal and interannual variations in atmospheric oxygen and implications for the global carbon cycle, *Nature, 358*, 723–727, 1992.

Kiehl, J. T., and K. E. Trenberth, Earth's annual global mean energy budget, *Bull. Am. Meteor. Soc., 78*(12), 197–208, 1997.

Kindermann, J., G. Würth, G. H. Kohlmaier, and F.-W. Badeck, Interannual variation of carbon exchange fluxes in terrestrial ecosystems, *Global Biogeochem. Cycles, 10*(4), 737–755, 1996.

Kleypas, J. A., R. W. Buddemeier, D. Archer, J.-P. Gattuso, C. Langdon, and B. N. Opdyke, Geochemical consequences of increased atmospheric carbon dioxide on coral reefs, *Science, 284*, 118–120, 1999.

Knox, F., and M. McElroy, Changes in atmospheric CO_2: influence of marine biota at high latitudes, *J. Geophys. Res., 89*, 4629–4637, 1984.

Lane, E., S. Peacock, and J. L. Restrepo, A model of glacial-interglacial changes in atmospheric carbon dioxide, *J. Clim.*, submitted, 2004.

Lee, K., S.-D. Choi, G. H. Park, R. Wanninkhof, T.-H. Peng, R. M. Key, C. L. Sabine, R. A. Feely, F. J. Millero, and A. Kozyr, An updated anthropogenic CO_2 inventory in the atlantic ocean, *Global Biogeochem. Cycles, 17*, 1116, doi:10.1029/2003GB002067, 2003.

Lee, K., R. Wanninkhof, T. Takahashi, S. C. Doney, and R. A. Feely, Low interannual variability in recent oceanic uptake of atmospheric carbon dioxide, *Nature, 396*, 155–158, 1998.

LeQuéré, C., O. Aumont, L. Bopp, P. Bousquet, P. Ciais, R. Francey, M. Heimann, C. D. Keeling, R. F. Keeling, H. Kheshgi, P. Peylin, S. C. Piper, I. C. Prentice, and P. J. Rayner, Two decades of ocean CO_2 sink and variability, *Tellus, Ser. B.*, in press, 2003.

LeQuéré, C., and N. Gruber, Satellite observation constraints on air-sea CO_2 flux variability, *Global Biogeochem. Cycles*, in preparation, 2004.

LeQuéré, C., J. C. Orr, P. Monfray, O. Aumont, and G. Madec, Interannual variability of the oceanic sink of CO_2 from 1979 through 1997, *Global Biogeochem. Cycles, 14*, 1247–1265, 2000.

Leuenberger, M., U. Siegenthaler, and C. C. Langway, Carbon isotope composition of atmospheric CO_2 during the last ice age from an antarctic ice core, *Nature, 357*, 1992.

Levitus, S., J. I. Antonov, T. P. Boyer, and C. Stephens, Warming of the World Ocean, *Science, 287*, 2225–2229, 2000.

Longhurst, A. R., A reply to Broecker's charges, *Global Biogeochem. Cycles, 5*(4), 315–316, 1991.

Mahowald, N., K. E. Kohfeld, M. Hansson, Y. Balkanski, S. P. Harrison, I. C. Prentice, M. Schulz, and H. Rodhe, Dust sources and deposition during the Last Glacial Maximum and current climate: A comparison of model results with paleodata from ice cores and marine sediments, *J. Geophys. Res., 104*, 15,895–15,916, 1999.

Maier-Reimer, E., and K. Hasselmann, Transport and storage of CO$_2$ in the ocean – an inorganic ocean-circulation carbon cycle model, *Clim. Dyn., 2*, 63–90, 1987.

Marino, B. D., M. B. McElroy, R. J. Salawitch, and W. G. Spaulding, Glacial-to-interglacial variations in the carbon isotopic composition of atmospheric CO$_2$, *Nature, 357*, 461–466, 1992.

Marland, G., R. J. Andres, T. A. Boden, C. Johnston, and A. Brenkert, Global, regional and national CO$_2$ emission estimates from fossil fuel burning, cement production and gas flaring: 1751-1996 (revised March 1999), *Carbon Dioxide Inf. Anal. Cent.*, *Data Report, ORNL NDP-030*, Oak Ridge Natl. Lab., Oak Ridge, Tenn., 1998.

Martin, J. H., Glacial-interglacial CO$_2$ change: the iron hypothesis, *Paleoceanogr., 5*(1), 1–13, 1990.

Matear, R. J., and A. C. Hirst, Climate change feedback on the future oceanic CO$_2$ uptake, *Tellus, Ser. B., 51*, 722–733, 1999.

Matsumoto, K., J. L. Sarmiento, and M. A. Brzezinski, Silicic acid leakage from the Southern Ocean as possible mechanism for explaining glacial atmospheric pCO$_2$, *Global Biogeochem. Cycles, 16*(10), doi:10.1029/2001GB001442, 2002.

Matsumoto, K., J. L. Sarmiento, R. M. Key, J. L. Bullister, K. Caldeira, J.-M. Campin, S. C. Doney, H. Drange, J.-C. Dutay, M. Follows, Y. Gao, A. Gnanadesikan, N. Gruber, A. Ishida, F. Joos, K. Lindsay, E. Maier-Reimer, J. C. Marshall, R. J. Matear, P. Monfray, A. Mouchet, R. Najjar, G.-K. Plattner, R. Schlitzer, R. Slater, P. S. Swathi, I. J. Totterdell, M.-F. Weirig, Y. Yamanaka, A. Yool, and J. C. Orr, Evaluation of ocean carbon cycle models with data-based metrics, *Geophys. Res. Lett., 31*, L07303, doi:10.1029/2003GL018970, 2004.

McElroy, M. B., Marine biological controls on atmospheric CO$_2$ and climate, *Nature, 302*, 328–329, 1983.

McKinley, G. A., 2002, *Interannual variability of the air-sea fluxes of carbon dioxide and oxygen*, Ph.d. thesis, Massachussetts Institute of Technology, Cambridge, MA.

McNeil, B. I., R. J. Matear, J. Bullister, R. M. Key, and J. Sarmiento, Anthropogenic CO$_2$ uptake by the oceans using the global chorofluorocarbon dataset, *Science, 299*, 235–299, 2003.

McNeil, B. I., B. Tilbrook, and R. J. Matear, Accumulation and uptake of anthropogenic CO$_2$ in the southern ocean, south of australia from 1968 to 1996, *J. Geophys. Res., c12*, 31,431–31,445, 2001.

Milliman, J. D., Production and accumulation of calcium carbonate in the ocean: Budget of a nonsteady state, *Global Biogeochem. Cycles, 7*(4), 927–957, 1993.

Mitchell, J. F. B., D. J. Karoly, G. C. Hegerl, F. W. Zwiers, M. R. Allen, and J. Marengo, Detection of climate change and attribution of causes, in *Climate Change 2001: The Scientific Basis. Contribution of Working Group I to the Third Assessment Report of the Intergovernmental Panel on Climate Change*, edited by J. T. Houghton, Y. Ding, D. J. Griggs, M. Noguer, P. van der Linden, X. Dai, K. Maskell, and C. A. Johnson, Chapter 12, pp. 527–585, Cambridge University Press, Cambridge, 2001.

Monnin, E., A. Indermühle, A. Dällenbach, J. Flückiger, B. Stauffer, T. F. Stocker, D. Raynaud, and J.-M. Barnola, Atmospheric CO$_2$ concentrations over the last glacial termination, *Science, 291*, 112–114, electronic copy, 2002.

Murnane, R. J., J. L. Sarmiento, and C. LeQuéré, The spatial distribution of air-sea fluxes and the interhemispheric transport of carbon by the oceans, *Global Biogeochem. Cycles, 13*, 287–305, 1999.

Neftel, A., E. Moor, H. Oeschger, and B. Stauffer, Evidence from polar ice cores for the increase in atmospheric CO$_2$ in the past two centuries, *Nature, 315*, 45–47, 1985.

Neftel, A., H. Oeschger, J. Schwander, B. Stauffer, and R. Zumbrunn, Ice core sample measurements give atmospheric CO$_2$ content during the past 40,000 yr, *Nature, 295*, 220–223, 1982.

Nevison, C. D., T. J. Lueker, and R. F. Weiss, Quantifying the nitrous oxide source from coastal upwelling, *Global Biogeochem. Cycles, 18*(GB1018), doi:10.1029/2003GB002110, 2004.

Oeschger, H., U. Siegenthaler, U. Schotterer, and A. Gugelmann, A box diffusion model to study the carbon dioxide exchange in nature, *Tellus, 27*(2), 168–192, 1975.

Opdyke, B. N., and J. C. G. Walker, Return of the coral reef hypothesis: basin to shelf partitioning of $CaCO_3$ and its effect on atmospheric pCO_2, *Geology, 20*, 733–736, 1992.

Orr, J. C., E. Maier-Reimer, U. Mikolajewicz, P. Monfray, J. L. Sarmiento, J. R. Toggweiler, N. K. Taylor, J. Palmer, N. Gruber, C. L. Sabine, C. LeQuéré, R. M. Key, and J. Boutin, Global oceanic uptake of anthropogenic carbon dioxide as predicted by four 3-D ocean models, *Global Biogeochem. Cycles, 15*(1), 43–60, 2001.

Pacala, S. W., G. C. Hurtt, D. Baker, P. P. P, R. A. Houghton, R. A. Birdsey, L. Heath, E. T. Sundquist, R. F. Stallard, P. Ciais, P. Moorcroft, J. P. Caspersen, E. Shevliakova, B. Moore, G. Kohlmaier, E. Holland, M. Gloor, M. E. Harmon, S.-M. Fan, J. L. Sarmiento, C. L. Goodale, D. Schimel, and C. B. Field, Consistent land- and atmosphere-based U.S. carbon sink estimates, *Science, 292*, 2316–2320, 2001.

Peltier, W. R., Ice age paleotopography, *Science, 265*, 195–201, 1994.

Peng, T.-H., R. Wanninkhof, J. L. Bullister, R. A. Feely, and T. Takahashi, Quantification of decadal anthropogenic CO_2 uptake in the ocean based on dissolved inorganic carbon measurements, *Nature, 396*, 560–563, 1998.

Peng, T.-H., R. Wanninkhof, and R. A. Feely, Increase of anthropogenic CO_2 in the Pacific Ocean over the last two decades, *Deep Sea Res. II, 50*, 3065–3082, 2003.

Petit, J. R., J. Jouzel, D. Raynaud, N. I. Barkov, J.-M. Barnola, I. Basile, M. Bender, J. Chappellaz, M. Davis, G. Delaygue, M. Delmotte, V. M. Kotlyakov, M. Legrand, V. Y. Lipenkov, C. Lorius, L. Pépin, C. Ritz, E. Saltzman, and M. Stievenard, Climate and atmospheric history of the past 420,000 years from Vostok ice core, Antarctica, *Nature, 399*, 429–436, 1999.

Peylin, P., P. Bousquet, C. LeQuéré, P. Friedlingstein, S. Sitch, G. McKinley, N. Gruber, P. Ciais, and P. Rayner, Interannual CO_2 fluxes as deduced by inverse modeling and by models of the biogeochemical carbon cycle, *Global Biogeochem. Cycles*, submitted, 2004.

Plattner, G.-K., F. Joos, T. F. Stocker, and O. Marchal, Feedback mechanisms and sensitivities of ocean carbon uptake under global warming, *Tellus, Ser. B., 53*, 564–592, 2001.

Prather, M., D. Ehhalt, F. Dentener, R. Derwent, E. Dlugokencky, E. Holland, I. Isaksen, J. Katima, V. Kirchhoff, P. Matson, P. Midgley, and M. Wang, Atmospheric chemistry and greenhouse gases, in *Climate Change 2001: The Scientific Basis. Contribution of Working Group I to the Third Assessment Report of the Intergovernmental Panel on Climate Change*, edited by J. T. Houghton, Y. Ding, D. J. Griggs, M. Noguer, P. van der Linden, X. Dai, K. Maskell, and C. A. Johnson, Chapter 4, pp. 527–585, Cambridge University Press, Cambridge, 2001.

Prentice, I. C., G. D. Farquhar, M. J. R. Fasham, M. L. Goulden, M. Heimann, V. J. Jaramillo, H. S. Keshgi, C. LeQuéré, R. J. Scholes, and D. W. R. Wallace, 2001, *IPCC WGI Third Assessment Report*, Chapter Chapter 3. The carbon cycle and atmospheric CO_2, Cambridge: Cambridge University Press.

Quay, P. D., B. Tilbrook, and C. S. Wong, Oceanic uptake of fossil fuel CO_2: Carbon-13 evidence, *Science, 256*, 74–79, 1992.

Ramaswamy, V., O. Boucher, J. Haigh, D. Hauglustaine, J. Haywood, G. Myhre, T. Nakajima, G. Y. Shi, and S. Solomon, Radiative forcing of climate change, in *Climate Change 2001: The Scientific Basis. Contribution of Working Group I to the Third Assessment Report of the Intergovernmental Panel on Climate Change*, edited by J. T. Houghton, Y. Ding, D. J. Griggs, M. Noguer, P. van der Linden, X. Dai, K. Maskell, and C. A. Johnson, Chapter 6, pp. 527–585, Cambridge University Press, Cambridge, 2001.

Rayner, P., I. Enting, R. Francey, and R. Langenfelds, Reconstructing the recent carbon cycle from atmospheric CO_2, $\delta^{13}C$ and O_2/N_2 observations, *Tellus, Ser. B., 51B*, 213–232, 1999.

Riebesell, U., I. Zondervan, B. Rost, P. D. Tortell, R. E. Zeebe, and F. M. M. Morel, Reduced calcification of marine plankton in response to increased atmospheric CO_2, *Nature, 407*, 364–367, 2000.

Rocha, C. L. D. L., M. A. Brzezinski, M. J. DeNiro, and A. Shemesh, Silicon-isotope composition of diatoms as an indicator of past oceanic change, *Nature, 395*, 680–683, 1998.

Roedenbeck, C., S. Houweling, M. Gloor, and M. Heimann, Time-dependent atmospheric CO_2 inversions based on interannually varying tracer transport, *Tellus, Ser. B., 55*(2), 488–497, 2003.

Roethlisberger, R., R. Mulvaney, E. W. Wolff, M. A. Hutterli, M. Bigler, S. Sommer, and J. Jouzel, Dust and sea salt variability in central East Antarctica (Dome C) over the last 45 kyrs and its implications for southern high-latitude climate, *Geophys. Res. Lett., 29*(20), 24.1 – 24.4, 1963, doi:10.1029/2002GL015186, 2002.

Sabine, C. L., R. A. Feely, N. Gruber, R. F. Key, K. Lee, J. L. Bullister, R. Wanninkhof, C. S. Wong, D. W. R. Wallace, B. Tillbrook, F. J. Millero, T.-H. Peng, A. Kozyr, , T. Ono, and A. R. Rios, The oceanic sink for anthropogenic CO$_2$, *Science, 305*, 367–371, electronic copy, 2004.

Sabine, C. L., R. A. Feely, R. M. Key, J. L. Bullister, F. J. Millero, K. Lee, T.-H. Peng, B. Tillbrook, T. Ono, and C. S. Wong, Distribution of anthropogenic CO$_2$ in the Pacific ocean, *Global Biogeochem. Cycles, 16*(4), 30.1–30.17, 1083, doi:10.1029/2001GB001639, 2002.

Sabine, C. L., R. M. Key, K. M. Johnson, F. J. Millero, J. L. Sarmiento, D. W. R. Wallace, and C. D. Winn, Anthropogenic CO$_2$ inventory of the Indian ocean, *Global Biogeochem. Cycles, 13*(1), 179–198, 1999.

Sanyal, A., N. G. Hemming, G. N. Hanson, and W. S. Broecker, Evidence for a higher ph in the glacial ocean from boron isotopes in foraminifera, *Nature, 373*, 234–236, 1995.

Sarmiento, J. L., Oceanic uptake of anthropogenic CO$_2$: the major uncertainties, *Global Biogeochem. Cycles, 5*(4), 309–313, 1991.

Sarmiento, J. L., and N. Gruber, Anthropogenic carbon sinks, *Physics Today, 55*, 30–36, 2002.

Sarmiento, J. L., N. Gruber, M. A. Brzezinski, and J. P. Dunne, High-latitude controls of thermocline nutrients and low-latitude biological productivity, *Nature, 427*, 56–60, 2004.

Sarmiento, J. L., T. M. C. Hughes, R. J. Stouffer, and S. Manabe, Simulated response of the ocean carbon cycle to anthropogenic climate warming, *Nature, 393*, 245–249, 1998.

Sarmiento, J. L., and C. LeQuéré, Oceanic carbon dioxide uptake in a model of century-scale global warming, *Science, 274*, 1346–1350, 1996.

Sarmiento, J. L., C. LeQuéré, and S. W. Pacala, Limiting future atmospheric carbon dioxide, *Global Biogeochem. Cycles, 9*(1), 121–137, 1995.

Sarmiento, J. L., J. C. Orr, and U. Siegenthaler, A perturbation simulation of CO$_2$ uptake in an ocean general circulation model, *J. Geophys. Res., 97*(C3), 3621–3645, 1992.

Sarmiento, J. L., and E. T. Sundquist, Revised budget for the oceanic uptake of anthropogenic carbon dioxide, *Nature, 356*, 589–593, 1992.

Sarmiento, J. L., and J. R. Toggweiler, A new model for the role of the oceans in determining atmospheric pCO$_2$, *Nature, 308*, 621–624, 1984.

Schimel, D., D. Alves, I. Enting, M. Heimann, F. Joos, D. Raynaud, T. Wigley, M. Prather, R. Derwent, D. Ehhalt, P. Fraser, E. Sanhueza, X. Zhou, P. Jonas, R. Charlson, H. Rohde, S. Sadasivan, K. Shine, Y. Fouquart, V. Ramaswamy, S. Solomon, J. Srinivasan, D. Albritton, I. Isaken, M. Lal, and D. Wuebbles, 1996, *Climate Change 95, The Science of Climate Change*, Chapter 2. Radiative Forcing of Climate Change, pp. 65–131, Cambridge, England: Intergovt. Panel on Clim. Change.

Schimel, D., I. Enting, M. Heimann, T. Wigley, D. Raynaud, D. Alves, and U. Siegenthaler, 1994, *Climate Change 94, Radiative Forcing of Climate Change*, Chapter CO$_2$ and the carbon cycle, pp. 38–71, Cambridge, England: Intergovt. Panel on Clim. Change.

Schimel, D. S., J. I. House, K. A. Hibbard, P. Bousquet, P. Ciais, P. Peylin, B. H. Braswell, M. J. Apps, D. Baker, A. Bondeau, J. Canadell, G. Churkina, W. Cramer, A. S. Denning, C. B. Field, P. Friedlingstein, C. Goodale, M. Heimann, R. A. Houghton, J. M. Melillo, B. M. III, D. Murdiyarso, I. Noble, S. W. Pacala, I. C. Prentice, M. R. Raupach, P. J. Rayner, R. J. Scholes, W. L. Steffen, and C. Wirth, Recent patterns and mechanisms of carbon exchange by terrestrial ecosystems, *Nature, 414*, 169–172, 2001.

Schrag, D. P., G. Hampt, and D. W. Murray, Pore fluid constraints on the temperature and oxygen isotopic composition of the glacial ocean, *Science, 272*, 1930–1932, 1996.

Severinghaus, J. P., 1995, *Studies of the terrestrial O$_2$ and carbon cycles in sand due gases and in Biosphere 2*, Ph.d., Columbia Univ., New York.

Shackelton, N. J., Carbon-13 in uvigerina: tropical rainforest history and the equatorial carbonate dissolution cycles, in *The fate of fossil fuel CO_2 in the Oceans*, edited by N. Andersen and A. Malahoff, pp. 401–428, Plenum Press, New York, 1977.

Shiller, A. M., Calculating the oceanic CO_2 increase: A need for caution, *J. Geophys. Res., 86* (C11), 11083–11088, 1981.

Shiller, A. M., Reply to comment by *chen et al.*, on "calculating the oceanic CO_2 increase: A need for caution", by A.M Shiller, *J. Geophys. Res., 87* (C3), 2086, 1982.

Siegenthaler, U., and F. Joos, Use of a simple model for studying oceanic tracer distributions and the global carbon cycle, *Tellus, Ser. B., 44*, 186–207, 1992.

Siegenthaler, U., and J. L. Sarmiento, Atmospheric carbon dioxide and the ocean, *Nature, 365*, 119–125, 1993.

Siegenthaler, U., and T. Wenk, Rapid atmospheric CO_2 variations and ocean circulation, *Nature, 308*, 624–626, 1984.

Siegenthaler, U., and T. Wenk, Modelling the ocean's role for el niño-related CO_2 variations, Environmental Pollution Monitoring and Research Programme, Geneva, Switzerland, 1989.

Sigman, D., D. C. McCorkle, and W. R. Martin, The calcite lysocline as a constraint on glacial/interglacial low-latitude production changes, *Global Biogeochem. Cycles, 12* (3), 409–427, 1998.

Sigman, D. M., M. A. Altabet, R. Francois, D. C. McCorkle, and J.-F. Gaillard, The isotopic composition of diatom-bound nitrogen in southern ocean sediments, *Paleoceanogr., 14*, 118–134, 1999.

Sigman, D. M., M. A. Altabet, D. D. McCorkle, R. Francois, and G. Fischer, The $\delta^{15}N$ of nitrate in the Southern Ocean: Consumption of nitrate in surface waters, *Global Biogeochem. Cycles, 13* (4), 1149–1166, 1999.

Sigman, D. M., M. A. Altabet, D. D. McCorkle, R. Francois, and G. Fischer, The $\delta^{15}N$ of nitrate in the Southern Ocean: Nitrogen cycling and circulation in the ocean interior, *J. Geophys. Res., 105* (C8), 19599–19614, 2000.

Sigman, D. M., and E. A. Boyle, Glacial/interglacial variations in carbon dioxide: searching for a cause, *Nature, 407*, 859–869, 2000.

Sowers, T., R. B. Alley, and J. Jubenville, Ice core records of atmospheric N_2O covering the last 106,000 years, *Science, 301*, 945–948, 2003.

Spero, H. J., J. Bijma, D. W. Lea, and B. E. Bemis, Effect of seawater carbonate concentration on foraminiferal carbon and oxygen isotopes, *Nature, 390*, 497–500, 1997.

Stephens, B. B., and R. F. Keeling, The influence of antarctic sea ice on glacial-interglacial CO_2 variations, *Nature, 404*, 171–174, 2000.

Stute, M., M. Forster, H. Frischkorn, A. Serejo, J. Clark, P. Schlosser, W. Broecker, and G. Bonani, Cooling of tropical brazil ($5°C$) during the last glacial maximum, *Science, 269*, 379–383, 1995.

Takahashi, T., S. C. Sutherland, C. Sweeney, A. Poisson, N. Metzl, B. Tilbrook, N. Bates, R. Wanninkhof, R. A. Feely, C. Sabine, J. Olafsson, and Y. Nojiri, Global sea-air CO_2 flux based on climatological surface ocean pCO_2, and seasonal biological and temperature effects, *Deep Sea Res. II, 49* (9-10), 1601–1622, 2002.

Tans, P. P., J. A. Berry, and R. F. Keeling, Oceanic $^{12}C/^{13}C$ observations: a new window on ocean CO_2 uptake, *Global Biogeochem. Cycles, 7* (2), 353–368, 1993.

Tans, P. P., I. Y. Fung, and T. Takahashi, Observational constraints on the global atmospheric CO_2 budget, *Science, 247*, 1431–1438, 1990.

Toggweiler, J. R., Variations of atmospheric CO_2 driven by ventilation of the ocean's deepest water, *Paleoceanogr., 14* (5), 571–588, 1999.

Toggweiler, J. R., A. Gnanadesikan, S. Carson, R. Murnane, and J. L. Sarmiento, Representation of the carbon cycle in box models and GCMs: 1. solubility pump, *Global Biogeochem. Cycles, 17* (1), 26.1–26.11, 1026, doi:10.1029/2001GB001401, 2003.

Toggweiler, J. R., and J. L. Sarmiento, Glacial to interglacial changes in atmospheric carbon dioxide: the critical role of ocean surface water in high latitudes, in *The Carbon Cycle and Atmosperic CO$_2$: Natural Variations Archean to Present*, edited by E. T. Sundquist and W. S. Broecker, Geophys. Monogr. Ser., 32, pp. 163–184, AGU, Washington, D.C., 1985.

Walker, J. C., P. B. Hays, and J. F. Kasting, A negative feedback mechanism for the long term stabilization of earth's surface temperature, *J. Geophys. Res., 86*, 9976–9782, 1981.

Wallace, D. W. R., Monitoring global ocean carbon inventories, *Ocean Obs. Syst. Dev. Panel, OOSDP Background Report, 5*, Texas A&M Univ., Texas, 1995.

Wallace, D. W. R., Storage and transport of excess CO$_2$ in the oceans: the JGOFS/WOCE global CO$_2$ survey, in *Ocean circulation and climate*, edited by G. Siedler, J. Church, and J. Gould, pp. 489–524, Academic Press, San Diego, 2001.

Wanninkhof, R., R. A. Feely, D. K. Atwood, G. Berberian, D. Wilson, P. P. Murphy, and M. F. Lamb, Seasonal and lateral variations in carbon chemistry of surface water in the eastern equatorial Pacific during 1992, *Deep Sea Res. II, 42*(2-3), 387–409, 1995.

Watson, A. J., D. C. E. Bakker, A. J. Ridgewell, P. W. Boyd, and C. S. Law, Effect of iron supply on Southern Ocean CO$_2$ uptake and implications for glacial atmospheric CO$_2$, *Nature, 407*, 730–733, 2000.

Weaver, A. J., M. Eby, A. F. Fanning, and E. C. Wiebe, Simulated influence of carbon dioxide, orbital forcing and ice sheets on the climate of the last glacial maximum, *Nature, 394*, 847–853, 1998.

Webb, R. S., D. H. Rind, S. J. Lehman, R. H. Healy, and D. Sigman, Influence of ocean heat transport on the climate of the last glacial maximum, *Nature, 385*, 695–699, 1997.

Winguth, A. M. E., D. Archer, E. Maier-Reimer, U. Mikolajewicz, and J.-C. Duplessy, Sensitivity of paleonutrient tracer distribution and deep sea circulation to glacial boundary conditions, *Paleoceanogr., 14*, 304–323, 1999.

Winguth, A. M. E., M. Heimann, D. Kurz, E. Maier-Reimer, U. Mikolajewicz, and J. Segschneider, El Niño-Southern Oscillation related fluctuations of the marine carbon cycle, *Global Biogeochem. Cycles, 8*(1), 39–63, 1994.

Yung, Y. L., T. Lee, C.-H. Wang, and Y.-T. Shieh, Dust: A diagnostic of the hydrologic cycle during the last glacial maximum, *Science, 271*, 962–963, 1996.